THE UNIVERSITY OF CHICAGO

EFFECTS OF CLIMATE CHANGE ON INTERACTIONS BETWEEN A FOREST PEST AND ITS NATURAL ENEMIES

A DISSERTATION SUBMITTED TO
THE FACULTY OF THE DIVISION OF THE BIOLOGICAL SCIENCES
AND THE PRITZKER SCHOOL OF MEDICINE
IN CANDIDACY FOR THE DEGREE OF
DOCTOR OF PHILOSOPHY

DEPARTMENT OF ECOLOGY AND EVOLUTION

BY
JIAWEI LIU

CHICAGO, ILLINOIS
JUNE 2022

TABLE OF CONTENTS

LIST OF FIGURES

LIST OF TABLES

ACKNOWLEDGMENTS

First, I want to express my deepest thanks to my advisor, Dr. Greg Dwyer. Greg, you are an incredible advisor, and a super nice person to work and chat with. I still remember that you told me to sit in the front rows of the classroom when I took your class in my first year of PhD. At that time I was timid and nervous to talk loud as a foreigner, but you gave me the courage to believe in myself. At the end of my first year, when I encountered difficulties in finding a lab, it was you again that offered me an opportunity, and encouraged me to step in the brand new field of disease ecology and modelling. During the five years' time in your lab, you have taught me tons of skills in research, writing and presenting, while always encouraging me that my English is good. This means so much to me, because your words let me stay positive and confident for most of time. My project was not going smoothly, but you always offered me a great deal of help in figuring things out, especially in the past few months. I am sure that I could not have found a path to graduation without you.

The former and current members in the Dwyer lab are also incredible colleagues to work with. My project is based on the work by Colin Kyle, who provided me valuable experience and knowledge in programming and understanding the code. Chentong Li has taught me many useful mathematical principles and methods. Spencer Carran and Joe Mihaljevic also gave me helpful suggestions on coding and learning commands for Linux. I am enjoying working together with the current members in the lab, Katie Dixon, Will Koval and Sophia Horigan. You are always helpful in giving me unique suggestions and insights that I cannot think of by myself, and always friendly in daily life. I feel relaxed when working in the lab with you, and the atmosphere in our team is impressively awesome because you are all willing to share information and opinions with each other.

I would like to thank my Dissertation Committee of Dr. Mercedes Pascual, Dr. Sarah Cobey and Dr. Tim Wootton. You all have contributed to my project greatly with your

questions and suggestions from the committee meetings. Your professional perspectives have helped me figure out shortcomings in my methods, and many more interesting questions to answer, while being incredibly valuable to my potential career in scientific research. I also appreciate the chances you offered to me at the end of each committee meeting to talk about my concerns. I want to thank our collaborators Jiali Wang and Rao Kotamarthi at Argonne National Laboratory for sharing their weather projections with us. Jiali taught me how to read the weather projection data, and figured out some important issues in the projections that had confused me for a long time. I also want to thank Andrew Liebhold and Alison Hunter for the information on spongy moth habitats in the United States and Canada.

I feel fortunate to have the great faculties and staffs in the Department of Ecology and Evolution. I want to give my special thanks to Dr. Manyuan Long, who provided me an opportunity to visit the University of Chicago and the Department of Ecology and Evolution when I was at college. I spent an unforgettable summer in his lab, and had great chances to talk to Dr. Joy Bergelson and Dr. Martin Kreitman to know about this department. This meaningful summer trip and the conversation with Manyuan, Joy and Marty made up my mind to apply for a PhD in Ecology and Evolution, and I feel proud that I finally become a member of this community. Manyuan also gave me helpful suggestions and encouragement when I was at a loss in finding a lab, which I will never forget. I would also like to thank Dr. Audrey Aronowsky, the Director of Graduate Education. Audrey, you are always extremely helpful in figuring out a variety of issues. When I turn to you for help, I can get the exact information I want every time. I am able to focus more on my research because you are here to support me in dealing with different procedures, so I owe you many thanks.

My cohort and the other graduate students in the Biological Sciences Division are all fascinating and brilliant people, who have taught me important lessons as a researcher and a person. I would like to especially thank Kat Belsmith as my student mentor of my first lab rotation in Dr. Joy Bergelson's lab. Kat was incredibly responsible and considerate

in planning the experiments and answering my questions, teaching me these commendable attitudes in scientific research as well as in daily life.

I would like to thank the Chinese Scholarship Council for awarding me a two-year fellowship as a PhD student. I was benefited from this fellowship in my PhD application and the first two years. I am thankful that it is available to support Chinese students to pursue further education abroad.

Finally, I need to thank my parents and all the friends in China and in the United States. We have all experienced the hard times of COVID in the past two years, and I would like to thank every kind message sent by my friends. I am not a social person, but I realize that you all care for me. I live alone in this difficult time period, but I never feel lonely because of you. My parents are always my strongest backup with their unconditional love and support. The phone calls with you at night let me feel that you are always with me and I never walk alone. I can never achieve anything without you. I owe you thanks more than I can express.

ABSTRACT

Climate change can often lead to severe but complicated effects on ecosystems. Previous studies of the effects of climate change on ecosystems have often focused on single species, thereby neglecting species interactions and underlying mechanisms. To comprehensively understand how climate change influences ecosystems, interactions among multiple species should be considered. Here we provide an example of why species interactions are important for understanding and predicting the effects of climate change on a forest pest species, the spongy moth (*Lymantria dispar*). The transmission and survival of the spongy moth specialist fungal pathogen *Entomophaga maimaiga* have been proved to be strongly affected by weather conditions. By combining a mechanistic disease model with a climate change model, we show that in most locations over the spongy moth habitat in North America, climate change will lead to increased temperature and decreased relative humidity, thereby suppressing the fungal infection in the future. The insect population density is likely to increase in the future, causing a higher level of defoliation. We further extend the model to allow for a viral pathogen and generalist predators, as well as long-term dynamics of the insect host and its both pathogens. Additional parameters on fungus-virus competition and fungus survival are estimated by fitting the long-term fungus-virus models to defoliation data in New England. By projecting the effects of climate change on insect outbreak patterns, we show that hotter and drier weather in the future is likely to cause more frequent spongy moth outbreaks, with moderately larger outbreak amplitudes, when the fungal and viral pathogen interact with each other. Generalist predators tend to strengthen the effects of climate change on spongy moth outbreaks, probably because of their ability to suppress the insect density together with the pathogens. Our results indicate that spongy moth outbreaks are likely to be more severe in the future because the fungal pathogen is not favored by climate change, emphasizing the necessity of considering species interactions to understand effects of climate change, while providing insights into forest protection and pest management.

CHAPTER 1

OVERVIEW: EFFECTS OF CLIMATE CHANGE ON A FOREST-DEFOLIATING INSECT AND ITS NATURAL ENEMIES

Effects of climate change on ecosystems and the role of species interactions

The word "climate change" has often been mentioned in news reports and scientific studies covering a large variety of fields. Many of us may hear words like "global warming" and "greenhouse gas emissions" as our first impressions of climate change. Public attention to climate change was first drawn by concerns that climate change could strongly affect the Earth and resources that human beings rely on. For example, melting glaciers may drive rises in the average sea levels (Change, 2007). The basic but profound way in which climate change affects the global environment is to disrupt ecosystems, causing consequences such as species abundance changes, range shifts and community reorganization (Walther, 2010). The phenology and physiology of different organisms are likely to be altered by climate change, thus resulting in changes in local resource abundance and species habitats. Such disruptions in ecosystems can lead to large-scale environmental changes such as deforestation and desertification, which can dramatically affect the lives of human beings.

Understanding how climate change will affect the dynamics of certain species in their specific ecosystems is thus important to understand the ecological consequences of climate change and to predict its effects in the future, so that losses in resources or biodiversity can be avoided. Most studies on climate change in ecology, however, only focus on single-species (Urban et al., 2016), thereby neglecting the ecological principle that every species interacts with multiple other species (Lawton, 1999). Allowing for species interactions in studies of

climate change is thus crucial for achieving a more realistic, comprehensive and accurate understanding of the extent to which climate change may alter natural ecosystems, but it is difficult because of the lack of high-quality data on species-interaction mechanisms, so that many interaction patterns and mechanisms are still poorly known (Urban et al., 2016). Early efforts indicate that climate change can influence multiple species in the same ecosystem, but they mainly depend on regressions and statistical analyses, while again neglecting the interaction mechanisms (Kausrud et al., 2008; Millon et al., 2014). The few cases that project the effects of climate change while mechanistically considering species interactions provide evidence showing that climate change can influence the dynamics of multiple species simultaneously and severely (Iyengar et al., 2016; Mordecai et al., 2019; Rasher et al., 2020). However, these studies still lack knowledge on underlying species interactions. Mordecai et al. (2019) and Rasher et al. (2020) performed laboratory experiments to develop insight into species interaction mechanisms, but laboratory experiments are often not accurate enough to reveal mechanisms operating in nature. Thus, an essential requirement for more realistic studies on effects of climate change on interacting species is to acquire more knowledge and data on species-interaction mechanisms in the field.

Understanding effects of climate change in outbreaking insects

To provide a practical example of why it is important to understand the effects of climate change on species interactions, we focus on an outbreaking insect pest which causes severe damage to forests. Outbreaking insects often have large-amplitude population cycles over a long time period, mainly driven by interactions with pathogens or parasitoids (Anderson and May, 1980; Varley et al., 1974). As the concentration of CO_2 is a major concern of climate change, effects of climate change on trees and forests are thus important topics; however, we may not be able to understand for such effects if we focus on tree growth alone without considering outbreaking insects. Previous work has argued that tree growth and

forest productivity are likely to increase because of more CO_2 in the atmosphere (Gustafson et al., 2018; Kim et al., 2017), but such conclusions are too optimistic because they neglect interactions among trees, outbreaking defoliator insects and their natural enemies.

Evidences for effects of climate change on outbreaking insects have been found in several previous studies. Population cycles of forest insects can be strongly affected by climate change, but whether outbreak probabilities will increase or decrease following a warming period with high temperatures depends on the species (Haynes et al., 2014; Pureswaran et al., 2018). Such differences may come from the species-specific physiology and habitat of each insect species, but most researches have attempted to connect and compare insect population data to weather data, so that the underlying mechanisms were either guessed or inferred from statistical analyses. Mechanistic information and data on interactions between forest insects and their natural enemies, such as pathogens and parasitoids, are essential for a more comprehensive understanding of theses species-specific responses to climate change. The few existing studies on the effects of climate change on insects that consider species interactions emphasize the role of parasitoids. For example, climate change may have eliminated cycles in larch budmoth that were previously driven by parasitoids (Iyengar et al., 2016), but direct evidences are missing. Moreover, it is also hard to translate effects of climate change on parasitoid physiology into change in insect populations because of limited information on mechanisms of interactions between insect hosts and parasitoids (Tougeron et al., 2020). Studies on effects of climate change on the interactions between forest insects and pathogens are even rarer. To explain the complex effects that climate change can have on forest ecosystems, it is necessary to consider multi-species interactions between outbreaking insects and their natural enemies, making understanding of interaction mechanisms and collection of high-quality mechanistic data in the field priority tasks to accomplish before realistic conclusions can be drawn.

Study system: the spongy moth and its natural enemies

To understand the importance of including species interactions when studying climate change, we chose the spongy moth (*Lymantria dispar*) as the insect host in our study system. The spongy moth was introduced from Europe in 1868 or 1869 (Elkinton and Liebhold, 1990) , and has long been an important defoliating insect in the hardwood forests of North America (Liebhold et al., 1992). The spongy moth has undergone large-amplitude population cycles for many years with cycle period of 5 to 10 years, mainly driven by a specialist lethal baculovirus (Johnson et al., 2006; Liebhold et al., 2000). Small mammals have been known to be generalist predators for this insect species, introducing variations in the time between insect population peaks (Dwyer et al., 2004; Elkinton et al., 1996). Since 1989, the introduction of another specialist pathogen, the fungus *Entomophaga maimaiga* (Andreadis and Weseloh, 1990; Hajek et al., 1996), has dramatically altered the interactions between *L. dispar* and its natural enemies, while sporadic outbreaks terminated by the fungus have replaced the fairly regular boom-bust population cycles driven by the virus before the fungus introduction, as found in Johnson et al. (2006). The fact that fungal transmission and survival are favored by wet and cool weather (Hajek, 1999; Weseloh and Andreadis, 1992) connects climate change with species interactions, making the spongy moth system a useful system for studying the potential effects of climate change on forest ecosystems. We know that weather variables directly change the fungal transmission and survival, and we want to further know how spongy moth dynamics are in turn changed, while considering additional and simultaneous effects caused by interactions with other species such as the viral pathogen and generalist predators.

Mechanistic models are useful for studying the dynamics of interacting species, especially in predator-prey and host-pathogen systems. In outbreaking insects, larval-stage insects are relatively easy to rear, so that laboratory and field experiments on artificial epizootics (epidemics in animals) can be performed to obtain mechanistic data on interactions between

the insect host and its specialist pathogens. Previous work by our colleagues has constructed models describing both within-epizootic and long-term dynamics driven by the interaction between the insect host and the viral pathogen (Dwyer et al., 1997, 2000, 2004), as well as the single-epizootic dynamics driven by the interaction between insect host and the fungal pathogen (Kyle et al., 2020). Here we combine and extend these existing models into a long-term two-pathogen model. By further adding in the weather projections generated by down-scaled climate change models (Wang and Kotamarthi, 2014, 2015), we aim to make realistic and comprehensive projections on future spongy moth dynamics and outbreak patterns, thus providing insights into forest protection and pest management.

Chapter summaries and conclusions

In Chapter 2, we combine the single-epizootic fungus model developed by Kyle et al. (2020) with the down-scaled climate change model developed by our colleagues (Wang and Kotamarthi, 2015), to project the fraction of spongy moths infected by the fungal pathogen *E. maimaiga* across the range of spongy moth habitats in North America. We choose several host and pathogen densities that have been either observed or estimated. Then we run our eco-climate models for 10 years with historical weather projections and for another 10 years with weather projections at the end of the 21st century and compare the model output. Multiple scenarios commonly show the trend that climate change will generally decrease the fraction infected by the fungal pathogen, thus leading to higher insect population densities and defoliation levels. The weather projections show that in most locations within the range of spongy moth, there tend to be decreased relative humidity and increased temperature at the end of 21st century, which will not favor the fungal transmission. Our findings on the decrease of fungal infection in the future thus correspond to climate change driven alterations in weather conditions.

However, we have not included the viral pathogen and generalist predators in the models

in Chapter 2. Moreover, the projections in Chapter 2 are based on averages across only 10 years with fixed host and pathogen densities at the beginning of each year. To understand the effects of climate change on the interactions between the spongy moth and its multiple natural enemies over the long term, in Chapter 3, we extend the model to allow for the interaction between the virus and the fungus, as well as the effects of generalist predators. We fit the models to defoliation data in New England to estimate additional parameters for which we have limited information. Then we run the long-term fungus-virus models with their best parameter estimates for a long time period, using historical and future weather projections respectively, to compare differences in summary statistics such as number of insect population peaks, peak intervals and amplitudes, to show the effects of climate change on spongy moth population dynamics. We also discuss the role of generalist predators by comparing the model output and summary statistics generated by models with and without the influence of generalist predators on long-term insect host dynamics. In representative locations from the spongy moth habitat, we show that there will be a moderately increase in the number of spongy moth outbreaks in the future, with shorter intervals between outbreaks and higher amplitudes. The severity of effects of climate change also depends on how many species we allow for. Invoking both pathogens and generalist predators leads to much higher outbreak amplitudes and more obvious differences in outbreak patterns in the future as opposed to historically. Having two pathogens but not generalist predators generates overall lower outbreak amplitudes and less obvious changes from the past to the future.

We conclude that the fungal pathogen *E. maimaiga* is the key factor showing effects of climate change, since the fungal pathogen's transmission and survival are directly dependent on weather conditions. If we eliminate the fungus, so that the virus is the only pathogen, all effects of climate change are eliminated. Moreover, generalist predators help the pathogens to suppress the spongy moth density at a relatively low level until a severe outbreak happens. When the fungus is likely to play a much weaker role in the future in controlling the spongy

moth, generalist predators and virus will do an inadequate job of suppressing the spongy moth, so more outbreaks will occur more frequently. Altogether, we show that an understanding of interaction mechanisms among multiple species is essential for understanding ecological consequences of climate change.

CHAPTER 2

PROJECTED EFFECTS OF CLIMATE CHANGE ON A FUNGAL PATHOGEN OF A FOREST PEST INSECT

2.1 Abstract

Ecological studies of climate change have focused on individual species, neglecting the interactions between species that regulate population numbers. A crucial example of this neglect comes from models of tree growth, which project positive effects of climate change on North American forests without accounting for alterations in the interactions between forest-defoliating insects and the pathogens that control them. To understand how climate change will affect an important forest insect under the influence of species interactions, we first combined a physics-based climate change model with a validated single-epizootic model of the interaction between the spongy moth *Lymantria dispar* and its fungal pathogen *Entomophaga maimaiga*. Our model projects that climate change will severely restrict *E. maimaiga*, thereby greatly increasing *L. dispar* defoliation. Climate-change driven alterations in species interactions are likely to have dire unanticipated consequences for ecosystems.

2.2 Introduction

Mathematical models of tree growth project that higher CO_2 concentrations are likely to lead to increased forest productivity (Gustafson et al., 2018; Kim et al., 2017), especially if trees can acclimate to the drought stress that accompanies higher temperatures (Sperry et al., 2019). As forest modelers have recognized (Sturtevant and Fortin, 2021), however, tree-growth models neglect the fundamental ecological principle that every species interacts with multiple other species (Lawton, 1999). Forest trees are thus embedded in a web of interactions that includes defoliating insects, which lower tree growth and survival by removing

foliage (Fei et al., 2019), and pathogens of defoliating insects, which increase tree growth and survival by killing defoliating insects (Dwyer et al., 2004). Understanding how climate change will affect North American forests thus requires an understanding not just of how climate change will affect tree growth but also of how climate change will affect interactions between defoliating insects and their pathogens. Such an understanding, however, is sorely lacking.

The ecological literature as a whole has similarly neglected the species interaction principle: most studies of the ecological consequences of climate change have focused on how climate change affects particular species rather than on how climate change affects webs of species interactions (Urban et al., 2016). Our lack of understanding of the effects of climate change on insect-pathogen interactions in particular therefore reflects a lack of understanding of the effects of climate change on species interactions in general.

To test the hypothesis that climate change will alter interactions between forest insects and their pathogens, and thus to carry out a specific test of the general hypothesis that climate change will alter species interactions, we constructed a mathematical model of the interaction between the spongy moth, *Lymantria dispar*, an invasive pest of North American hardwood forests (Tobin et al., 2012), and its fatal, species-specific fungal pathogen *Entomphaga maimaiga* (Hajek et al., 1996). Between the introduction of *L. dispar* in 1869 and the introduction of *E. maimaiga* in 1989, *L. dispar* defoliation had severe negative impacts on hardwood forests in eastern North America (Morin and Liebhold, 2016). In the pre-*E. maimaiga* era, spongy moth outbreaks did not collapse until they had reached densities high enough to allow for epizootics of a fatal, species-specific nucleopolyhedrovirus that belongs to the baculovirus family (Dwyer et al., 2004).

As is often the case for animal pathogens (McCallum et al., 2001), the transmission of both the nucleopolyhedrovirus and *E. maimaiga* is higher in high density spongy moth populations, but cool and moist weather can allow for *E. maimaiga* epizootics even in low density

spongy moth populations (Hajek, 1999). This is important because weather conditions in eastern North America since the introduction of *E. maimaiga* have been sufficiently cool and moist that *E. maimaiga* epizootics have greatly reduced *L. dispar* defoliation (Liebhold et al., 2022). Climate change, however, is projected to lead to increases in temperature and reductions in relative humidity in eastern North America (Wang and Kotamarthi, 2015). Climate change may therefore interfere with the ability of *E. maimaiga* to reduce *L. dispar* defoliation, with negative consequences for hardwood forests in North America. To assess the likelihood of such an outcome, we constructed an ecological model that describes the effects of weather on the *E. maimaiga*-*L. dispar* interaction, and we combined our ecological model with a climate-change model to form what we call an "eco-climate" model. Here we use our eco-climate model to project the effects of climate change on the *E. maimaiga*-*L. dispar* interaction.

The few previous efforts to project the effects of climate change on species interactions (Mordecai et al., 2019; Rasher et al., 2020) estimated model parameters using laboratory experiments that considered only the effects of temperature. Laboratory experiments can provide insight into underlying mechanisms but often make inaccurate projections of ecological phenomena in the field (Carpenter, 1996), while species interactions in nature are often affected by weather variables other than temperature (Urban et al., 2016). We therefore instead estimated parameters from field data, and we considered multiple weather variables. To identify underlying mechanisms, we fit our ecological models to a combination of experimental and observational data (Kyle et al., 2020), and we used statistical model selection (Burnham and Anderson, 2010) to choose between fifteen models, each of which made different assumptions about the mechanisms driving the *E. maimaiga*-*L. dispar* interaction. The model that best describes our data includes effects of temperature, relative humidity, rainfall, and the densities of *E. maimaiga* and *L. dispar*, whereas models that neglect weather or host and pathogen densities or that allow for only one or two weather variables provide

substantially worse explanations for the data.

Our climate-change model uses a technique known as "dynamic down-scaling" to convert the continental-scale projections of standard climate-change models to the forest scales at which *E. maimaiga* epizootics occur (Wang and Kotamarthi, 2015; Zobel et al., 2018). The dynamic down-scaling projections show that temperature will increase and relative humidity will decrease at the vast majority of locations in eastern North America, but that rainfall will increase in almost as many locations as it will decrease (Figure 2.2). Because increased rainfall has positive effects on the *E. maimaiga*-*L. dispar* interaction, while increased temperatures and decreased relative humidity have negative effects on the interaction (Kyle et al., 2020), the dynamic down-scaling simulations alone are insufficient to project how climate change will affect the interaction. We therefore combined our dynamically down-scaled climate-change model with our *E. maimaiga*-*L. dispar* model to form an eco-climate model. The eco-climate model thus integrates the effects of temperature, rainfall, relative humidity and *E. maimaiga* and *L. dispar* densities into an overall projection of the effects of climate change on the *E. maimaiga*-*L. dispar* interaction.

Because *E. maimaiga* transmission depends on spongy moth density, we made projections for a range of different spongy moth densities. *Lymantria dispar* densities at the beginning of epizootics in nature depend on how many spongy moths were killed in the previous generation, either by *E. maimaiga* or by generalist small mammal predators (Dwyer et al., 2004). Because densities of generalist small mammal predators are in turn determined by the production of acorns by oak trees (Liebhold et al., 2000), projecting initial densities is difficult. We therefore made projections across the range of densities at which we observed insect outbreaks and fungus epizootics in nature (Kyle et al., 2020). Although *E. maimaiga* epizootics occasionally occur at densities slightly lower and slightly higher than the densities that we use here, focusing on commonly observed densities allowed us to avoid extreme scenarios, ensuring that our results are conservative.

Unfortunately, our eco-climate models project a general trend that climate change (predicted under the RCP 8.5 scenario) will severely reduce *E. maimaiga* infection rates, which is more obvious at the low and intermediate spongy moth densities at which *E. maimaiga* has suppressed spongy moth populations in the past. Because a female spongy moth can produce hundreds of offspring (Dwyer et al., 2004), the reductions in *E. maimaiga* infection rates projected by our model will allow spongy moth populations to rapidly reach higher densities, at which more severe defoliation may occur. An analysis of the effects of stochasticity suggests that these projections are if anything overly optimistic, while a consideration of alternative scenarios, including the RCP 4.5 scenario and scenarios with higher and lower initial *E. maimaiga* densities, shows that the projections are robust to errors in model assumptions.

2.3 Methods

2.3.1 Overview

In this section, we are going to introduce how our different versions of eco-climate change models are constructed. We will first walk through the equations for the SEIR ecological models showing the *L. dispar*-*E. maimaiga* interactions during a single epizootic. Because several processes in the ecological models are related to weather variables, we are able to combine them with the down-scaled climate change models to study the effect of climate change, by running the models with different projected weather datasets in the past or in the future. Then we will talk about how to generate maps over the entire spongy moth habitat region in North America, to show the differences in historical and future projections in all the locations. We mainly plot out relative differences of fraction infected by fungus between the future and the historical projections. In some cases, we use a regression to transform insect densities into defoliation percentage, to get a more intuitive view on what

consequences climate change will bring to the forests through affecting the insect-pathogen interactions.

2.3.2 The SEIR ecological models

The ecological part of our model consists of a standard "SEIR" model from theoretical epidemiology (Keeling and Rohani, 2008), which we modified to describe the effects of weather. In a previous study (Kyle et al., 2020), we estimated the model's parameters from data that we collected during *E. maimaiga* epizootics in larval spongy moth populations (only larvae are susceptible) at a range of densities in the years 2010, 2011, and 2012, along a 300 km-long north/south transect in Michigan, USA. Here we briefly summarize the model structure, which is described in more detail in Kyle et al. (2020).

Weather conditions in the model change on a daily basis, roughly matching the time scale over which weather systems move through the range of *L. dispar* in North America. Because the model also includes stochasticity, it consists of a set of random ordinary differential equations, integrated on a daily time scale. For each day τ, the model is:

$$\overbrace{\frac{dS_\tau}{dt}}^{\substack{\text{change in}\\ \text{susceptible}\\ \text{host density}}} = -\overbrace{\nu_{R,\tau}}^{\substack{\text{resting spore}\\ \text{transmission rate}}}\overbrace{S_\tau}^{\substack{\text{host}\\ \text{density}}}\overbrace{R_\tau(0)}^{\substack{\text{resting spore}\\ \text{density}}} - \overbrace{\nu_{C,\tau}}^{\substack{\text{conidia}\\ \text{transmis-}\\ \text{sion rate}}} S_\tau \overbrace{C_\tau}^{\substack{\text{conidia}\\ \text{density}}}, \tag{2.1}$$

$$\overbrace{\frac{dE_{\tau,1}}{dt}}^{\substack{\text{change in exposed}\\ \text{class 1}}} = \nu_{R,\tau}S_\tau R_\tau(0) + \nu_{C,\tau}S_\tau C_\tau - \overbrace{\underbrace{m}_{\substack{\text{no. of}\\ \text{exposed}\\ \text{classes}}}\ \underbrace{\lambda}_{\substack{\text{speed of}\\ \text{kill of}\\ \text{fungus}}}\ E_{\tau,1}}^{\text{aging into next exposed class}}, \tag{2.2}$$

$$\overbrace{\frac{dE_{\tau,j}}{dt}}^{\substack{\text{change in exposed}\\ \text{class j}}} = \overbrace{m\lambda E_{\tau,j-1}}^{\substack{\text{aging out of}\\ \text{previous class}}} - \overbrace{m\lambda\ \underbrace{E_{\tau,j}}_{\substack{\text{host density in}\\ \text{exposed class j}}}}^{\substack{\text{aging into}\\ \text{next class}}}, \qquad j = 2, ..., m, \tag{2.3}$$

$$\overbrace{\frac{dC_\tau}{dt}}^{\substack{\text{change in cadavers}\\ \text{producing conidia}}} = \overbrace{m\lambda E_{\tau,m}}^{\substack{\text{death of hosts}\\ \text{in final}\\ \text{exposed class}}} - \overbrace{\underbrace{\mu_{C,\tau}}_{\substack{\text{decay rate of}\\ \text{cadavers producing}\\ \text{conidia}}} C_\tau}^{\text{cadaver decay}}. \tag{2.4}$$

Here we indicate the day during the epizootic by τ, and so on day τ we numerically integrate from time $t = 0$ to time $t = 1$. As we describe below, the stochastic terms are incorporated into the transmission functions $\nu_{R,\tau}$ and $\nu_{C,\tau}$. Because stochasticity is incorporated into the model independently of weather, and because we estimated the amount of stochasticity from our epizootic data (Kyle et al., 2020), stochasticity in the model allows for errors in the model fit that cannot be ascribed to measurement error (which our model-fitting showed was modest (Kyle et al., 2020), but in any case we do not need to include here). Stochasticity in the model thus constitutes what is referred to in the ecological literature as "process error", meaning that it accounts for processes in nature that are not accounted for in the model.

The state variables are the density of uninfected or "susceptible" larvae $S_\tau(t)$, the density of resting spores $R_\tau(0)$, the density of exposed larvae in class j, $E_{\tau,j}(t)$, and the density of conidia $C_\tau(t)$. Resting spore density is symbolized as $R_\tau(0)$ to indicate that it is constant during the resting-spore transmission period, which runs from $\tau = T_g$ until $\tau = T$, where T_g and T are parameters that we fit to the epizootic data. We thus set $R_\tau(0)$ to a constant value of $R_\tau(0)$ for $T_g \leq \tau \leq T$, and we set it to zero for $\tau < T_g$ and $\tau > T$.

By including m exposed classes, we allow for a distributed delay between infection and death, which follows a gamma distribution with a mean delay of $1/\lambda$ and variance $1/(m\lambda^2)$ (Keeling and Rohani, 2008). A gamma distribution provides a reasonable approximation to the distribution of *E. maimaiga* incubation times (Kyle et al., 2020).

On day τ, the conidial decay rate $\mu_{C,\tau}$ and the transmission rates $\nu_{R,\tau}$ for resting spores $R_\tau(0)$, and $\nu_{C,\tau}$ for conidia $C(t)$ are determined by the weather projected by our dynamically

down-scaled climate-change model (Wang and Kotamarthi, 2015), and by a stochastic term. Because larval infection risk increases as larvae increase in size, and because this increase in size causes infection rates during epizootics to show sharp increases late in the larval season when larvae are larger (Kyle et al., 2020), we assumed that transmission increases with larval size. Without increases in larval size the fit of the model to the data was quite poor, and so allowing for larval growth ensured that the model provided a good fit to the data.

Larval size is in turn described by a larval growth function. Because larvae grow faster when temperatures are higher, for temperatures above 10° C, the lowest temperature at which larvae can grow, larval size in the growth function increases linearly with temperature. Because spongy moth eggs hatch in response to an accumulation of degree days, the timing of spongy moth larval emergence in the model also depends on degree-day accumulation (Kyle et al., 2020). This is important partly because it means that larval emergence in the model occurs earlier as temperatures increase due to climate change. Degree days (DD) are calculated by summing up daily average temperature $T(i)$ over a certain time period, while considering the lower threshold T_{min} and upper threshold T_{max}, as the following equations show:

$$DD = \sum_{i=t_0}^{t_1} dd(i) \tag{2.5}$$

$$dd(i) = 0 \qquad if \quad T(i) < T_{min} \tag{2.6}$$

$$dd(i) = T(i) - T_{min} \quad if \quad T(i) \in [T_{min}, T_{max}] \tag{2.7}$$

$$dd(i) = T_{max} - T_{min} \quad if \quad T(i) > T_{max} \tag{2.8}$$

To incorporate weather into the model we assumed that the functions for $\nu_{C,\tau}$, $\nu_{R,\tau}$ and $\mu_{C,\tau}$ depend on the weather, and we fit the parameters of these functions to our epizootic data, using observed values of temperature, relative humidity, and rainfall as covariates. To

construct a weather-dependent transmission function for resting spores we first assumed that the resting spore transmission rate $\nu_{R,\tau}$ is a logistic function of accumulated daily rainfall (mm $\times$ 10/day) over the previous 10 days $p(\tau)$:

$$\nu_{R,\tau} = D(\tau)\left(\frac{\psi_1}{1+\psi_2\exp(-\psi_3 p(\tau))} - \frac{\psi_1}{\psi_2+1}\right)\exp(\epsilon_{R,\tau}). \tag{2.9}$$

This function is constructed to ensure that when cumulative rainfall $p(\tau) = 0$, resting spore transmission is zero. The function also includes stochasticity, as represented by $\epsilon_{R,\tau}$, which symbolizes a normally distributed random variate with zero mean and with a non-zero standard deviation, where the standard deviation was estimated by fitting the model to the data. The parameters ψ_1-ψ_3 were likewise estimated from the data (Kyle et al., 2020). The symbol $D(\tau)$ represents the larval growth function.

Because conidia production increases with relative humidity (Hajek, 1999), we assumed that the conidia transmission rate $\nu_{C,\tau}$ increases exponentially with minimum daily relative humidity $m(\tau)$ on day τ;

$$\nu_{C,\tau} = D(\tau)\psi_4\exp(\psi_5 m(\tau))\exp(\epsilon_{C,\tau}). \tag{2.10}$$

Here $D(\tau)$ is again the larval growth function, and the parameters ψ_4 and ψ_5 were estimated from the data (Kyle et al., 2020). As in equation (2.9), stochasticity is represented by $\epsilon_{C,\tau}$, which symbolizes a normally distributed random variate with a zero mean and with a non-zero standard deviation that was estimated from the data.

Because high temperatures inhibit conidia production (Hajek, 1999), we assumed that conidia decay $\mu_{C,\tau}$ is an exponentially increasing function of daily maximum temperature,

so that conidia survival falls with temperature;

$$\mu_{C,\tau} = \psi_6 \exp(\psi_7 h(\tau)). \tag{2.11}$$

Here $h(\tau)$ is the maximum temperature on day τ, and the parameters ψ_6-ψ_7 were again estimated from the epizootic data (Kyle et al., 2020).

Because the model equations (2.1)-(2.4) are only integrated for one day at a time, we update their initial conditions at the beginning of each day, according to:

$$\begin{aligned} S_\tau(0) &= S_{\tau-1}(1), && (2.12)\\ R_\tau(0) &= R_{\tau-1}(0) \text{ for } T_g \le \tau \le T, && (2.13)\\ &= 0 \text{ for } \tau < T_g \quad \text{or} \quad \tau > T, && (2.14)\\ E_{\tau,j}(0) &= E_{\tau-1,j}(1), && (2.15)\\ C_\tau(0) &= C_{\tau-1}(1). && (2.16) \end{aligned}$$

Here $S_{\tau-1}(1)$ is the density of susceptible hosts at $t = 1$ on day $\tau - 1$, which means at the end of day $\tau - 1$, while $S_\tau(0)$ is the density of susceptible hosts at $t = 0$ on day τ, which means at the beginning of day τ, and similarly for the other state variables. We repeat that the resting spore density is constant during the resting spore transmission period and is otherwise zero. As we will describe in the Results section, we have varied the initial density of hosts $S_0(0)$ and resting spores $R_{T_g \le \tau \le T}(0)$ across scenarios.

When larvae in the SEIR model have completed development to enter the stage of pupation, the epizootic is over. The model then calculates the cumulative fraction of the host population that became infected during the epizootic. In each year, the epizootic starts when eggs hatch after 317 DD with 3 $^\circ C$ as the lower threshold and 40 $^\circ C$ as the higher threshold (Russo et al., 1993). The epizootic ends when pupation occurs 568.5 DD after hatch, with 7.65 $^\circ C$ as the lower threshold and 41 $^\circ C$ as the higher threshold (Carter et al.,

1992). Resting spores start germination 100.16 DD after hatch, and end germination 267.03 DD after hatch, both with 10 $^{\circ}C$ as the lower threshold (Kyle et al., 2020).

To construct the weather-only version of the SEIR model, we assumed that *E. maimaiga* transmission is unaffected by the density of conidia or resting spores, and we continued to track larval growth. The weather-only model therefore tracks only the density of susceptible larvae S and the density of larvae in exposure class E_i, according to:

$$\begin{aligned} \frac{dS_\tau}{dt} &= -\overbrace{\nu_{F,\tau}}^{\text{transmission rate of the fungus}} S_\tau. && (2.17)\\ \frac{dE_{1,\tau}}{dt} &= \nu_{F,\tau} S - m\lambda E_{1,\tau}, && (2.18)\\ \frac{dE_{i,\tau}}{dt} &= m\lambda E_{i-1,\tau} - m\lambda E_{i,\tau}, \qquad i = 2, ..., m. && (2.19) \end{aligned}$$

Although in this model larvae do not produce conidia, we included exposed larvae to allow for the possibility that larvae would not yet be dead at the end of the epizootic. Model selection then showed that the version of this model that best describes the epizootic data uses a weather-dependent function $\nu_{F,\tau}$ that depends on daily rainfall and maximum temperature, as follows;

$$\nu_{F,\tau} = D(\tau)\left(\frac{\psi_8}{1+\psi_9\exp(-\psi_{10}p(\tau)} - \frac{\psi_8}{\psi_9+1}\right)\exp(-\psi_{11}h(\tau))\exp(\epsilon_{F,\tau}). \quad (2.20)$$

As in the full eco-climate model, $p(\tau)$ is the accumulated rainfall over the previous 10 days, $h(\tau)$ is the daily maximum temperature on day τ, and $D(\tau)$ is the larval growth function. Also as in the eco-climate model, $\epsilon_{F,\tau}$ is a normally distributed random variate, with mean zero and a standard deviation estimated from the data. As in equation (2.9) in the eco-climate model, $\nu_{F,\tau}$ is a logistic function that describes transmission as a function of cumulative rainfall, again constructed so that $\nu_{F,\tau}$ is 0 when no rain occurs, in other words when $p(\tau) = 0$. The values of the parameters ψ_8-ψ_{11} and the standard deviation of $\epsilon_{F,\tau}$

were estimated from the data, and are given in Kyle et al. (2020).

Here we also show results for a version of the SEIR model that includes the *E. maimaiga*-*L. dispar* interaction but that includes only the effects of relative humidity on the interaction, which we refer to as the "relative-humidity-only model". In this model the conidia transmission rate $\nu_{C,\tau}$ is again an exponential function of minimum daily relative humidity, as in the eco-climate model, but the resting spore transmission rate $\nu_{R,\tau}$ and the conidia decay rate $\mu_{C,\tau}$ no longer depend on weather covariates. The first two of these functions, however, continue to depend on larval size, which in turn depends on degree days;

$$\nu_{R,\tau} = D(\tau)\psi_{12}\exp(\epsilon_{R,\tau}). \tag{2.21}$$

$$\nu_{C,\tau} = D(\tau)\psi_{13}\exp(\psi_{14}m(\tau))\exp(\epsilon_{C,\tau}). \tag{2.22}$$

$$\mu_{C,\tau} = \psi_{15}. \tag{2.23}$$

Here m_τ is again the minimum relative humidity on day τ, and $D(\tau)$ is again the larval growth function. The normally distributed random variates $\epsilon_{R,\tau}$ and $\epsilon_{C,\tau}$ again allow for stochasticity, and both have zero means and standard deviations that were estimated from the epizootic data. As with the other models, the values of the coefficients ψ_{12} - ψ_{15} and the standard deviations for $\epsilon_{R,\tau}$ and $\epsilon_{C,\tau}$ were estimated from the epizootic data, and their values are again given in Kyle et al. (2020).

Conidia of *E. maimaiga* are airborne, and are therefore in principle capable of dispersing significant distances. Given the sensitivity of conidia to local weather conditions, however, it seems likely that any effects of migration would be outweighed by local weather conditions. We therefore expect that conidia dispersal leads at most to some averaging of the infection rate over space. The extent of conidia dispersal is any case poorly known; accordingly, to avoid the additional uncertainty that would accompany estimation of conidia dispersal rates, we assumed that individual locations function as independent populations, with no

migration between populations, but with complete mixing within a location. Our approach therefore allows for high variation between locations, in turn allowing for the possibility that climate change will have positive effects in some locations. We therefore argue that neglecting long-distance dispersal of conidia is a conservative approach.

2.3.3 Climate change model

To allow for inherent variability in weather, the dynamic down-scaled model is stochastic (Wang and Kotamarthi, 2015), and so its projections consist of averages over multiple realizations. Averaging allows the model to reduce the influence of outlier conditions and low probability events. By using the model projections for both 1995-2004 and 2085-2094, we ensured that all weather data came from the same source.

2.3.4 Comparison of weather in our study plots to weather across the range of L. dispar

As we mentioned in section 2.3.2, the ecological parameters for our eco-climate model were estimated from data that we collected in the lower peninsula of Michigan during the spongy moth (*L. dispar*) larval seasons from 2009 to 2012 (Kyle et al., 2020). As part of this data collection effort, we quantified rainfall, relative humidity and temperature every day of the larval season at each of our 3 study sites in each year. Because the study sites were located along a 300 km-long north-south transect, the weather data include substantial variation in each weather variable. Indeed, as Figure 2.1 shows, the variation in the weather variables in our data encompasses most of the variation in the same weather variables across the range of spongy moth in eastern North America for the same periods, and the mean of each variable was similar to the corresponding mean across the range of spongy moth. This similarity is important because we estimated model parameters from epizootic data collected in the state of Michigan, but Figure 2.1 suggests that our models should produce accurate

projections for the entire range of *L. dispar*. Therefore, we use our parameterized model to make projections across the eastern and midwestern United States and the province of Ontario, Canada (to our knowledge Ontario is the only Canadian province for which *L. dispar* defoliation data are available). To focus on forests known to be suitable for *L. dispar*, we make projections only for areas that have experienced *L. dispar* defoliation in the past (Morin and Liebhold, 2016).

2.3.5 Generating the maps

Because the model is stochastic, to make projections for the maps we averaged over model realizations. This means that, at any given map location in any given year, we averaged the fraction infected over 100 realizations or "runs" of the model with the same initial conditions for host and pathogen densities, to produce an average at each map location in that year. To produce overall averages for historical versus future conditions, at each map location we first averaged across the historical period, meaning the years 1995-2004, to produce an historical average for each map location. We then averaged across the future period, meaning the years 2085-2094, to produce a future average for each map location. The maps then show the difference in the average projection for each map location, divided by the historical average and multiplied by 100, to produce a relative percent change in the infection rate. We repeated this process for each model and scenario that we describe below. In each scenario, the initial conditions for running the model remain constant all the time.

In all but the defoliation maps, we plot relative percent changes. This means that we plotted $100(S_f - S_p)/S_p$, where S_f is the future value of a statistic, and S_p is the past value of the statistic, meaning either a weather variable or a fraction infected.

In the defoliation maps, we instead plot the absolute percent change in defoliation $100(D_f - D_p)$, where D_f and D_p are the fraction of foliage defoliated in the future and past, respectively. To generate values of D_f and D_p, we used a published regression model

(Liebhold et al., 1993) to translate the eco-climate model's projections of spongy moth egg mass densities at the end of one larval period into defoliation levels in the following year. Spongy moth sex ratios are generally close to 50:50, and so we multiplied larval densities in the model by 0.5 to translate larval densities into egg mass densities.

We summarize the maps in terms of the mean and the upper 5th and 95th percentiles of the distribution of outcomes across locations. We also calculate the percentage of sites with the relative difference of fraction infected or the absolute difference of defoliation greater than 0, to see to what extent the climate change will suppress the fungal pathogen in the future.

2.3.6 Effects of stochasticity on the model projections

A key feature of our eco-climate model is that it explicitly allows for stochasticity in disease dynamics; allowing for such stochasticity ensured that the model was able to fully capture the variation in the data (Kyle et al., 2020). Like the other ecological parameters in our models, the level of stochasticity was estimated from our field data on *E. maimaiga* infection rates, as we described above. Because the models additionally allow for variation in weather conditions, stochasticity in the models represents variation in the model projections due to errors in the model structure. The model's projections therefore allow for stochastic variation that is above and beyond the day-to-day and year-to-year variation inherent in the weather projections of the dynamic down-scaled climate change model. Here we analyze the effects of this variation on the full eco-climate model and on the weather-only model.

To do this, we calculated the distribution of outcomes at each location in each model. This means that, for each model, we used the model to generate 100 stochastic realizations of the model's projections at each location on the map. In any set of 100 realizations, the weather conditions were the same in each realization, but the realizations nevertheless differed because of the stochastic terms in the models.

In Section 2.3.5, we show the mean projection at each location, to characterize overall trends in model projections. To instead characterize the variation in the model projections, here we instead show maps of the model projections at the upper 75th and lower 25th percentiles of the distribution at each location. The projections of relative percent changes at these percentiles were calculated as follows.

First, to ensure that we were calculating distributions of outcomes for time periods of the same lengths, we paired each historical year, meaning years during the time interval 1995-2004, with the corresponding future year, meaning years during the time interval 2085-2094. This means that 1995 was paired with 2085, 1996 was paired with 2086, and so on. We then generated 100 realizations for each historical year and each future year. Next, we calculated the 10^4 possible differences between the realizations for each set of paired years; because we had 10 sets of paired years, this gave us 10^5 total differences between the historical and future time intervals. As in maps for the mean projection of fraction infected, in practice we calculated relative percent differences again.

Variation was sufficiently high that the 5th/95th percentiles show extreme outcomes, giving the false impression that there are no trends. In calculating percentiles of differences, we therefore calculated the upper 75th and lower 25th percentiles across the 10^5 differences at each geographical location. Then we summarize these maps again in terms of the upper 5th and 95th percentiles of the distribution of outcomes across locations. In what follows, it is therefore important to keep in mind the distinction between the percentiles calculated across locations and the percentiles calculated across realizations.

2.4 Results

2.4.1 Effect of climate change under intermediate fungus density

We start the Results section with the scenario considering that the initial fungus resting spore density for each year is constantly 5.71×10^{-3} m^{-2}, which is an intermediate estimated value from Kyle et al. (2020). We put projected weather data for the past and future from the down-scaled climate change model (Wang and Kotamarthi, 2015) into our full eco-climate model and its weather-only version. The past represents the period 1995-2004, while the future represents the period 2085-2094, under the Relative Concentration Pathway or "RCP" 8.5 scenario.

In the full eco-climate model considering the effects of both weather and fungus density, we have tested the effects of climate change on fraction infected by the fungal pathogen *E. maimaiga* for four different initial insect host densities. Our maps in Figure 2.3 project that climate change will severely reduce *E. maimaiga* infection rates at the low and intermediate spongy moth densities at which *E. maimaiga* has suppressed spongy moth populations in the past. At the two lowest insect densities that we considered, the model projects relative reductions in infection rates of 19.9-23.8%, with a lower 5th percentile of more than 30% at both densities, and with 98.9-99.3% of locations showing reductions. At higher host densities, climate change is projected to lead to more modest reductions, but these more modest reductions are projected to lead to large increases in defoliation, with a mean increase across locations of roughly 20%, with upper 95th percentiles of at least 40% increases, and with more than 98% of locations showing increases, as shown in Figure 2.4. At the end of an epizootic, each survived female spongy moth can produce hundreds of offspring (Dwyer et al., 2004). As a result, the reductions in *E. maimaiga* infection rates projected by our model at low and intermediate host densities will allow spongy moth populations to rapidly reach high densities. The model then projects that at high densities there will be steep increases

in *L. dispar* defoliation. The climate change will therefore cause more harm to forests in the way of suppressing the fungal pathogen and increasing the defoliator insect host density.

Part of the reason why climate change has such strong effects in our full eco-climate model is that the pathogen transmission term in the model depends on the densities of both *E. maimaiga* and *L. dispar*; the transmission term is therefore nonlinear, but it is also weather-dependent. Modest changes in nonlinear transmission terms in SEIR models can lead to large changes in pathogen infection rates (Keeling and Rohani, 2008), and so in our model even modest changes in climate conditions lead to large changes in *E. maimaiga* infection rates. To illustrate this point, we made additional projections in Figure 2.5, using an alternative "weather-only" model that includes effects of weather but that does not include the nonlinear transmission term; significantly, this model projects reductions in the *E. maimaiga* infection rate that are substantially less severe than the reductions projected by the eco-climate model. The mean decrease of the infection rate is 9.75%, and about 95% of locations are showing reductions, which is less compared to the full eco-climate model. Models that unrealistically neglect nonlinear species-interaction terms can thus lead to unrealistically optimistic projections of the effects of climate change.

2.4.2 Effects of stochasticity on the model projections

As mentioned in Section 2.3.6, we summarize the model projections at the upper 75th and lower 25th percentiles of the distribution at each location, to analyze the effects of variation caused by stochasticity on the full eco-climate model and the weather-only model. We also summarize these maps again in terms of the upper 5th and 95th percentiles of the distribution of outcomes across locations. To repeat, it is important to keep in mind the distinction between the percentiles calculated across locations and the percentiles calculated across realizations.

For the full eco-climate model, Figure 2.6 then shows the upper 75th percentiles of

realizations. At the two lowest host densities, the lower 5th percentiles across locations are 16.6% and 15.4% reductions, respectively, while the upper 95th percentiles are 38.7% and 32.9% increases (see Table 2.1 for a summary and a comparison to the averages in Figure 2.3). For the same two densities Figure 2.7 shows that at the lower 25th percentile of realizations the lower 5th percentiles across locations are 54.0% and 53.1% reductions, while the upper 95th percentiles are 33.3% and 20.6% reductions. At the mean fraction infected at the two lowest densities, as shown in Figure 2.3, the lower 5th percentiles are in contrast 35.8% and 33.2% reductions, while the upper 95th percentiles are 7.58% and 6.71% reductions.

The projections of the eco-climate model at the two lowest densities are thus more optimistic at the upper 75th percentiles of projections than at the means, in that higher infection rates occur at almost 50% of sites across the landscape at the upper 75th percentiles; over the rest of the landscape, however, the extent of the reductions at the upper 75th percentiles remains quite severe, although not as severe as in the mean projections. At the lower 25th percentiles in contrast, the model projections show more severe reductions across all locations and all densities. The model's projections are thus moderately less severe at the upper 75th percentile, while being much more severe at the lower 25th percentile. Stochasticity thus leads to substantial variation in the model projections, but in general a consideration of stochasticity suggests that the projections based on averages (Figure 2.3) are if anything optimistic.

It is also useful to compare variation in the projections of the eco-climate model to variation in the projections of the weather-only model. From Figure 2.3 and 2.5, we showed that the average projections of the weather-only model are consistently less severe than the average projections of the eco-climate model; consistent with this result, the projections of the weather-only model at the upper 75th and lower 25th percentiles are less severe than the corresponding projections of the eco-climate model. Figure 2.8 shows that, at the upper 75th percentile of realizations of the weather-only model, 97.5% of locations show increases

in the *E. maimaiga* infection rate; at the upper 75th percentile for the eco-climate model in contrast, no more than than 62% of locations show increases at any density (Figure 2.6, also see Table 2.1 for a summary comparison of the two models).

At the lower 25th percentiles of realizations, the percentage of locations showing reductions in weather-only model (Figure 2.9) is similar to the corresponding case for the full eco-climate model (Figure 2.7), but the severity of the reductions is lower for the weather-only model. For the weather-only model, the lower 5th percentile across locations is a 39.6% reduction, while the upper 95th percentile is a 21.1% reduction, whereas at the two lowest densities for the eco-climate model the corresponding values are 54.0% and 53.1% reductions at the lower 5th percentiles, and 33.3% and 20.6% reductions at the upper 95th percentiles. The reductions in the infection rate at the lower 25th percentiles are thus much less severe for the weather-only model than for the eco-climate model.

The weather-only model therefore also projects substantial variability in the effects of climate change; unlike the case of the eco-climate model, however, a consideration of stochasticity in the weather-only model leads to more optimistic projections than the mean projections. Allowing for stochasticity thus makes the unrealistically optimistic projections of the weather-only model even more unrealistically optimistic.

2.4.3 Alternative Scenarios I: Variation in Resting Spore Density and Changes in Model Structure

Little is known about what determines variation in resting spore densities (Hajek, 1999), and so we assumed that resting spore densities are constant over time and space. We then used values of resting spore densities that we estimated when fitting our models to *E. maimaiga* infection rates in our previous work (Kyle et al., 2020). Although in principle resting spore densities can be estimated by using a microscope to count resting spores in soil samples (Hajek, 1999), in practice little is known about how resting spore density is

translated into infections among larvae; in particular, it is unclear how deep resting spores can be buried before they cease to be able to infect larvae. We therefore instead estimated a resting spore density for each population in our data set, thus estimating what is essentially an effective resting spore density for each population.

An important feature of this approach is that it can lead to different estimates of resting spore densities for different models. Notably, for the relative-humidity-only model, the fitting algorithm attempted to improve the model's generally poor fit to the data by increasing the resting spore density (Kyle et al., 2020). Resting spore densities are therefore higher for the relative-humidity-only model than for the full eco-climate model.

For the full eco-climate model in Section 2.4.1 and 2.4.2, the resting spore density we use is 5.71×10^{-3} m^{-2}, a value that is the second highest of the seven that we estimated in our previous work (a table for these estimates will be given in Chapter 3). Because our argument is that climate change is likely to severely reduce *E. maimaiga* infection rates, and because high resting spore densities ameliorate the effects of climate change by raising infection rates, using a high value is conservative. Variation across sample populations was not particularly high, however, with a standard error of 2.38×10^{-3} m^{-2}, so our default value is within one standard error of the mean value of 4.75×10^{-3}.

For purposes of comparison, here we show cases in which the resting-spore density is instead either the second-lowest value, 6.91×10^{-4} m^{-2} (the lowest value was an extreme outlier), and the case for which the resting-spore density is instead the highest value, 1.83×10^{-2} m^{-2}. At more than 2 standard errors higher than the mean, the highest value is quite extreme, which is why we used the second highest value first.

As Figure 2.10 shows, the highest value of the resting spore density leads to less severe reductions in the infection rate, as compared to Figure 2.3 (see Table 2.2 for a comparison and an overall summary). This is especially true at the second-highest spongy moth density, at which the mean is a 3.79% reduction, with a lower 5th percentile of an 8.58% reduction,

and an upper 95th percentile of a 0.66% reduction. In Figure 2.3, the corresponding map for the second-highest spongy moth density are a mean of a 10.2% reduction, with a lower 5th percentile of a 21.2% reduction and an upper 95th percentile of a 2.27% reduction.

At the two lowest and most important spongy moth densities in Figure 2.10 the relative reductions are again less severe than in Figure 2.3, but the changes are not as strong as at the higher *L. dispar* densities. At the lowest density, the mean is a 10.7% reduction, with a lower 5th percentile of a 17.1% reduction and an upper 95th percentile of a 3.22% reduction. The corresponding case in Figure 2.3 instead gives a mean of a 23.8% reduction, a lower 5th percentile of a 35.8% reduction, and an upper 95th percentile of a 7.58% reduction. At the second lowest density, the mean is an 8.07% reduction, with a lower 5th percentile of a 14.7% reduction and an upper 95th percentile of a 2.53% reduction. The corresponding case in Figure 2.3 instead gives a mean of a 19.9% reduction, a lower 5th percentile of a 33.2% reduction, and an upper 95th percentile of a 6.71% reduction.

High resting spore densities thus lead to less severe but still substantial reductions in the *E. maimaiga* infection rate at low spongy moth densities. This occurs because in both the model and nature resting spores are responsible for a substantial fraction of *E. maimaiga* infections at the beginning of epizootics, leading in turn to more intense overall epizootics. Higher resting spore densities can thus ameliorate the negative effects of climate change. The effects are modest, however, because in general conidia play a more important role than resting spores in driving epizootics (Kyle et al., 2020).

More concretely, the result that reductions in the *E. maimaiga* infection rate are still severe even when the resting spore density is high shows that climate change would still have meaningfully negative impacts on *E. maimaiga* epizootics even if the resting spore density estimate that we used in Section 2.4.1 and 2.4.2 is for some reason biased to be lower than realistic values. If the resting spore density estimate that we used in Section 2.4.1 and 2.4.2 is instead biased to be higher than realistic values, then climate change would have more

severely negative impacts on *E. maimaiga* epizootics (Figure 2.11) than shown in Figure 2.3. We therefore argue that our conclusions are robust to variation in resting spore density.

Next we show projections for the relative-humidity-only model, while varying the resting spore density. As Figures 2.12-2.14 show, and as summarized in Table 2.2, the results are qualitatively similar to the results for the full eco-climate model, except that the projected reductions are moderately less severe. Unrealistically including the effects of only one weather variable thus leads to unrealistically moderate projections, although the effect is not nearly as strong as the effect of eliminating the nonlinear transmission term, as in the weather-only model.

2.4.4 Alternative Scenarios II: RCP 4.5

Here we show results for the RCP 4.5 climate-change scenario, a more optimistic alternative to the RCP 8.5 scenario. As in our other alternative scenarios, here we again consider higher and lower values of the resting spore density, again taken from values estimated in our previous work (Kyle et al., 2020), and again we vary the model structure. We thus consider the full eco-climate model, the relative-humidity-only model, and the weather-only model.

First, in Figure 2.15, we show the projections of the dynamic down-scaled climate change model for the RCP 4.5 scenario. As the figure shows, the model's projected changes are qualitatively similar to the RCP 8.5 case, in that rainfall rises in more than 40% of locations, while relative humidity falls over most of the landscape and temperature increases over most of the landscape. As expected these changes are a little more modest than for the RCP 8.5 scenario (compare Figure 2.15 to Figure 2.2), but the changes are in the same direction for both scenarios.

Because the *E. maimaiga-L. dispar* interaction is quite sensitive to weather, the more modest changes in weather projected under the RCP 4.5 scenario lead to reductions in the *E. maimaiga* infection rate that are only slightly less severe than the reductions under the

RCP 8.5 scenario. To show this, in Fiure. 2.16 we first present projections for the same intermediate resting spore density that we used for the RCP 8.5 scenario, except that here we use the RCP 4.5 scenario.

Figure 2.16 then shows that under the RCP 4.5 scenario the mean relative change in the fraction infected with *E. maimaiga* at the lowest spongy moth density is a 15.3% reduction, the lower 5th percentile is a 25.8% reduction, and the upper 95th percentile is a 4.49% reduction (see Table 2.3 for a summary). For the same spongy moth density under the RCP 8.5 scenario, the mean change is a 23.8% reduction, the lower 5th percentile is a 35.8% reduction, and the upper 95th percentile is a 7.58% reduction. Figure 2.16 further shows that, at the second lowest density under the RCP 4.5 scenario, the mean relative change is a 14.1% reduction, the lower 5th percentile is a 23.7% reduction, and the upper 95th percentile is a 5.33% reduction. For the same spongy moth density under the RCP 8.5 scenario, the mean change is a 19.9% reduction, the lower 5th percentile is a 33.2% reduction, and the upper 95th percentile is a 6.71% reduction. For the two highest densities, the projections under the RCP 4.5 scenario are similar to or moderately less severe than for the RCP 8.5 scenario. The cases of higher and lower resting spore densities under the RCP 4.5 scenario likewise lead to changes that are only moderately less severe than the corresponding cases under the RCP 8.5 scenario (Figures 2.17 and 2.18). The projections of the eco-climate model under the RCP 4.5 scenario are thus in general only moderately less severe than the reductions projected under the RCP 8.5 scenario.

To continue our consideration of the RCP 4.5 scenario, in Figures 2.19-2.21 we show projections for the relative-humidity-only model under the RCP 4.5 scenario. Again the RCP 4.5 scenario leads to only modest changes in the model projections relative to the RCP 8.5 scenario shown in Figures 2.12-2.14 (see Table 2.3 for a summary).

Finally, Figure 2.22 shows the projections of the weather-only model for the RCP 4.5 scenario. As in the other models, comparison of Figure 2.22 to Figure 2.5 shows that the

projections of the weather-only model are only moderately different if we use the RCP 4.5 scenario instead of the RCP 8.5 scenario (see Table 2.3 for a summary).

2.5 Discussion

Our model's projections of reduced *E. maimaiga* infection rates and increased *L. dispar* defoliation rates are important because the spongy moth feeds preferentially on oaks, *Quercus* spp., and has therefore been an important factor driving "oak decline" (Morin and Liebhold, 2016), the replacement of oaks by maples, *Acer* spp., in North American hardwood forests (Haavik et al., 2015). Compared to oaks, maples provide fewer resources for native insects, songbirds and small mammals (Radcliffe et al., 2021); the effects of climate change on the *E. maimaiga*-*L. dispar* interaction are thus likely to affect many other animal species, providing additional examples of the species interaction principle. Meanwhile, the nucleopolyhedrovirus may experience a resurgence because of reduced competition with *E. maimaiga* (Kyle et al., 2020), but the inability of the nucleopolyhedrovirus to prevent defoliation before 1989 suggests that a virus resurgence would be insufficient to prevent increases in defoliation levels. Generalist small mammal predators were also often unable to prevent *L. dispar* defoliation before 1989 (Dwyer et al., 2004), and are therefore similarly unlikely to prevent defoliation in the future.

Nonlinear terms are fundamental to species-interaction models in general (Kot, 2001), and so our work suggests that most species interactions will show strong effects of climate change. Recent forest models have in contrast included effects of insect defoliation without tracking insect or pathogen densities (Sturtevant and Fortin, 2021), and thus without including nonlinear species-interaction terms. It is important to emphasize, however, that our model tracks defoliation but not tree growth, and so a full understanding of the effects of climate change on North American forests ultimately requires a merger of eco-climate models and forest models.

The projections of our eco-climate model are supported by the occurrence in 2015-2018 of the first region-wide spongy moth outbreak in New England since the introduction of *E. maimaiga* in 1989 (Elkinton et al., 2019) (note that smaller outbreaks had occurred earlier). The New England outbreak followed several years of hot, dry weather, suggesting that climate change may have already begun to reduce the severity of *E. maimaiga* epizootics, but a single region-wide spongy moth outbreak of course cannot confirm that our model is correct. Another issue to be solved is that our eco-climate model is still based on the single-epizootic SEIR model to show the changes in fungus infection, and to infer changes in host density in the future. To reach a more general conclusion considering host and pathogen reproduction and the effect of generalist predators, a long-term model describing dynamics between epizootics is thus required, and in Chapter 3 we will talk about our first efforts to construct that long-term model. Indeed, modeling species interactions is sufficiently difficult that our model's projections may be only moderately accurate; given that our model has survived extensive testing, however, our results provide strong evidence that the ecological consequences of climate change will be far worse than previously anticipated.

2.6 Tables and figures

Table 2.1: Summary of stochastic analyses on the full eco-climate model and weather-only model. Since host density has no effect on the weather-only model projections, we list it as N.A. in the table.

Scenario	Host density	Pct.sites > 0	Mean	5th, 95th Percentiles
Eco-Climate Model				
Averages,	25 Larvae/m2	1.09	-23.8	-35.8, -7.58
from Figure 2.3	50 Larvae/m2	0.71	-19.9	-33.2, -6.71
	100 Larvae/m2	0.83	-10.2	-21.2, -2.27
	250 Larvae/m2	2.07	-1.74	-5.76, -0.04
Upper 75th Percentiles	25 Larvae/m2	49.2	4.22	-16.6, 38.7
	50 Larvae/m2	47.5	2.23	-15.4, 32.9
	100 Larvae/m2	52.5	1.15	-4.87, 12.4
	250 Larvae/m2	60.4	0.14	-0.02, 0.46
Lower 25th Percentiles	25 Larvae/m2	0	-45.4	-54.0, -33.3
	50 Larvae/m2	0	-39.5	-53.1, -20.6
	100 Larvae/m2	0	-19.4	-39.5, -2.38
	250 Larvae/m2	0	-1.76	-5.55, -0.01
Weather-Only Model				
Averages from Figure 2.5	N.A.	5.13	-9.75	-19.1, 0.15
Upper 75th Percentiles	N.A.	97.5	14.4	1.94, 30.3
Lower 25th Percentiles	N.A.	0	-30.2	-39.6, -21.1

Table 2.2: Summary of alternative scenarios I: variation in resting spore density and changes in model structure.

Scenario	Host density	Pct.sites > 0	Mean	5th, 95th Percentiles
Eco-Climate Model: Resting Spore Variation				
Intermediate resting spores as in Figure 2.3	25 Larvae/m2	1.09	-23.8	-35.8, -7.58
	50 Larvae/m2	0.71	-19.9	-33.2, -6.71
	100 Larvae/m2	0.83	-10.2	-21.2, -2.27
	250 Larvae/m2	2.07	-1.74	-5.76, -0.04
High resting spores	25 Larvae/m2	1.42	-10.7	-17.1, -3.22
	50 Larvae/m2	1.05	-8.07	-14.7, -2.53
	100 Larvae/m2	1.40	-3.79	-8.58, -0.66
	250 Larvae/m2	2.96	-0.62	-2.38, -0.01
Low resting spores	25 Larvae/m2	2.78	-42.3	-64.7, -7.22
	50 Larvae/m2	2.47	-44.0	-66.4, -12.0
	100 Larvae/m2	1.95	-31.1	-54.4, -8.62
	250 Larvae/m2	1.18	-9.11	-22.0, -0.61
Relative-Humidity-Only Model: Resting Spore Variation				
Intermediate resting spores	25 Larvae/m2	1.34	-20.3	-39.0, -4.85
	50 Larvae/m2	1.56	-11.4	-27.4, -1.63
	100 Larvae/m2	3.89	-3.54	-11.7, -0.07
	250 Larvae/m2	5.47	-0.34	-1.51, 0.00
High resting spores	25 Larvae/m2	1.95	-9.90	-20.6, -1.43
	50 Larvae/m2	2.66	-5.36	-13.6, -0.54
	100 Larvae/m2	4.48	-1.72	-5.71, -0.03
	250 Larvae/m2	7.56	-0.18	-0.73, 0.02
Low resting spores	25 Larvae/m2	1.76	-34.9	-60.8, -8.52
	50 Larvae/m2	1.26	-24.5	-49.5, -5.83
	100 Larvae/m2	3.14	-9.40	-26.7, -0.25
	250 Larvae/m2	5.41	-1.12	-4.92, 0.00
Weather-Only Model				
N.A.	N.A.	5.13	-9.75	-19.1, 0.15

Table 2.3: Summary of Alternative Scenarios II: RCP 4.5

Scenario	Host density	Pct. sites > 0	Mean	5th, 95th Percentiles
Eco-Climate Model: Resting Spore Variation				
Intermediate resting spores as in Figure 2.3 but for RCP 4.5 scenario	25 Larvae/m2	0.95	-15.3	-25.8, -4.49
	50 Larvae/m2	0.65	-14.1	-23.7, -5.33
	100 Larvae/m2	0.12	-10.5	-19.2, -2.87
	250 Larvae/m2	0.37	-5.24	-10.8, -0.13
High resting spores	25 Larvae/m2	0.02	-8.75	-14.8, -3.63
	50 Larvae/m2	0.08	-7.81	-14.1, -2.84
	100 Larvae/m2	0.28	-5.86	-11.7, -1.01
	250 Larvae/m2	0.71	-3.25	-9.26, -0.05
Low resting spores	25 Larvae/m2	6.06	-24.2	-51.5, 1.21
	50 Larvae/m2	4.32	-24.5	-47.3, -1.22
	100 Larvae/m2	1.74	-20.5	-35.8, -5.92
	250 Larvae/m2	0.28	-11.2	-22.1, -1.53
Relative-Humidity-Only Model: Resting Spore Variation				
Intermediate resting spores	25 Larvae/m2	15.6	-11.1	-29.4, 7.14
	50 Larvae/m2	2.33	-11.3	-26.3, -1.70
	100 Larvae/m2	1.46	-7.83	-16.9, -0.97
	250 Larvae/m2	2.63	-3.71	-8.60, -0.02
High resting spores	25 Larvae/m2	11.9	-6.62	-17.1, 2.30
	50 Larvae/m2	2.37	-6.50	-14.7, -1.15
	100 Larvae/m2	1.93	-4.65	-9.50, -0.42
	250 Larvae/m2	3.02	-2.18	-5.90, -0.01
Low resting spores	25 Larvae/m2	23.3	-12.9	-42.1, 22.4
	50 Larvae/m2	6.63	-16.3	-38.2, 1.84
	100 Larvae/m2	1.42	-12.3	-29.2, -2.75
	250 Larvae/m2	0.95	-6.21	-11.6, -0.11
Weather-Only Model				
N.A.	N.A.	0.59	-11.2	-19.2, -4.17

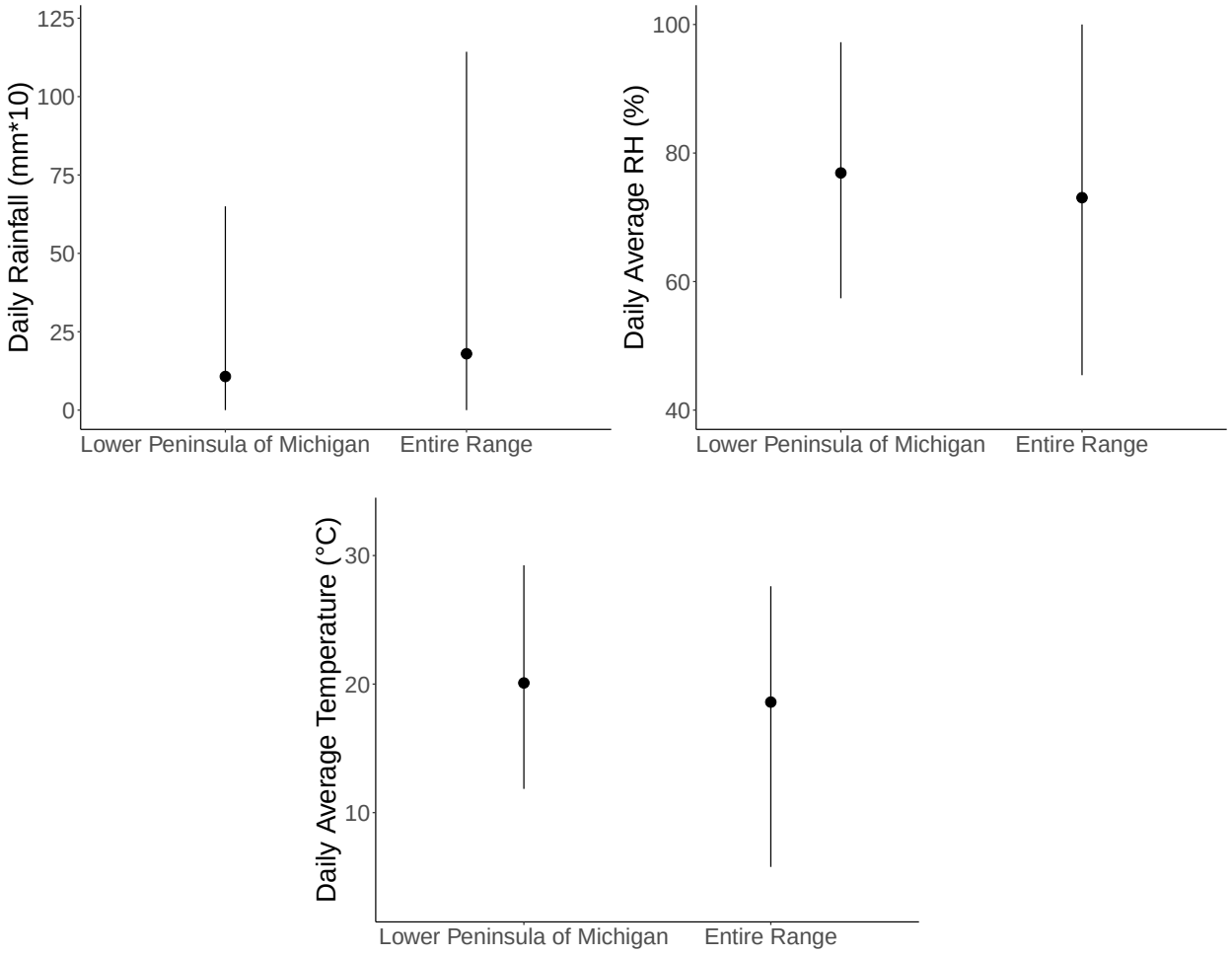

Figure 2.1: Comparison of weather data from our study plots to weather data from the National Center for Environmental Information (National Centers for Environmental Information and National Oceanic and Atmospheric Administration, 2022) for the range of *L. dispar*. Points indicate means and bars indicate upper 95th and lower 5th percentiles of the distribution of each variable.

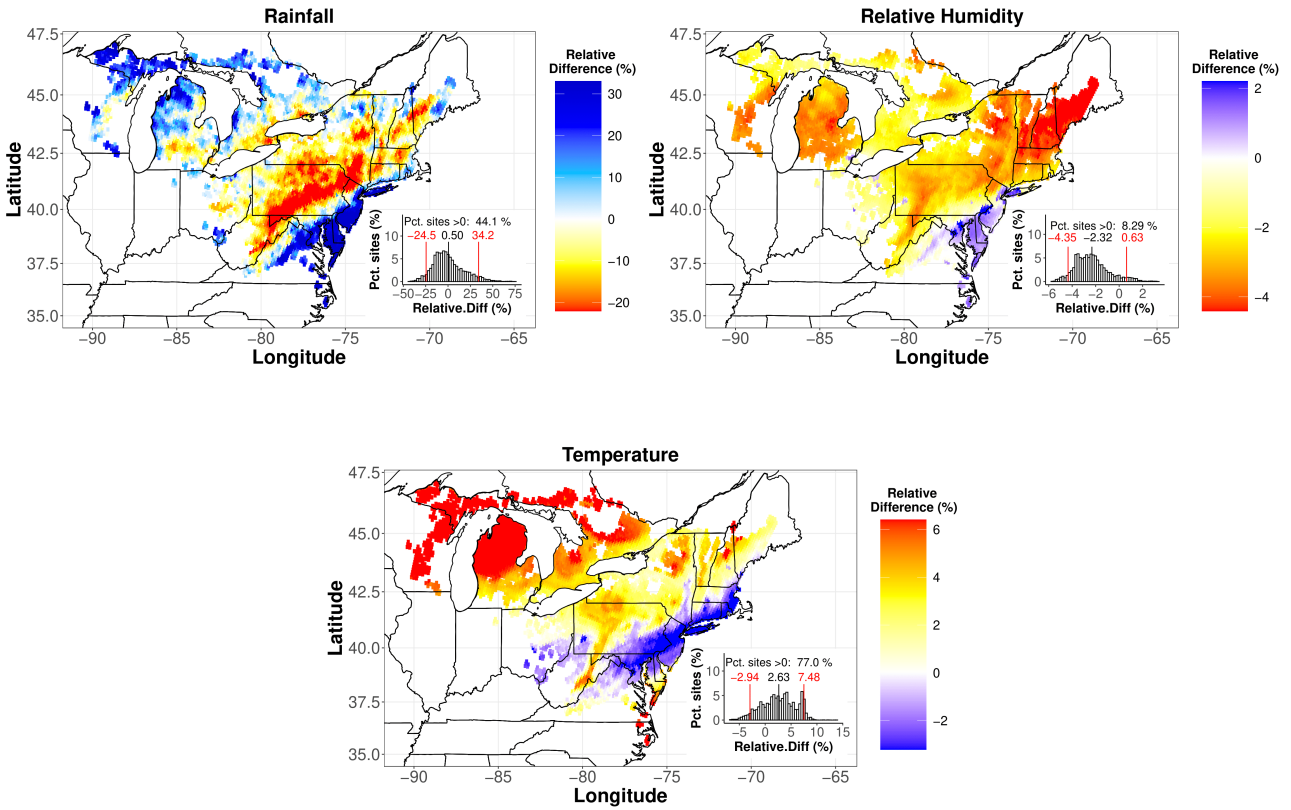

Figure 2.2: Projected relative percent changes (Section 2.3.5) due to climate change in rainfall, relative humidity, and average temperature during the *L. dispar* larval period across areas previously defoliated by *L. dispar* in the USA and Ontario, Canada. Projections were made on a grid with a spacing of 12 km between grid points. Here the past represents the period 1995-2004, while the future represents the period 2085-2094, under the Relative Concentration Pathway or "RCP" 8.5 scenario. Inset histograms show distributions across sites, with black vertical lines indicating means, and with red vertical lines indicating the 5th and 95th percentiles. For context, we note that mean values of the absolute changes in rainfall, relative humidity and temperature are respectively -2.37 mm/day, -2.31%, and +0.46 $^{\circ}C$.

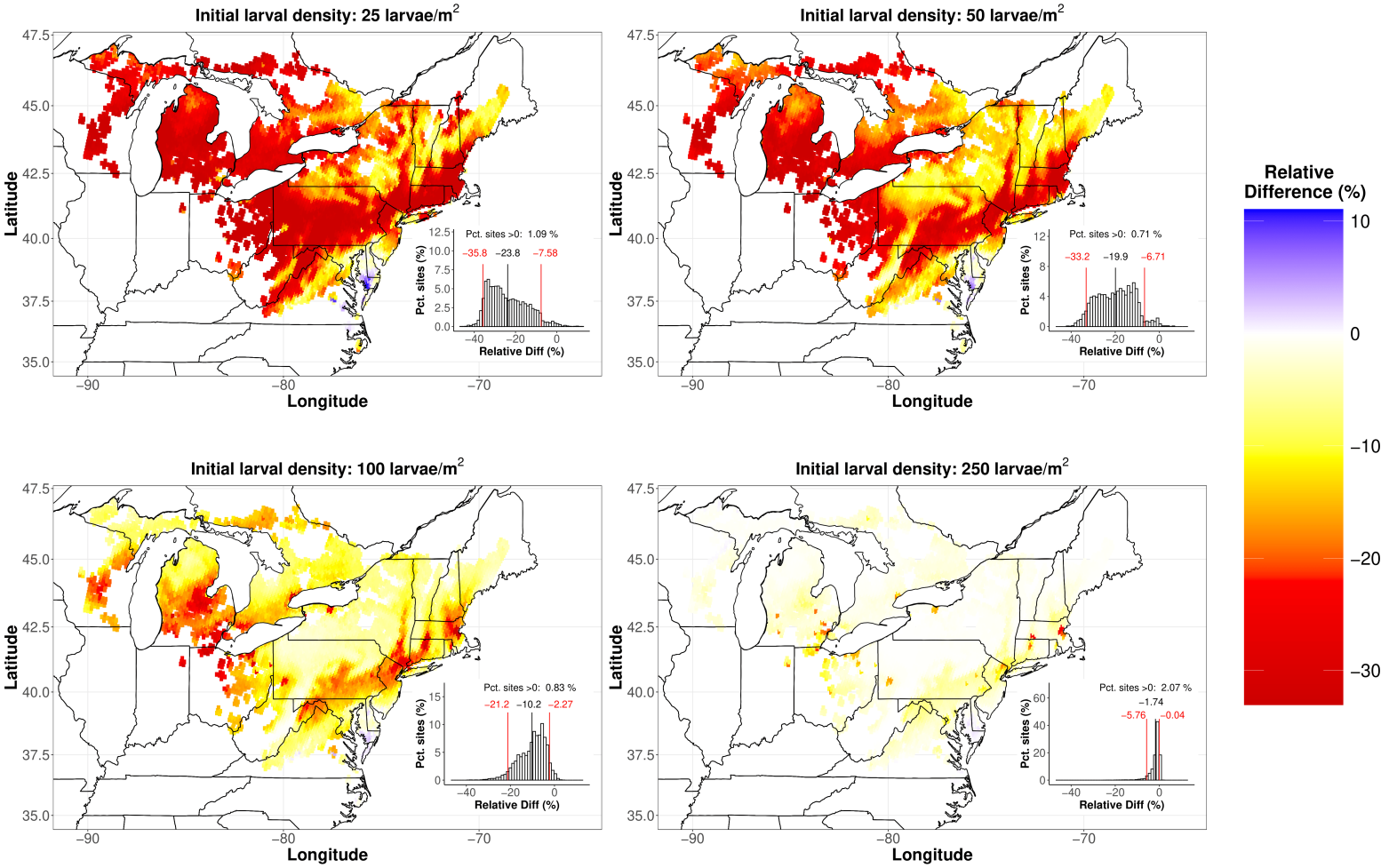

Figure 2.3: Eco-climate model projections of the effects of climate on the *E. maimaiga* infection rate for four different initial *L. dispar* densities. Here we show relative percent changes in the fraction infected, using the weather projections from Figure 2.2, and again using summary histograms.

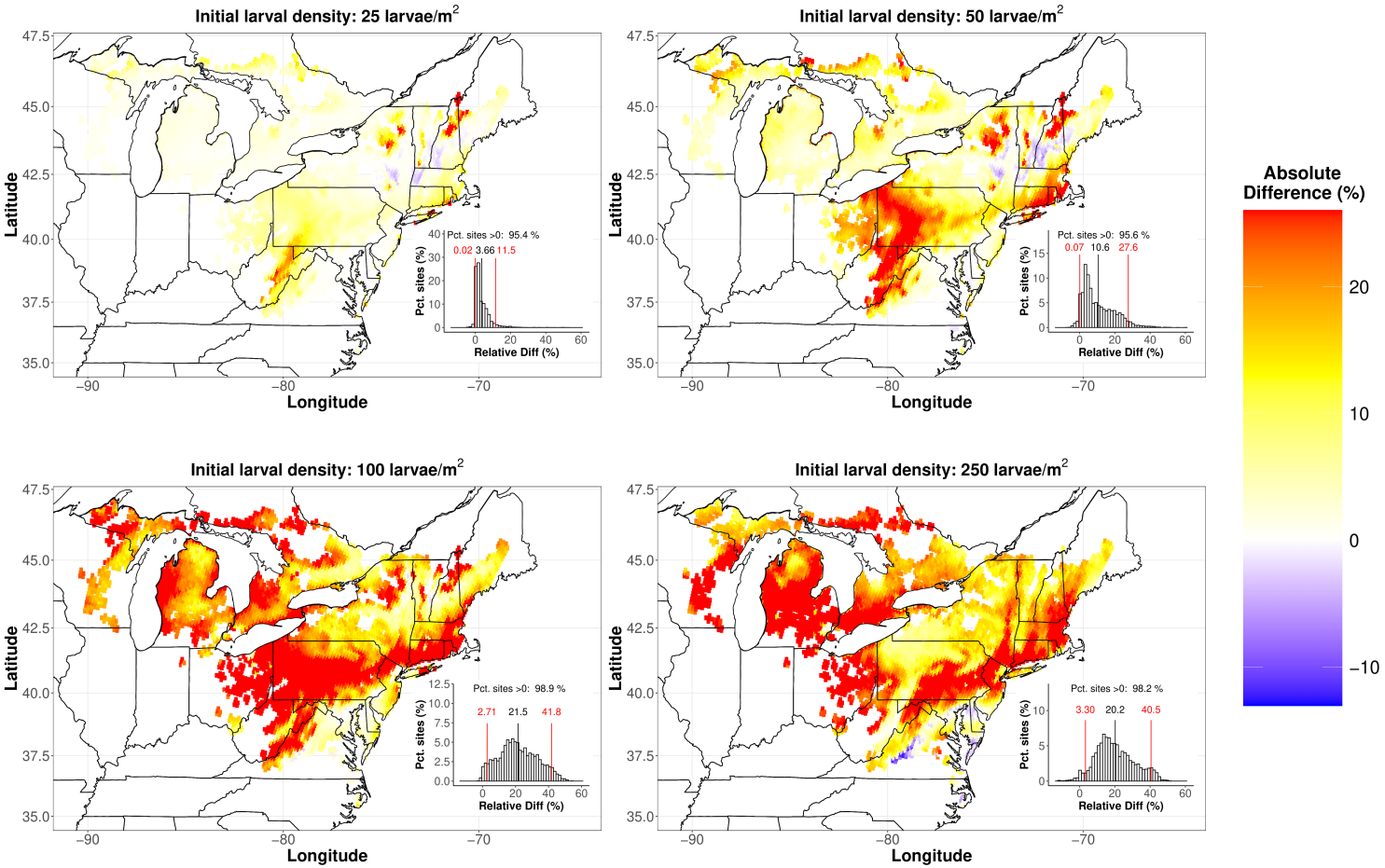

Figure 2.4: Projected changes in *L. dispar* defoliation levels due to climate change, calculated using a regression that converts *L. dispar* densities to percent defoliation (Liebhold et al., 1993). Because at high density the model (accurately) projects very high *E. maimaiga* mortality rates pre-climate change, projected pre-climate change defoliation rates are generally very low. To avoid inflating changes in defoliation we therefore show only absolute changes.

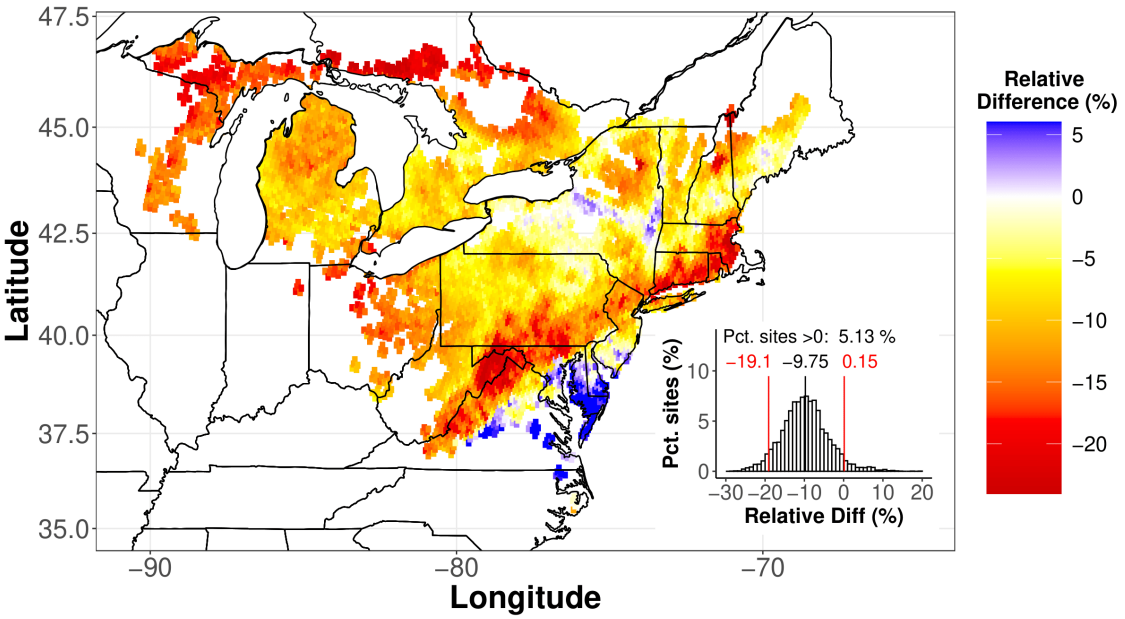

Figure 2.5: Projections of the effects of climate change on *E. maimaiga* infection rates for the weather-only model, as in Figure 2.3. Because the *E. maimaiga*-*L. dispar* interaction is not included in this model, host density has no effect on the model projections, and so we show only a single set of projections.

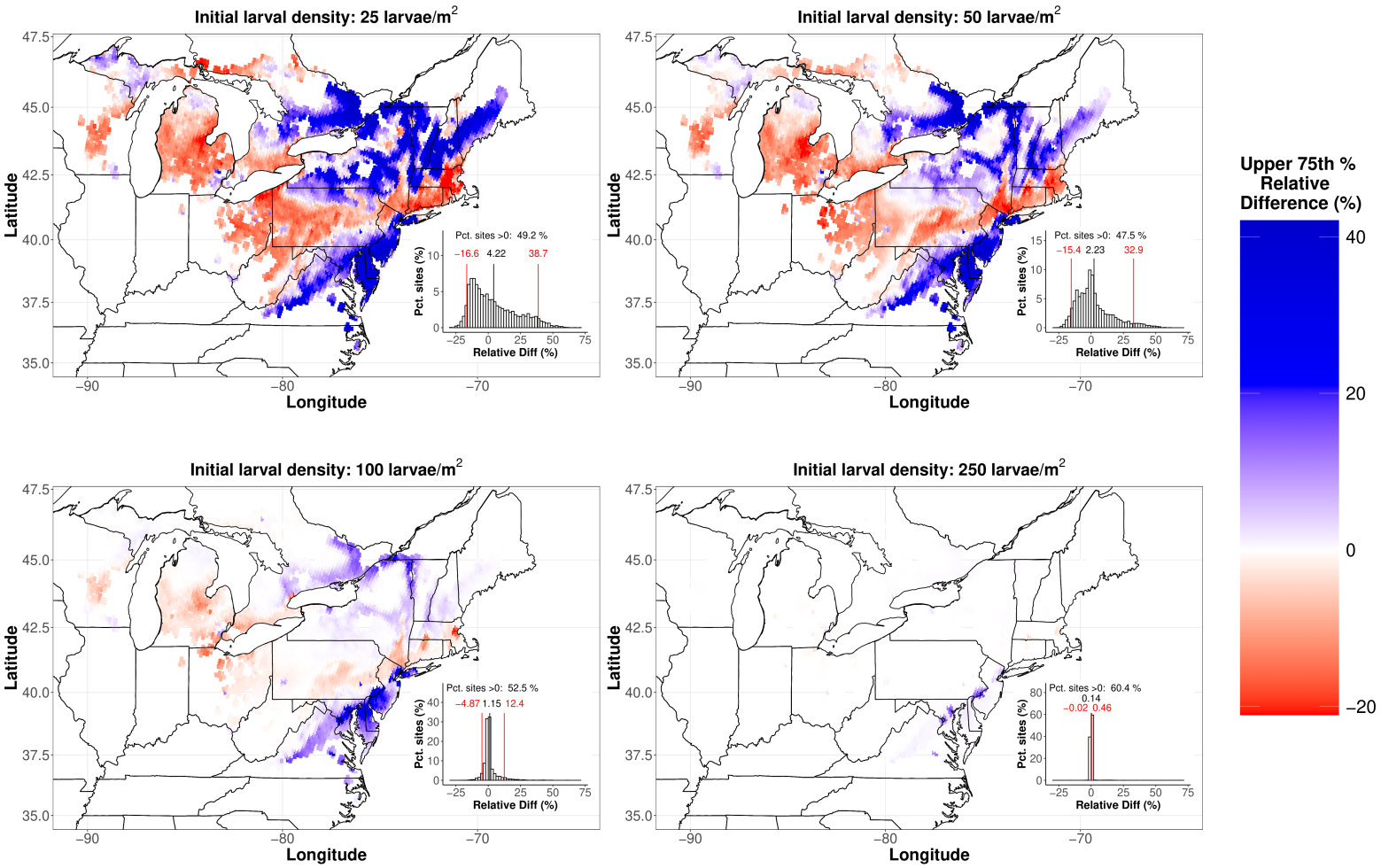

Figure 2.6: Upper 75th percentiles of the projections of the full eco-climate model, corresponding to Figure 2.3.

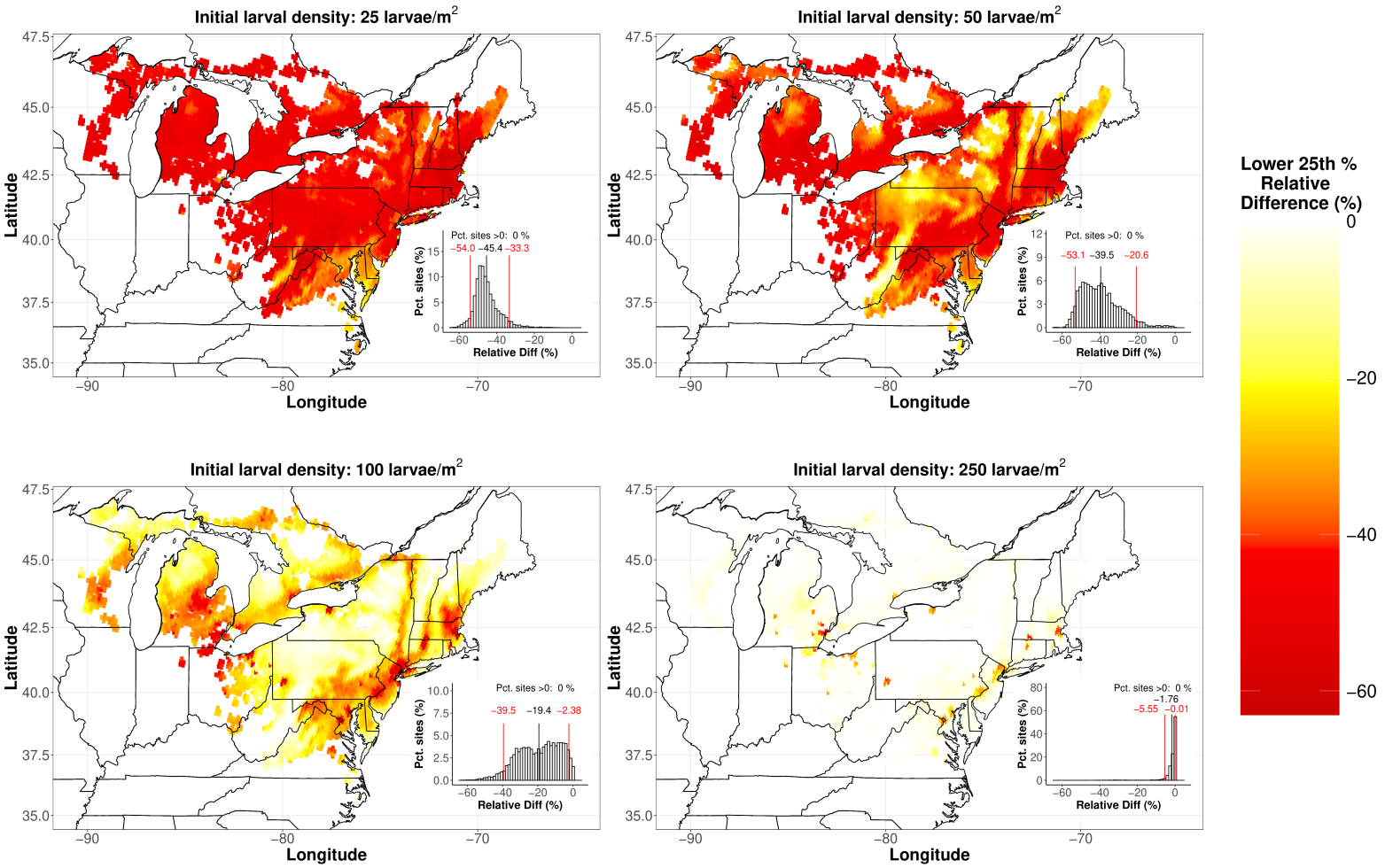

Figure 2.7: Lower 25th percentiles of the projections of the full eco-climate model, corresponding to Figure 2.3.

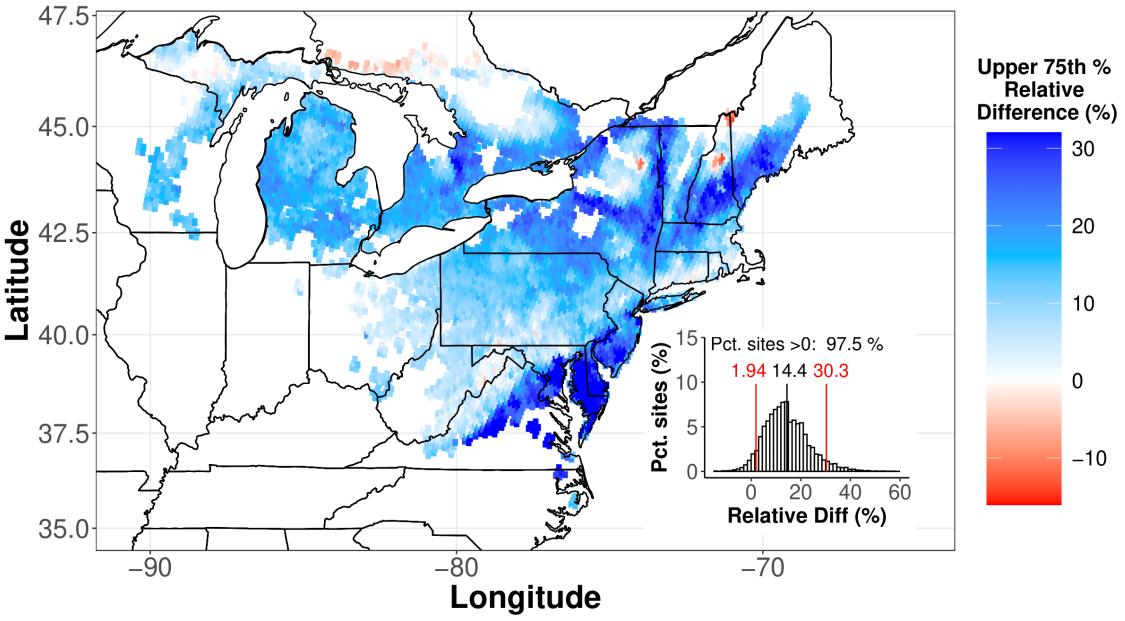

Figure 2.8: Upper 75th percentiles of the projections of the weather-only model, corresponding to Figure 2.5.

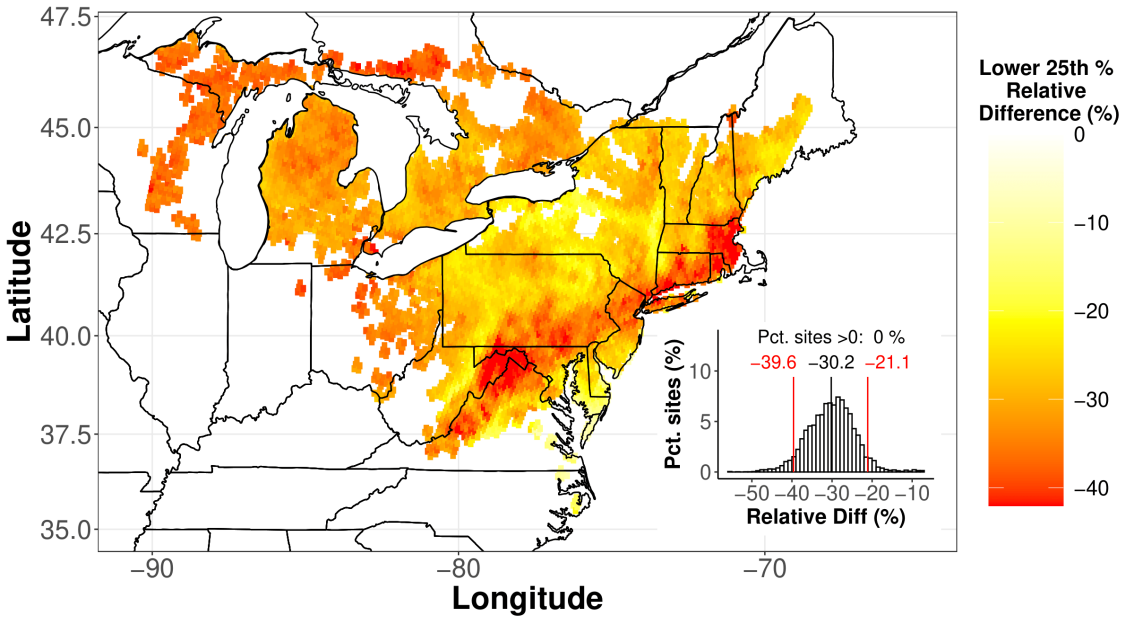

Figure 2.9: Lower 25th percentiles of the projections of weather-only model, corresponding to Figure 2.5.

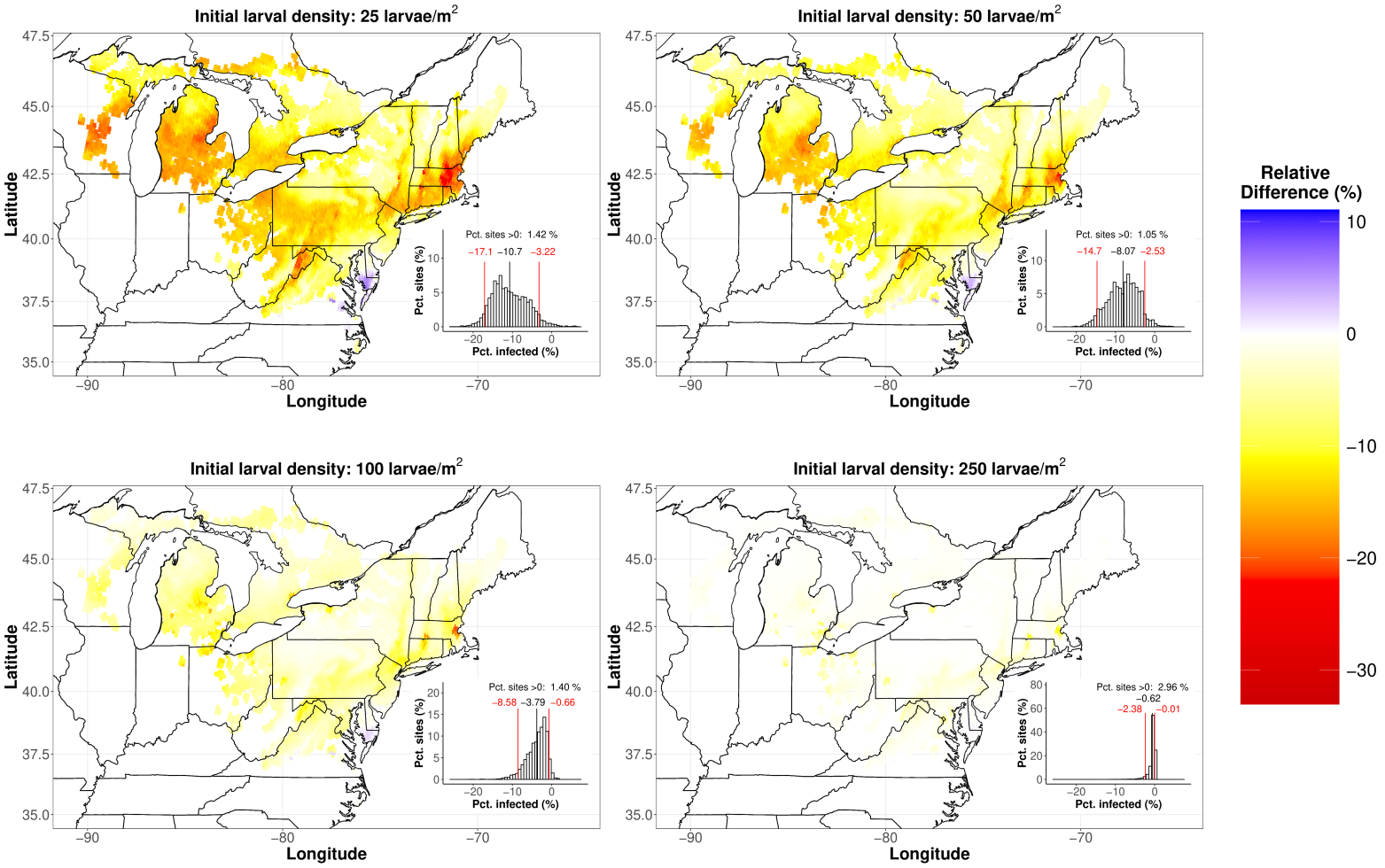

Figure 2.10: Projections of the full eco-climate model as in Figure 2.3, except that here we increase the resting spore density to 1.83×10^{-2} m^{-2} as opposed to the value of 5.71×10^{-3} m^{-2} that we used in the Figure 2.3.

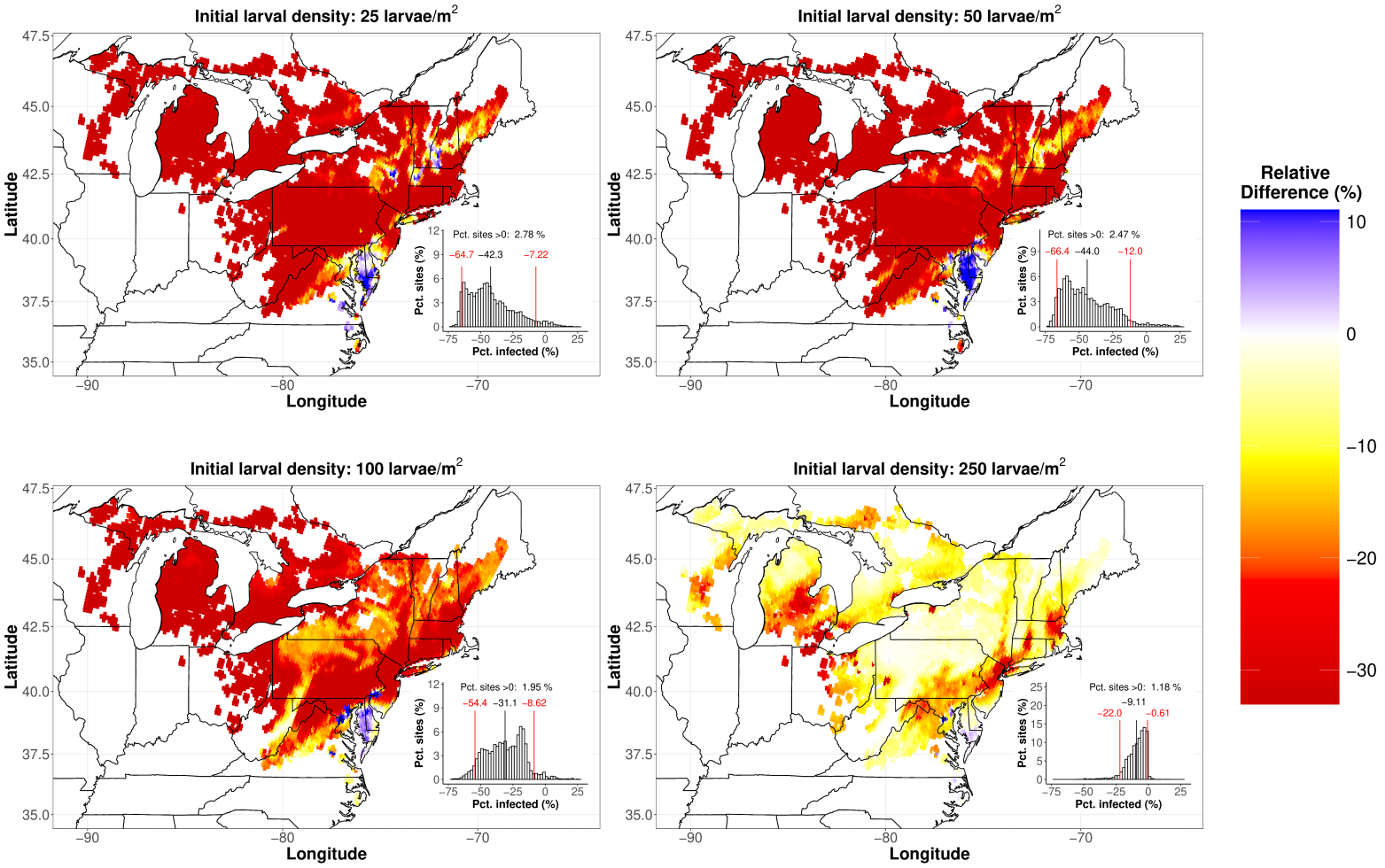

Figure 2.11: Projections of the full eco-climate model as in Figure 2.3, except that here we reduce the resting spore density to 6.91×10^{-4} m^{-2}, as opposed to the density of 5.71×10^{-3} m^{-2} that we used in the Figure 2.3.

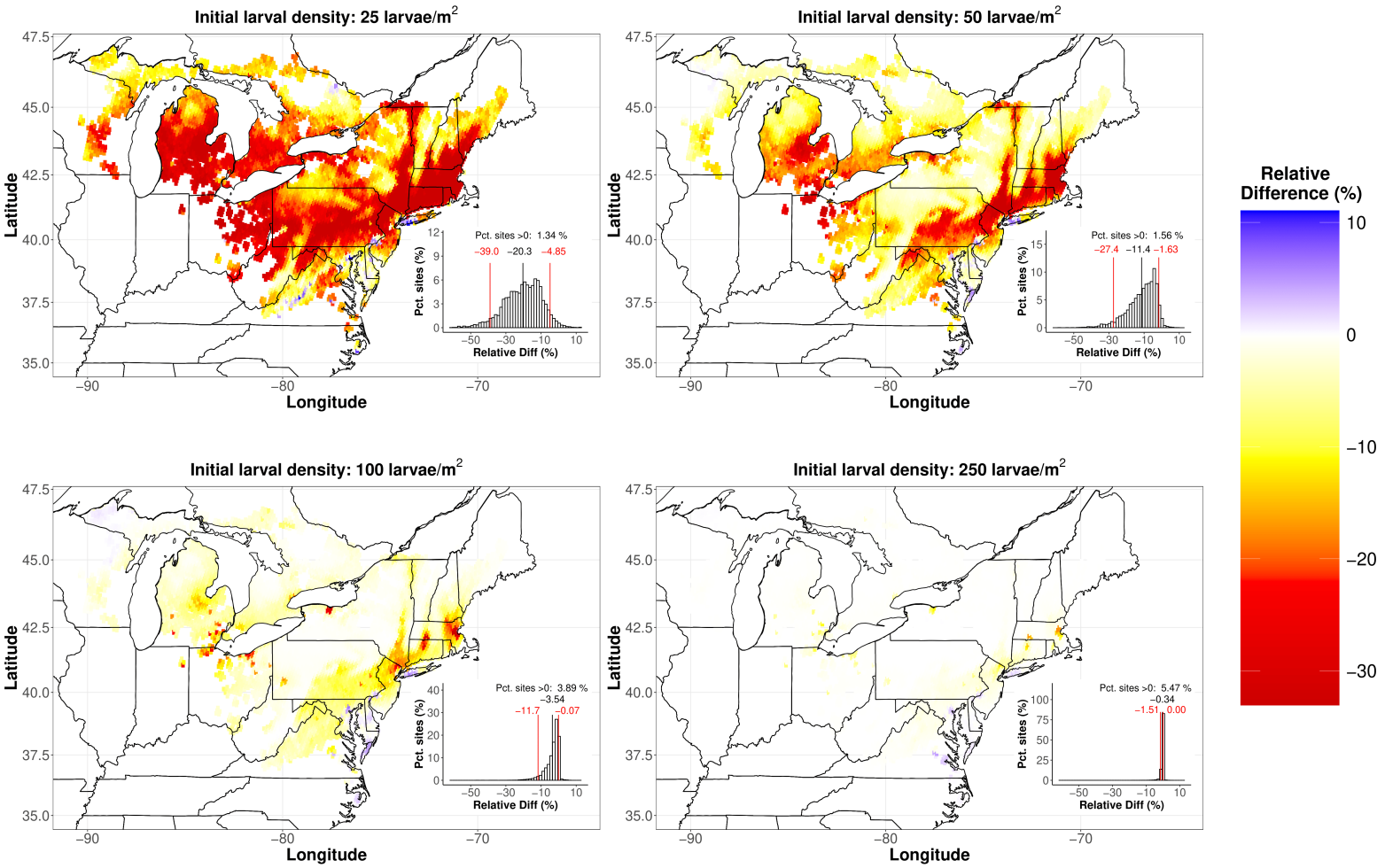

Figure 2.12: Projections of the relative-humidity-only model for an intermediate resting spore density of 0.227 m^{-2}.

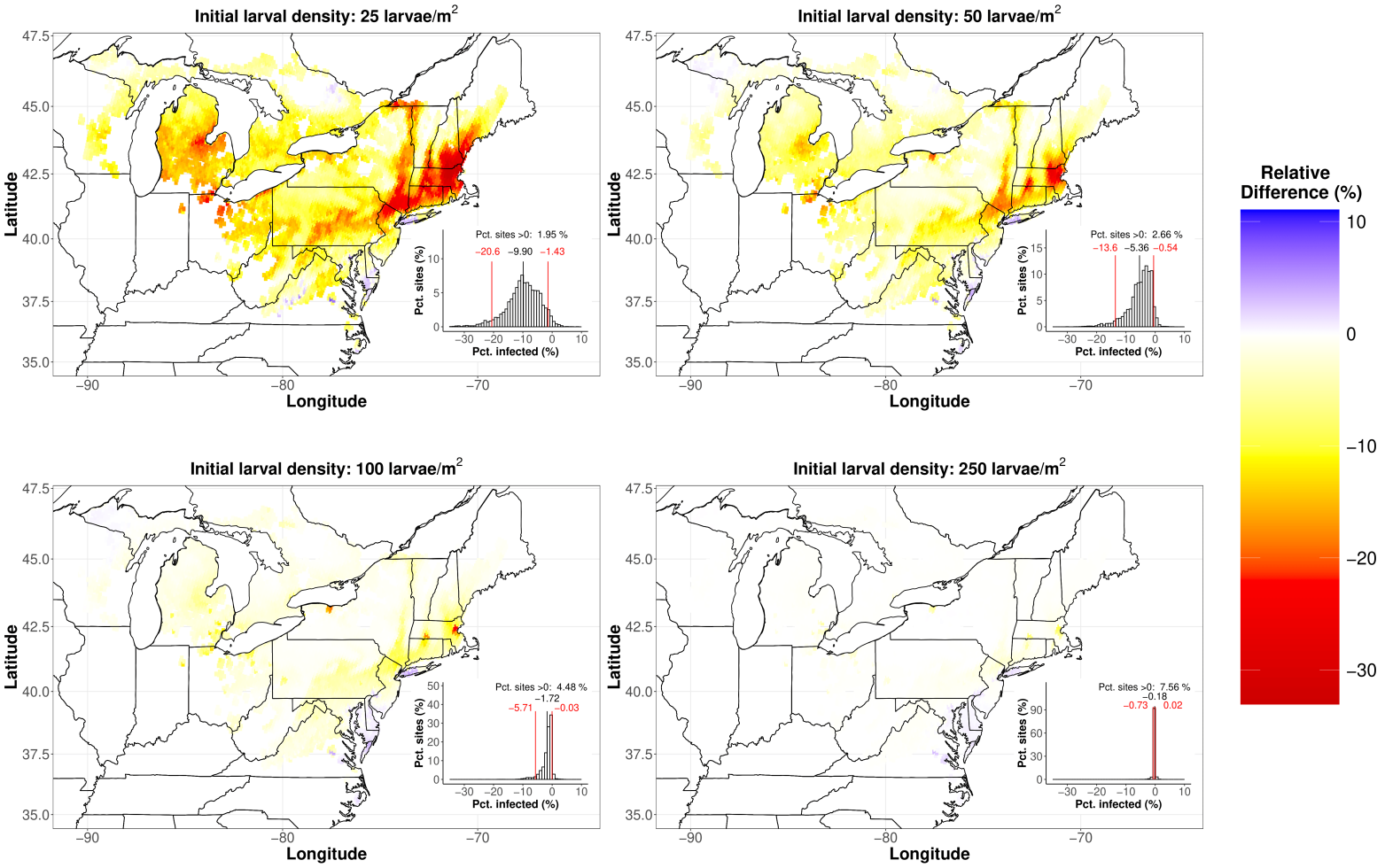

Figure 2.13: Projections of the relative-humidity-only model for a high resting spore density of 0.850 m^{-2}, as opposed to the density of 0.227 m^{-2} that we used in Figure 2.12.

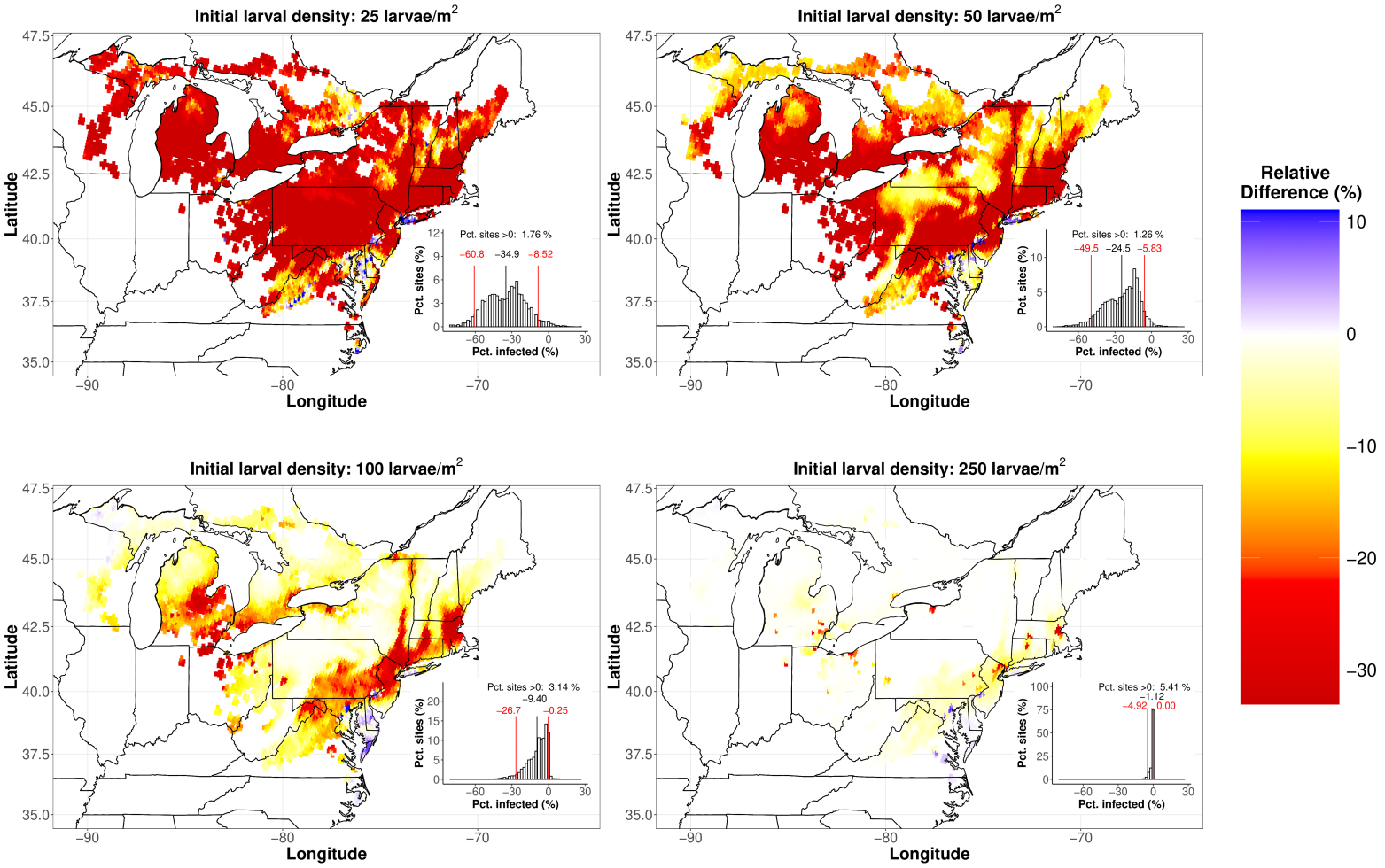

Figure 2.14: Projections of the relative-humidity-only model for a low resting spore density of 0.0371 m^{-2}, as opposed to the value of 0.227 m^{-2} that we used in Figure 2.12.

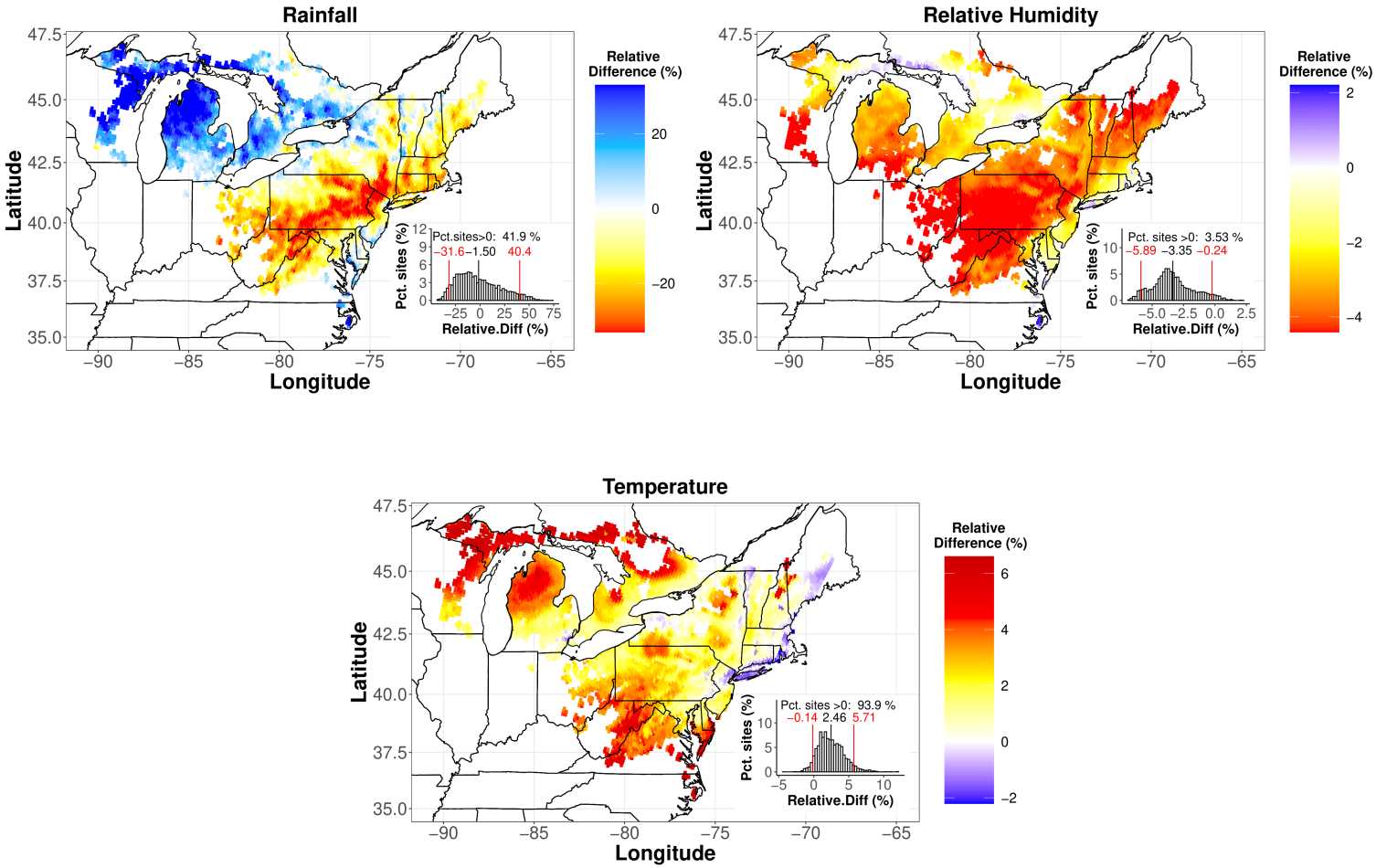

Figure 2.15: Projections of relative changes in rainfall, relative humidity, and temperature for the dynamically down-scaled climate-change model under the RCP 4.5 scenario, as opposed to the RCP 8.5 scenario that we used in Figure 2.2.

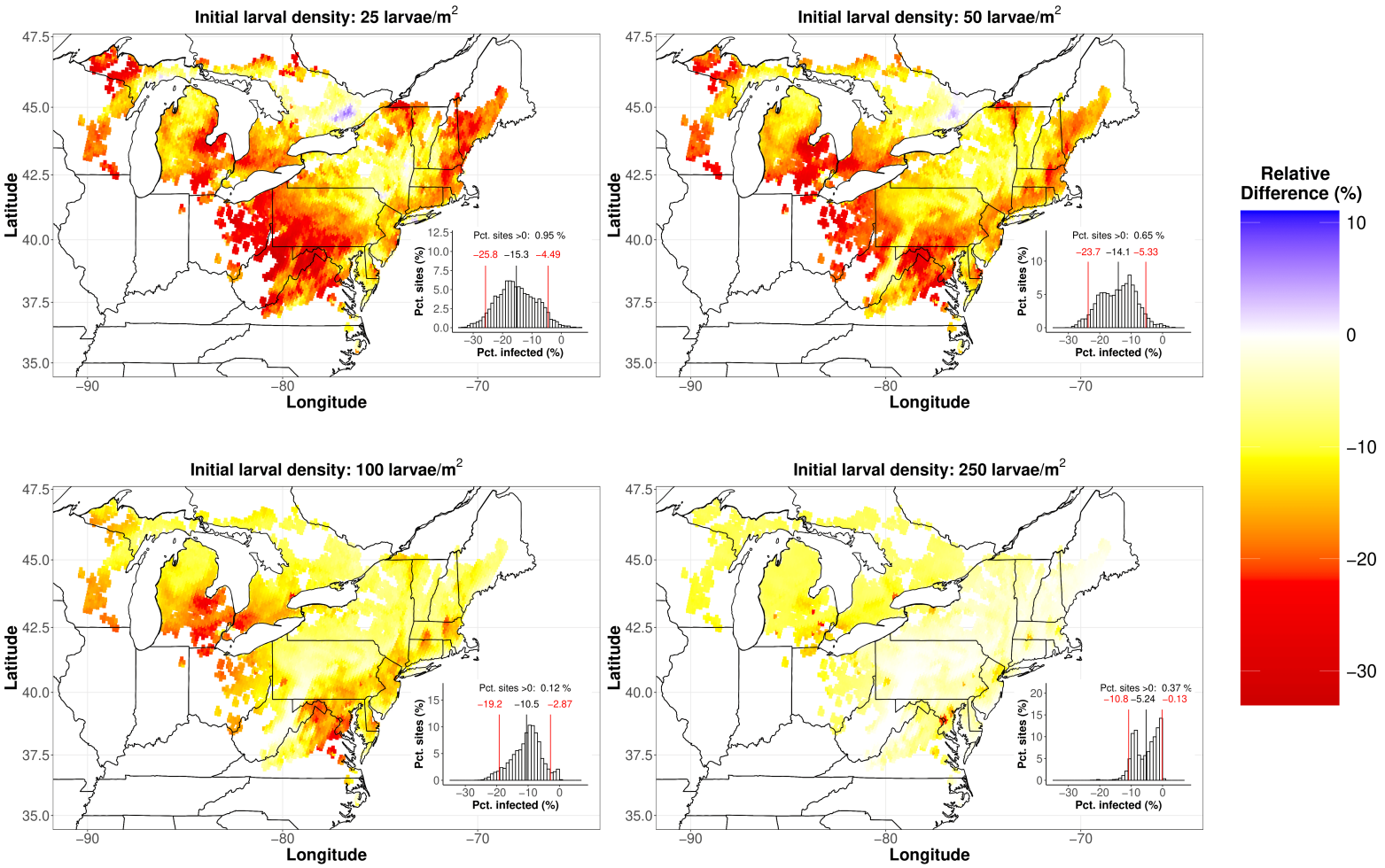

Figure 2.16: Projections of the full eco-climate model as in Figure 2.3, except that here we use the RCP 4.5 scenario.

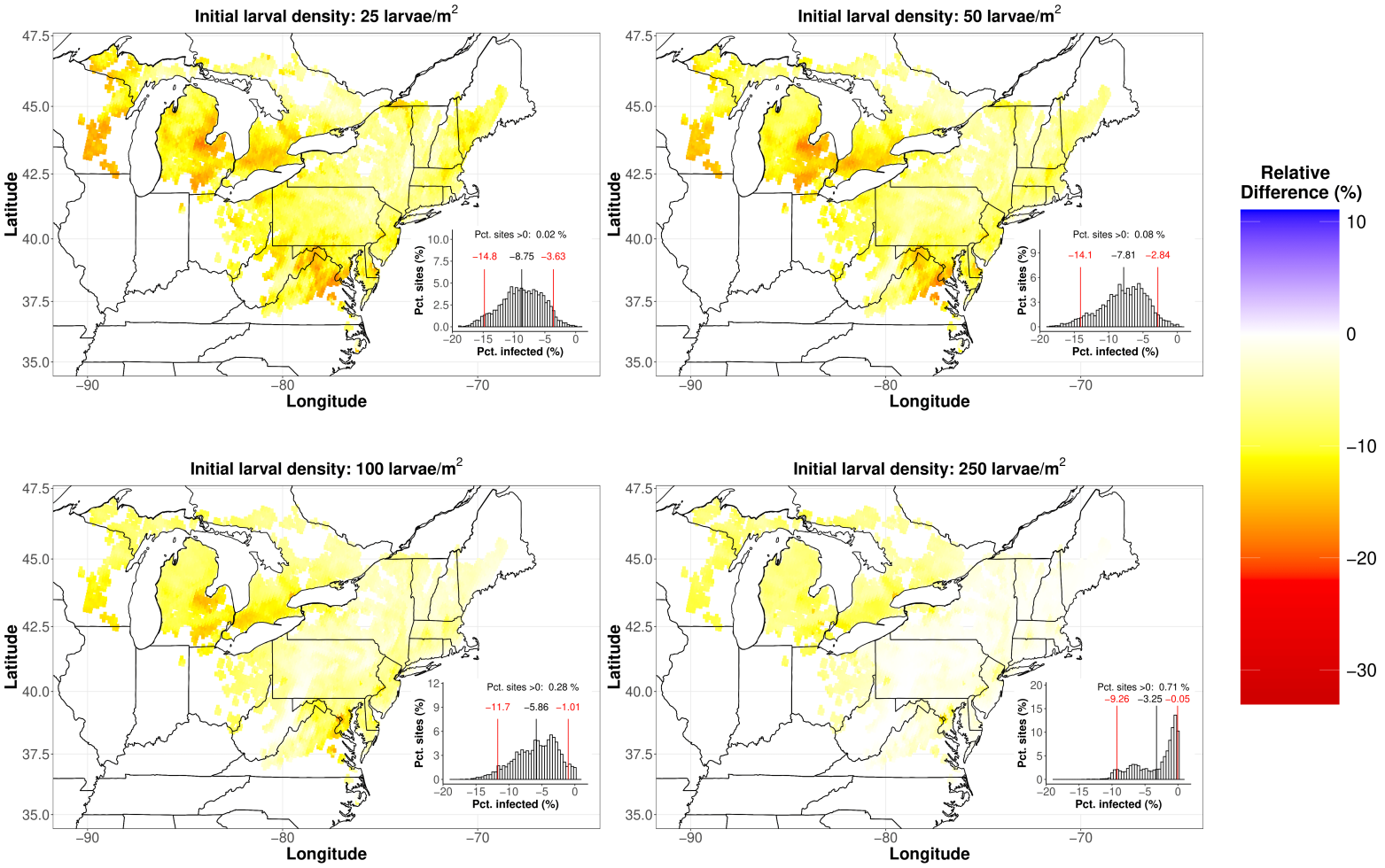

Figure 2.17: Projections of the full eco-climate model as in Figure 2.3, except that here we use the RCP 4.5 scenario, and we use a higher resting spore density of 1.83×10^{-2} m^{-2}.

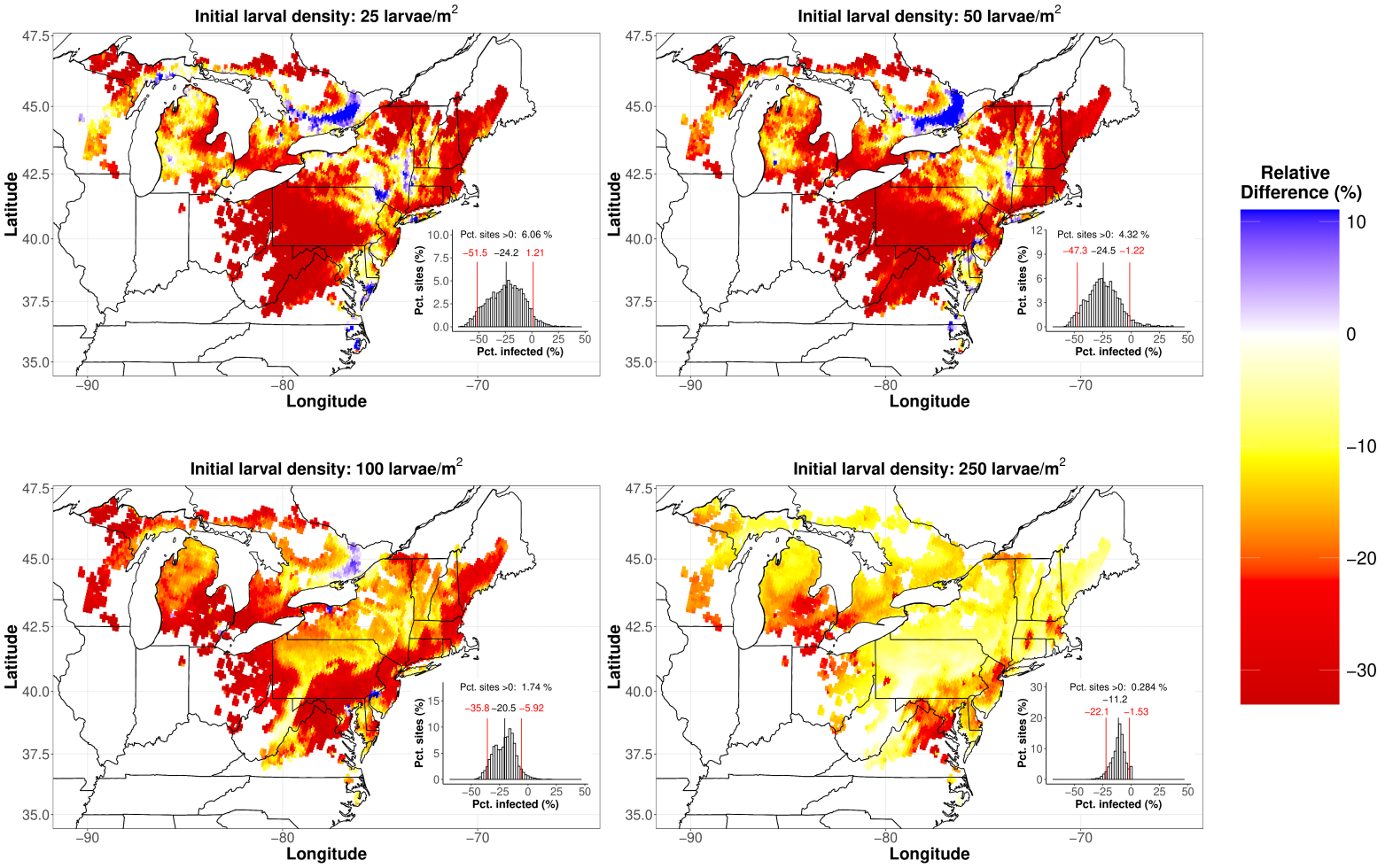

Figure 2.18: Projections of the full eco-climate model as in Figure 2.3, except that here we use the RCP 4.5 scenario, and we use a lower resting spore density of 6.91×10^{-4} m^{-2}.

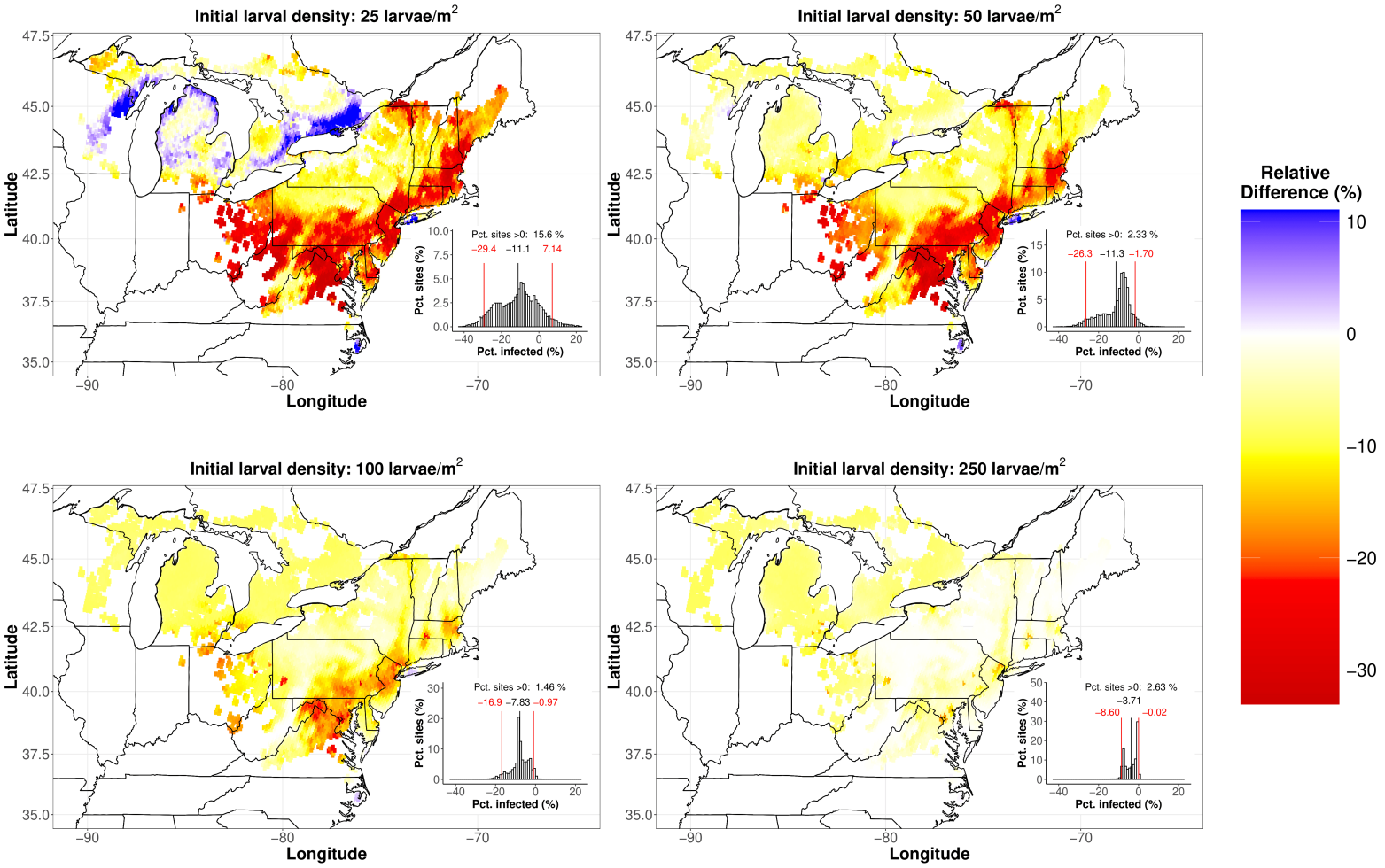

Figure 2.19: Projections of the relative-humidity-only model as in Figure 2.12, but for the RCP 4.5 scenario. Here the resting spore density is 0.227 m^{-2}.

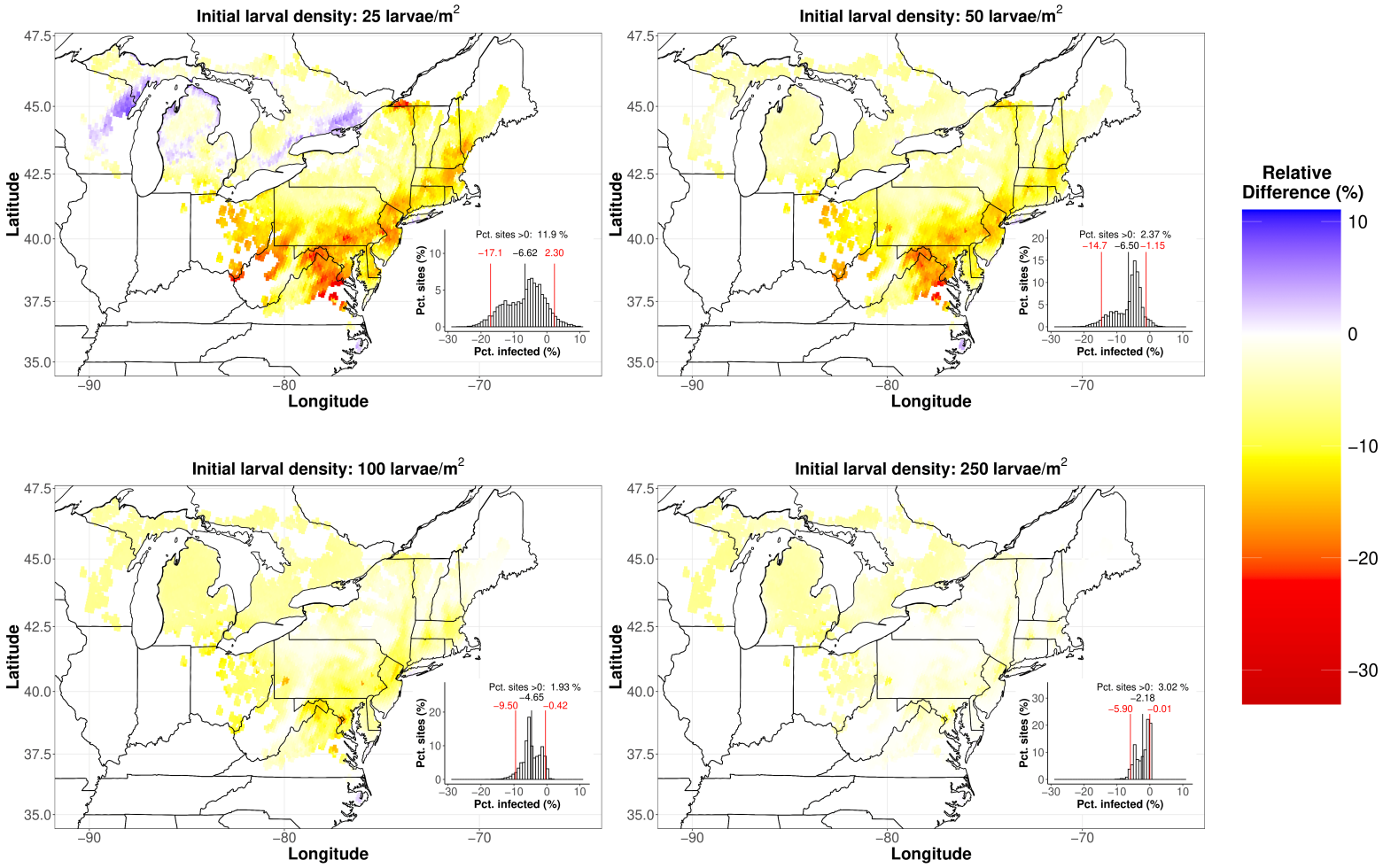

Figure 2.20: Projections for the relative-humidity-only model under the RCP 4.5 scenario as in Figure 2.19, but for a higher resting spore density of 0.850 m^{-2} as opposed to the value of 0.227 that we used in Figure 2.19.

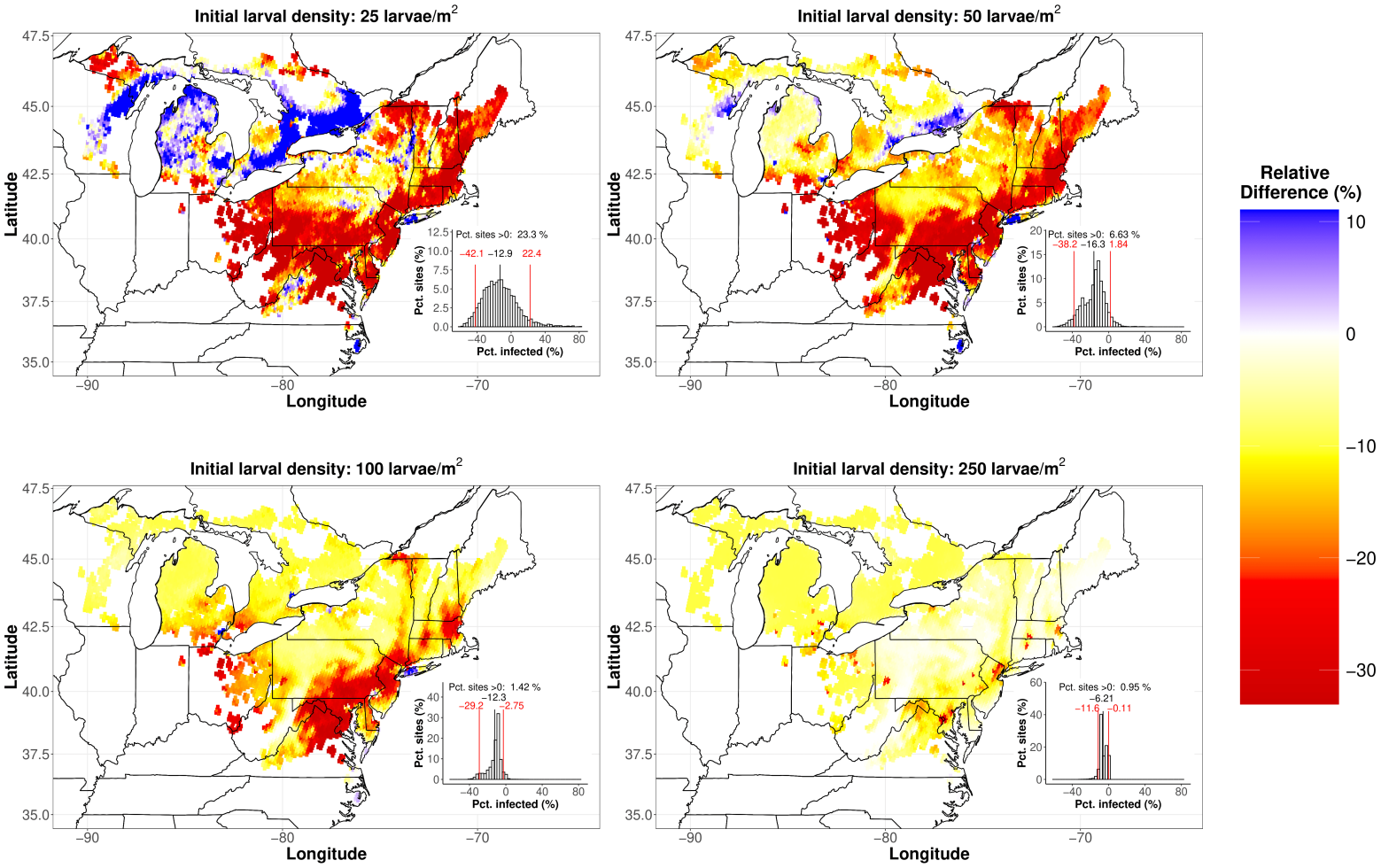

Figure 2.21: Projections for the relative-humidity-only model under the RCP 4.5 scenario as in Figure 2.19, but for a resting spore density of 0.0371 m^{-2} as opposed to the value of 0.227 that we used in Figure 2.19.

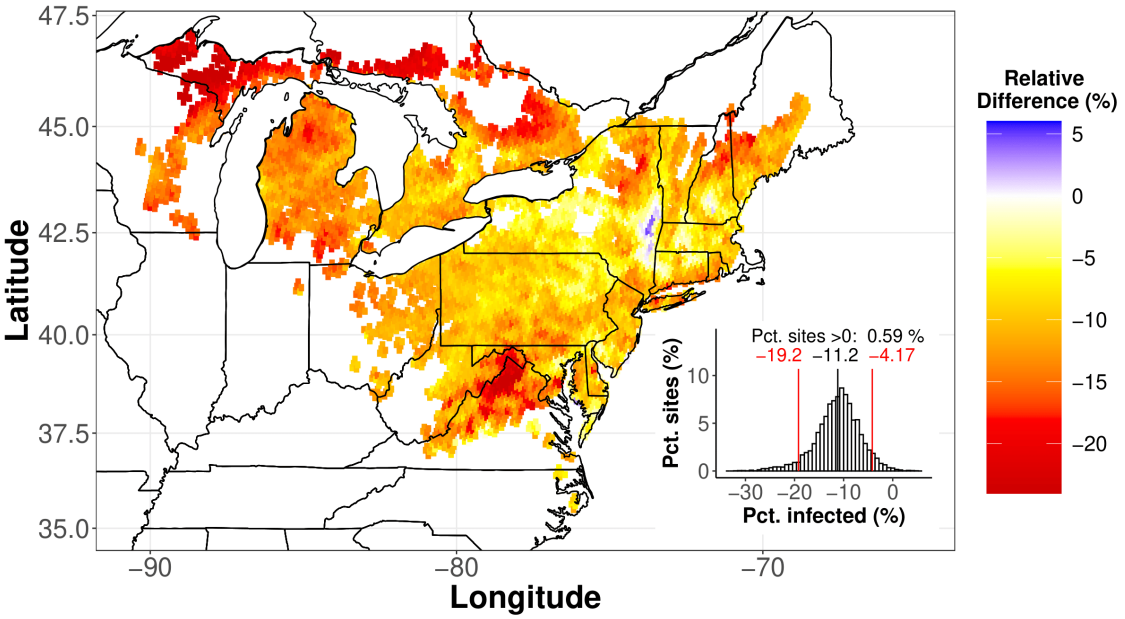

Figure 2.22: Projections of the weather-only model as in Figure 2.5, but for the RCP 4.5 scenario.

CHAPTER 3

PROJECTING THE EFFECTS OF CLIMATE CHANGE ON MULTI-SPECIES INTERACTIONS: THE SPONGY MOTH AND ITS NATURAL ENEMIES

3.1 Abstract

To study how climate change influences multi-species interactions over the long-term, here we extend the single-epizootic model from Chapter 2 to allow for multiple host generations, and we include the spongy moth baculovirus and the spongy moth's generalist predators. The resulting extended model projects an increased chance of spongy moth outbreaks in the future, when the weather conditions are typically hotter and/or drier. Models that realistically allow for both pathogens and the generalist predators project that climate change will cause outbreak amplitudes to strongly increase, whereas models that include the two pathogens but not the generalist predators project only very small increases in outbreak amplitudes. Our results thus show that a realistic accounting of species interactions can drastically alter our projections of the effects of climate change. Our work provides a clear example of how species interactions can seriously complicate efforts to understand the ecological consequences of climate change.

3.2 Introduction

Studies of the ecological consequences of climate change generally focus on individual species, and often rely on statistical correlations between species and climate, while neglecting underlying biological mechanisms. Indeed, even in well-studied animal species like fence lizards (*Sceloporus undulatus*), sockeye salmon (*Oncorhynchus nerka*) and speckled wood butterflies (*Pararge aegeria*), information on species interactions is either absent or missing

critical components (Urban et al., 2016). A basic principle in ecology nevertheless states that every species interacts with multiple other species (Lawton, 1999), while often an ultimate goal is to achieve a mechanistic understanding of the impact of climate change and species interactions, which cannot easily be achieved using correlations alone. Meanwhile, the few existing efforts to develop a mechanistic understanding of how climate change affects species interactions have relied on data collected in the laboratory (Mordecai et al., 2019; Rasher et al., 2020), but extrapolating from data collected in the laboratory to ecological phenomena in the field is notoriously difficult (Carpenter, 1996). An important area of ecological research is thus to use field data to understand the mechanistic consequences of climate change for species interactions.

Understanding the effects of climate change on species interactions is especially important in the case of outbreaking forest-defoliating insects, which often severely defoliate forests (Kamata and Liebhold, 2000). Many forest insects have long-period, large-amplitude outbreak cycles that are driven by interactions with parasitoids and pathogens (Anderson and May, 1980; Varley et al., 1974); moreover, climate change has strongly affected population cycles in several forest insects, leading to both higher and lower outbreak probabilities following years with high temperatures, depending on the insect (Haynes et al., 2014; Pureswaran et al., 2018). The mechanistic links between climate change and natural enemies of defoliator insects, however, are often poorly understood. Part of the problem is that although climate change is believed to have effects on parasitoid physiology, how these effects are translated into population change in host insects is unknown (Tougeron et al., 2020). For example, climate change is believed to have eliminated parasitoid-driven cycles in the larch budmoth (Iyengar et al., 2016), but empirical evidence for a connection between climate change and budmoth-specific parasitoids is almost completely unknown. There is also very limited information on how climate change can affect the pathogens of outbreaking insects, thus altering the insect population cycles.

To better understand how climate change affects outbreaks of forest insects, here we project the effects of climate change on the forest pest spongy moth, *Lymantria dispar*, while considering the interactions between this insect host and two species of lethal pathogens, as well as generalist predators. Spongy moth was introduced into Massachusetts, USA from Europe in 1868 or 1869 (Elkinton and Liebhold, 1990), and has since colonized most hardwood forests in the northeastern and midwestern United States and southeastern Canada, causing high levels of defoliation that often led to reduced tree growth and increased tree mortality (Dwyer et al., 2000; Woods and Elkinton, 1987). Although outbreaks were reliably terminated by the baculovirus, baculovirus epizootics (epizootics are epidemics in animals) typically only occurred when spongy moth densities were so high that defoliation was still often severe (Liebhold et al., 2022; U.S. Forest Service, 2022). The insect thus appeared to be in a host-pathogen population cycle driven by the baculovirus, with the complication that the time interval between outbreaks was extremely variable because of generalist predators such as the white-footed mouse *Peromyscus leucopus* that caused high mortality in low density spongy moth populations (Dwyer et al., 2004; Elkinton et al., 1996).

In 1989, however, the introduction of another fatal specialist pathogen, the fungal pathogen *Entomophaga maimaiga* (Andreadis and Weseloh, 1990), strongly altered these dynamics. Because *E. maimaiga* transmission and survival are enhanced by cool and moist weather, *E. maimaiga* epizootics can sometimes occur in populations that are at lower densities than the lowest densities at which baculovirus epizootics can occur. The introduction of *E. maimaiga* has therefore greatly reduced the frequency of large-scale spongy moth outbreaks (Tobin et al., 2012), reducing overall defoliation levels (Allstadt et al., 2013; Liebhold et al., 2022; U.S. Forest Service, 2022).

Our recent work with colleagues, however, has suggested that climate change may have severe effects on *E. maimaiga*, with dire effects for North American hardwood forests. Fungal transmission and survival are favored by high rainfall, high relative humidity, and cool

temperatures (Hajek, 1999; Weseloh and Andreadis, 1992); meanwhile, in the range of the spongy moth in North America, climate change is projected to lead to a little higher rainfall, increasing fungal transmission, but higher temperatures and lower relative humidity, reducing fungal transmission and survival (Wang and Kotamarthi, 2015). To project the effects of climate change on *E. maimaiga* in North America, we therefore began with a model produced by Kyle et al. (2020) that synthesized these different effects of weather conditions on *E. maimaiga* into overall projections of fungal infections rates; by combining the projections of this model with the projections of down-scaled climate models (Wang and Kotamarthi, 2014, 2015), as described in Chapter 2, we showed that in most locations within the range of the spongy moth in North America, fungal infection rates will be severely reduced, leading to higher defoliation levels and thus reduced tree survival and growth.

Our initial model, however, considered the effects of climate change only on single pathogen epizootics; because the pathogen only infects larvae (Hajek, 1999), the model thus tracks pathogen dynamics during only a single host generation. A key unanswered question is therefore, how will climate change affect the interaction between the fungal pathogen and the spongy moth over the long term? Because the spongy moth is an invasive pest (Liebhold et al., 1992), answering this question is of great importance for protecting hardwood forests in North America.

By quantifying the effects of climate change on spongy moth outbreaks, we are also able to ask broader questions about the effects of climate change on species interactions. This is partly because our initial model focused only on the fungal pathogen of the spongy moth, whereas the spongy moth is also infected by a fatal, species specific baculovirus (Woods and Elkinton, 1987). Indeed, before the introduction of the fungal pathogen, the baculovirus was the main source of mortality in spongy moth outbreaks, often leading to mortality rates of higher than 90% (Dwyer et al., 1997), and leading to long-term boom-bust population cycles (Dwyer et al., 2000).

Since the introduction of the fungal pathogen, however, viral infection rates have often been reduced relative to their pre-fungal values (Kyle et al., 2020), presumably because the virus has been out-competed by the fungus; recent observations have nevertheless made clear that the virus continues to be an important source of spongy moth mortality (Elkinton et al., 2019). It is nevertheless true that the introduction of the fungus substantially lowered spongy moth defoliation rates (Tobin et al., 2012); negative effects of climate change on the fungus may therefore lead to increased spongy moth defoliation, and thus to increased tree stress and mortality. Meanwhile, low-density spongy moth populations are often held in check by generalist predators for several generations (Elkinton et al., 1996), and in combination with stochasticity such generalist predators can dramatically alter spongy moth outbreak cycles (Dwyer et al., 2004). The interactions between the spongy moth, its two pathogens and its generalist predators thus offer a useful system for quantifying the effects of climate change on a multi-species ecosystem.

Moreover, a key feature of spongy moth population dynamics since the introduction of the fungal pathogen is that fairly regular boom-bust population cycles driven by the virus (Johnson et al., 2006) have been replaced by more sporadic outbreaks that are often terminated by the fungus. In particular, New England recently experienced its first region-wide outbreak since the introduction of *E. maimaiga* in 1989, and this outbreak was terminated by a combination of both viral and fungal mortality (Elkinton et al., 2019; U.S. Forest Service, 2022). Here we use the change in the dynamics of the spongy moth in New England as an opportunity to construct a model that can project the effects of the viral and fungal pathogens and generalist predators on the future dynamics of the spongy moth. Indeed, it is at least possible that the recent New England outbreak is due to the accumulation of hot and dry weather for several years, as indicated by data from weather stations in Massachusetts and Connecticut (see Section 3.3.5 and Figure 3.1). To allow for this possibility, our model attempts to explain the New England data in terms of both species interactions and weather.

We construct our model by extending the SEIR-type fungus-only model in our earlier work (Liu et al., 2022), described in Chapter 2, to allow for long-term spongy moth dynamics. This means that we first extend the SEIR-type model to allow for both pathogens, and then we allow for multiple host generations and generalist predators. To better understand the relative importance of different species interactions, we also consider models that include the two pathogens but not generalist predators, and that include the baculovirus and generalist predators but not the fungus.

By fitting ours models to defoliation data from New England, we show that the long period with no outbreaks after fungus introduction can be partly explained by a combination of weather and the interactions among insect hosts, pathogens and predators. In particular, a model that allows for two pathogens and generalist predators provides a better explanation for the data than a model that includes the two pathogens but not generalist predators.

By inserting the projections of down-scaled climate change models into our best-fit models of spongy moth dynamics, we show that models with the virus as the only pathogen project minimal effects of climate change, even though our virus-only model allows for strong effects of climate change on the timing of virus epizootics. Presence of generalist predators does not strengthen the effects of climate change in this case. Models with both the virus and the fungus in contrast project strong effects of climate change, such that climate change will lead to increases in likelihood of spongy moth outbreaks in the future; moreover, allowing for not just the two pathogens but also generalist predators leads to outbreak cycles with a much higher amplitude. Understanding of the ecological consequences of climate change for the spongy moth thus in turn requires a full understanding of the natural enemies that the spongy moth interacts with. Our work shows that a consideration of species interactions is essential for understanding the effect of climate change on long-term population cycles. Projections of the ecological consequences of climate change among multiple species and improvement of models require more high-quality mechanistic data from both laboratory

and field, as suggested by Urban et al. (2016).

3.3 Methods

3.3.1 Overview

Here we explain our long-term fungus-virus models, and how we fit those models to data for the spongy moth. We first explain the natural history of the spongy moth, its specialist pathogens and its generalist predators. We then use this explanation as motivation for the models that we construct. Lastly we explain how we fit our models to data.

Our models begin with a virus-only, single-epizootic model constructed by our lab and colleagues (Dwyer et al., 1997), which we combine with a fungus-only single-epizootic model that we previously fit to data on experiments and observations of fungus epizootics in the field (Kyle et al., 2020). The result is a two-pathogen, single-epizootic model. Because our goal is to understand how climate change will affect long-term dynamics of the insect host, we then extend our two-pathogen, single-epizootic model to allow for long-term dynamics.

We thus use an SEIR-type model (SEIR = Susceptible-Exposed-Infected-Removed) to describe host-pathogen dynamics within a single epizootic. Our SEIR model allows for two pathogens, and the fungal pathogen is able to take over early-stage virus-infected individuals after coinfection (Malakar et al., 1999). In our models that include generalist predators, insect hosts that survive the epizootic experience additional mortality due to the predators; in all models surviving hosts reproduce, thereby producing susceptible hosts that fuel the next generation's epizootic. The next generation's epizootic is begun by infectious pathogen particles that were generated during previous epizootics and that survived in the environment. Figure 3.2 provides a schematic diagram of our models.

Next we explain how we fit our model to data. Because our goal is to use the 2017 occurrence of an outbreak in New England as a way of studying changes in the spongy

moth's population dynamics, the data that we have available to fit our models are somewhat limited, especially compared to the complexity of the models. For many of our model parameters, we therefore use estimates produced in previous work (Dwyer et al., 1997, 2000, 2022; Fuller et al., 2012; Kyle et al., 2020). We then estimate the remaining parameters from a combination of estimates of fungal spore densities and spongy moth defoliation in two New England states, Massachusetts and Connecticut.

We then use our parameterized spongy moth models to project the effects of climate change. To do this, we insert the down-scaled projections of climate change models (Wang and Kotamarthi, 2015) into our models to project how climate change will alter spongy moth dynamics. To understand the importance of the spongy moth's interactions with its two pathogens and its generalist predators, we compare projections across models with different combinations of pathogens and predators.

3.3.2 Natural history and dynamics of the spongy moth

The spongy moth is one of the most widespread defoliating insects in the northern hemisphere. It was accidentally introduced into the New England area of the United States from Europe in 1868-1869 (Elkinton and Liebhold, 1990) and has since spread across much of the midwestern and northeastern United States and the eastern provinces of Canada (Liebhold et al., 1992), thus becoming a major pest of hardwood forests in North America. As we described, and as is often the case in forest-defoliating insects, the spongy moth has undergone large-amplitude population cycles for many years, reaching peak densities every 5 to 10 years (Johnson et al., 2006; Liebhold et al., 2000), following a host-pathogen cycle driven by the specialist baculovirus. Generalist predators such as the white-footed mouse (*Peromyscus leucopus*) introduce variation in the time intervals between spongy moth outbreaks (Dwyer et al., 2004; Elkinton et al., 1996), but rely on other food sources during the winter and therefore cannot control the insect on their own (Liebhold et al., 2000).

The fungal pathogen *Entomophaga maimaiga* first began to have epizootics in *L. dispar* populations in the northeastern United States in 1989 (Andreadis and Weseloh, 1990; Hajek et al., 1996). Unlike the baculovirus, which survives the winter by contaminating egg masses (Dwyer et al., 1997), the fungus survives the winter in the form of long-lived resting spores (Hajek, 1999). After larvae hatch out at the beginning of each epizootic, resting spores in the environment germinate later if there is enough free water, ejecting infectious spores known as "conidia" that begin the epizootic. Conidia continue to be produced among larvae in the first few larval stages or "instars", but in later instars larvae instead produce resting spores that stay dormant in the current epizootic and will germinate to start future epizootics (Hajek, 1999).

Field experiments and observational data have shown that the fungus is often able to outcompete the baculovirus (Smitley et al., 1995), and the fungus therefore became the dominant pathogen in most of the range of the spongy moth within a few years after its introduction (Hajek et al., 2015). During the 2017 New England outbreak, however, both pathogens occurred at high frequency (Elkinton et al., 2019).

3.3.3 Single-epizootic models

Previous work by colleagues produced parameterized SEIR-type models that described epizootics of the baculovirus alone (Dwyer et al., 1997) and the fungus alone (Kyle et al., 2020). Although the models are structurally similar, they differ in two important ways. First, in the fungus model both types of infectious spores, the resting spores and the conidia, are quite sensitive to weather conditions, but host infection risk is the same across individuals. In the virus model in contrast, the virus is largely unaffected by weather (Woods and Elkinton, 1987), but hosts vary greatly in their infection risk.

To allow for mixed virus-fungus epizootics, we combined the single-epizootic models from Dwyer et al. (1997) and Kyle et al. (2020) into one model. In this two-pathogen

single-epizootic model, the epizootic starts when larvae hatch. Larvae can then be infected by baculovirus particles, known as "occlusion bodies", fungal resting spores or fungal conidia. Infected larvae pass through multiple exposed classes before being killed by whichever pathogen they are infected with. Infectious cadavers then lead to additional infections, with the proviso that fungus-infected cadavers in late larval instars produce resting spores instead of conidia (Hajek, 1999).

A key feature of the biology of the fungus is that it kills faster than the baculovirus (Fuller et al., 2012; Kyle et al., 2020; Malakar et al., 1999). Because of this high speed of kill, and because hosts that have been exposed to both pathogens have been observed to contain both infectious viral occlusion bodies and fungal conidia (Malakar et al., 1999), it seems likely that the fungus can take over hosts that are in the early stages of baculovirus infection, but it does not seem likely that the baculovirus can take over fungus-infected larvae.

As we show in Figure 3.2, when hosts in the first few virus-exposed classes are coinfected by the fungus, they move into the first fungus-exposed class, and thus produce fungus spores at death. We also allow for the possibility that virus-infected insect hosts can be more susceptible to the fungus, because their immune system has been weakened by the baculovirus. These mechanisms have the advantage that they allow for the dominance of the fungus that has been observed in the field.

As in the single-epizootic fungus model, our combined model assumes that transmission and decay rates of fungus spores vary stochastically on a daily scale, and that both processes are affected by daily weather conditions (Kyle et al., 2020). We thus have a set of random differential equations, such that on day τ in the epizootic, the model equations are:

$$\overbrace{\frac{dS_\tau}{dt}}^{\substack{\text{change in}\\ \text{susceptible}\\ \text{host}\\ \text{density}}} = -\overbrace{\underbrace{\bar{\nu_v}}_{\substack{\text{average}\\ \text{virus}\\ \text{transmis-}\\ \text{sion rate}}}\left[\frac{S_\tau}{S(0)}\right]^{C^2}}^{\text{virus transmission}} \underbrace{P_\tau}_{\substack{\text{virus}\\ \text{killed}\\ \text{cadaver}\\ \text{density}}} \underbrace{S_\tau}_{\substack{\text{host}\\ \text{density}}} -(\overbrace{\nu_{R,\tau}}^{\substack{\text{resting}\\ \text{spore}\\ \text{transmis-}\\ \text{sion rate}}} \underbrace{R}_{\substack{\text{resting}\\ \text{spore}\\ \text{density}}} +\nu_{C,\tau}C_\tau)S_\tau \quad (3.1)$$

$$\overbrace{\frac{dE_{f,1,\tau}}{dt}}^{\substack{\text{change in}\\ \text{fungus}\\ \text{exposed}\\ \text{class 1}}} = (\nu_{R,\tau}R + \overbrace{\nu_{C,\tau}}^{\substack{\text{conidia}\\ \text{transmis-}\\ \text{sion rate}}} \underbrace{C_\tau}_{\substack{\text{conidia}\\ \text{density}}})(S_\tau + \underbrace{\zeta}_{\substack{\text{enhanced}\\ \text{suscepti-}\\ \text{bility}}} \overbrace{\sum_{i=1}^{n_1} E_{vf,i,\tau}}^{\substack{\text{Sum of virus}\\ \text{exposed}\\ \text{classes that}\\ \text{can be taken}\\ \text{over by the}\\ \text{fungus}}}) - \overbrace{m\delta_f E_{f,1,\tau}}^{\substack{\text{aging into}\\ \text{next fungus}\\ \text{exposed}\\ \text{class}}} \quad (3.2)$$

$$\overbrace{\frac{dE_{f,i,\tau}}{dt}}^{\substack{\text{change in}\\ \text{fungus exposed}\\ \text{class i}}} = \overbrace{\underbrace{m}_{\substack{\text{no. of}\\ \text{fungus}\\ \text{exposed}\\ \text{classes}}} \underbrace{\delta_f}_{\substack{\text{speed of}\\ \text{kill of}\\ \text{fungus}}} E_{f,i-1,\tau}}^{\substack{\text{aging out of}\\ \text{previous class}}} - \overbrace{m\delta_f \underbrace{E_{f,i,\tau}}_{\substack{\text{host density}\\ \text{in fungus}\\ \text{exposed class i}}}}^{\substack{\text{aging into}\\ \text{next class}}} \quad (i = 2, 3, \ldots, m) \quad (3.3)$$

$$\overbrace{\frac{dE_{vf,1,\tau}}{dt}}^{\substack{\text{change in}\\ \text{virus exposed}\\ \text{class 1,}\\ \text{which can}\\ \text{be taken over}\\ \text{by fungus}}} = \bar{\nu_v}P_\tau S_\tau \left[\frac{S_\tau}{S(0)}\right]^{\overbrace{C^2}^{\substack{\text{C.V. of}\\ \text{virus}\\ \text{transm-}\\ \text{ission}}}} - \overbrace{\zeta(\nu_{R,\tau}R + \nu_{C,\tau}C_\tau)}^{\substack{\text{enhanced}\\ \text{fungus}\\ \text{transmi-}\\ \text{ssion}}} E_{vf,1,\tau} - n\delta_v E_{vf,1,\tau} \quad (3.4)$$

$$\overbrace{\frac{dE_{vf,j,\tau}}{dt}}^{\substack{\text{change in}\\ \text{virus exposed}\\ \text{class j,}\\ \text{which can}\\ \text{be taken over}\\ \text{by fungus}}} = \overbrace{\underbrace{n}_{\substack{\text{no. of}\\ \text{virus}\\ \text{exposed}\\ \text{classes}}} \underbrace{\delta_v}_{\substack{\text{speed of}\\ \text{kill of}\\ \text{virus}}} E_{vf,j-1,\tau}}^{\substack{\text{aging out of}\\ \text{previous class}}} - \overbrace{n\delta_v E_{vf,j,\tau}}^{\substack{\text{aging into}\\ \text{next class}}} - \zeta(\nu_{R,\tau}R + \nu_{C,\tau}C_\tau) \underbrace{E_{vf,j,\tau}}_{\substack{\text{host density}\\ \text{in virus}\\ \text{exposed class j}}}$$

$$(j = 2, 3, \ldots, \underbrace{n_1}_{\substack{\text{no. of virus exposed classes}\\ \text{which can be taken}\\ \text{over by fungus}}})$$

(3.5)

$$\overbrace{\frac{dE_{v,1,\tau}}{dt}}^{\substack{\text{change in the first}\\ \text{virus expose class}\\ \text{which cannot be taken}\\ \text{over by fungus}}} = \overbrace{n\delta_v E_{vf,n_1,\tau}}^{\substack{\text{aging out of the}\\ \text{final virus exposed}\\ \text{class which can be}\\ \text{taken over by fungus}}} - \overbrace{n\delta_v E_{v,1,\tau}}^{\substack{\text{aging into next}\\ \text{virus exposed class}}} \tag{3.6}$$

$$\overbrace{\frac{dE_{v,j,\tau}}{dt}}^{\substack{\text{change in the other}\\ \text{virus expose classes}\\ \text{which cannot be taken}\\ \text{over by fungus}}} = \overbrace{n\delta_v E_{v,j-1,\tau}}^{\substack{\text{aging out of previous}\\ \text{virus exposed class}}} - \overbrace{n\delta_v E_{v,j,\tau}}^{\substack{\text{aging into next}\\ \text{virus exposed class}}} \tag{3.7}$$

$$(j = 2, 3, \ldots, \underbrace{n - n_1}_{\substack{\text{no. of virus exposed classes}\\ \text{which cannot be taken}\\ \text{over by fungus}}})$$

$$\overbrace{\frac{dC_\tau}{dt}}^{\substack{\text{change in}\\ \text{fungus-infected}\\ \text{cadaver density}\\ \text{producing conidia}}} = \overbrace{(1 - X_{R,\tau})}^{\substack{\text{index on whether}\\ \text{fungus-infected}\\ \text{cadavers produce}\\ \text{conidia}}} \overbrace{m\delta_f E_{f,m,\tau}}^{\substack{\text{death of hosts}\\ \text{in the final}\\ \text{fungus exposed}\\ \text{class}}} - \overbrace{\underbrace{\mu_{C,\tau}}_{\substack{\text{decay rate of}\\ \text{cadavers}\\ \text{producing}\\ \text{conidia}}} C_\tau}^{\text{cadaver decay}} \tag{3.8}$$

$$\overbrace{\frac{dP_\tau}{dt}}^{\substack{\text{change in}\\ \text{virus-infected}\\ \text{cadaver density}}} = \overbrace{n\delta_v E_{v,n,\tau}}^{\substack{\text{death of hosts}\\ \text{in the final}\\ \text{virus exposed}\\ \text{class}}} - \overbrace{\underbrace{\mu_v}_{\substack{\text{decay rate of}\\ \text{virus-killed}\\ \text{cadavers}}} P_\tau}^{\text{cadaver decay}} \tag{3.9}$$

$$\overbrace{\frac{dP_{f,next,\tau}}{dt}}^{\substack{\text{change in cumulative fungus-killed}\\ \text{cadaver density producing}\\ \text{resting spores, used}\\ \text{in the long-term model}}} = \overbrace{X_{R,\tau}}^{\substack{\text{index on whether}\\ \text{fungus-infected}\\ \text{cadavers produce}\\ \text{resting spores}}} \overbrace{m\delta_f E_{f,m,\tau}}^{\substack{\text{death of hosts}\\ \text{in the final}\\ \text{fungus exposed}\\ \text{class}}} \tag{3.10}$$

$$\overbrace{\frac{dP_{f,\tau}}{dt}}^{\substack{\text{change in cumulative fungus-killed}\\ \text{cadaver density, used in}\\ \text{the long-term model}}} = m\delta_f E_{f,m,\tau} \tag{3.11}$$

$$\overbrace{\frac{dP_{v,next,\tau}}{dt}}^{\substack{\text{change in cumulative virus-killed}\\ \text{cadaver density, used}\\ \text{in the long-term model}}} = \overbrace{n\delta_v E_{v,n,\tau}}^{\substack{\text{death of hosts}\\ \text{in the final}\\ \text{virus exposed}\\ \text{class}}} \tag{3.12}$$

We thus use differential equations to describe the change in the densities of different classes of host and pathogens, such that hosts are expressed in units of individuals/m^2. Notably, $S(0)$ is the initial host density at the beginning of the epizootic, and the resting spore density R is assumed to be constant during the epizootic. The number of fungus-exposed host classes is m, and δ_f is the death rate of fungus-infected insects. Allowing for multiple exposed classes, each with an exponentially distributed incubation time, causes the

delay between fungus infection and death to follow a gamma distribution with mean $1/\delta_f$ and variance $1/(m\delta_f^2)$. Similarly, because there are n virus-exposed host classes, the delay between baculovirus infection and death follows a gamma distribution with with mean $1/\delta_v$ and variance $1/(n\delta_v^2)$ (Keeling and Rohani, 2008).

To allow the fungus take over virus-infected individuals, we divide the virus-exposed host classes into two partitions, such that the first n_1 of the n virus-exposed classes can be coinfected and killed by the fungus in the end. The value of n_1 depends on the speed of kill of the two pathogens, according to:

$$n_1 = \frac{\frac{1}{\delta_v} - \frac{1}{\delta_f}}{\frac{1}{\delta_v}} n = \left(1 - \frac{\delta_v}{\delta_f}\right) n \tag{3.13}$$

Once infected and taken over by the fungus, these early-stage virus-infected individuals move into the first exposed class of the fungus $E_{f,1,\tau}$, and then move through the same m fungus exposed classes as other fungus-infected individuals. The parameter ζ represents the enhanced susceptibility to fungus of these early-stage virus-infected individuals. Hosts in the final exposed class of either the fungus or the baculovirus then move into their respective classes of cadavers, thereby generating fungus conidia and virus occlusion bodies that have respective decay rates $\mu_{C,\tau}$ and μ_v. The symbol $X_{R,\tau}$ is then an index that determines whether the fungus-killed cadavers generate resting spores or conidia; if $X_{R,\tau} = 1$, fungus-infected cadavers produce resting spores, and if $X_{R,\tau} = 0$ fungus-infected cadavers produce conidia.

Because larval growth is temperature dependent (Elkinton and Liebhold, 1990), we use degree days to determine when the value of $X_{R,\tau}$ changes from 0 to 1. Equations (3.10) and (3.12) then describe the rate at which cadavers produce pathogens that persist in the environment over the winter. These two equations thus link epizootic dynamics to long-term dynamics.

Because stochasticity in our models is implemented on a daily basis, we update the

initial conditions for the model equations at the beginning of each day, according to:

$$S_\tau(0) = S_{\tau-1}(1), \tag{3.14}$$

$$E_{j,\tau}(0) = E_{j,\tau-1}(1), \tag{3.15}$$

$$C_\tau(0) = C_{\tau-1}(1). \tag{3.16}$$

$$P_\tau(0) = P_{\tau-1}(1). \tag{3.17}$$

Here $S_\tau(0)$ is the uninfected population at the beginning of day τ, while $S_{\tau-1}(1)$ is the uninfected population at the end of day $\tau - 1$, and similarly for the other state variables.

Weather conditions in our epizootic model affect the dynamics of the fungus in several ways, following our use of epizootic data to construct a single-epizootic fungus model (Kyle et al., 2020). First, cumulative degree days determine the time of larvae hatch and pupation, thus defining when the epizootic starts and ends, and the timing of resting spore germination and the end of conidia production. Also, rainfall increases resting spore transmission, while relative humidity increases conidia transmission, and temperature increases conidia decay. Also, because conidia infect larvae through airborne contact (Hajek, 1999), bigger larvae make for larger targets: we therefore allow the fungal transmission rates to increase with larval size, which is in turn determined by cumulative degree days.

In incorporating virus dynamics, we also modified previous virus-only models to allow for a weather effect on the virus (Dwyer et al., 1997, 2004), such that the speed of kill of initially infected larvae depends on temperature. In our initial efforts to combine the fungus and virus models, we first assumed that the speed of kill of initial virus infections was unaffected by weather, but in that case the fungus was unrealistically unable to outcompete the virus, even if the enhanced susceptibility of virus-infected individuals ζ was extremely high. In reality, however, temperatures at the beginning of virus epizootics are highly variable, and so the time of death of initially infected larvae is strongly determined by temperature (Dwyer et al.,

2022). This is important because if temperatures early in the epizootic are low enough that initial baculovirus infections occur a little earlier than or even after resting spore germination, then the fungus will dominate the subsequent epizootic, giving it a realistic competitive advantage. We therefore assumed that the timing of initial baculovirus deaths also depends on cumulative degree days, and we fit the dependency of this timing to the data. Additional details on how these variables or mechanisms are related to weather conditions are listed in the Appendix (Section 3.7.1).

3.3.4 Long-term Models

To study the effects of climate change on long-term spongy moth dynamics, we extended our single-epizootic two-pathogen SEIR model to allow for host and pathogen dynamics between epizootics, and thus between host generations. To match the one-year life cycle of the spongy moth, which is a common feature of outbreaking insects (Hunter, 1995), we use difference equations (Dwyer et al., 2000). The difference equations allow for post-epizootic mortality due to generalist predators, followed by reproduction of insects that survive to adulthood. Fungal resting spores and baculovirus occlusion bodies must then survive the winter. To allow for this biology, we extend previous long-term virus-only models Dwyer et al. (2004) and Fuller et al. (2012) as follows:

$$\overbrace{N_{t+1}}^{\text{host in gen'n } t+1} = \overbrace{\lambda}^{\text{baseline fecundity}} \underbrace{e^{\epsilon}}_{\substack{\text{stochasticity} \\ \text{in fecundity}}} \overbrace{N_t}^{\text{host in gen'n } t} \overbrace{[1 - \underbrace{I_{f,t}}_{\substack{\text{cumulative fraction} \\ \text{infected by} \\ \text{the fungus}}} - \underbrace{I_{v,t}}_{\substack{\text{cumulative fraction} \\ \text{infected by} \\ \text{the virus}}}]}^{\text{fraction surviving epizootic}} \times \overbrace{\left(1 - \frac{2abN_t}{b^2 + N_t^2}\right)}^{\text{fraction surviving from generalist predators}} + \overbrace{g}^{\substack{\text{immigration to avoid} \\ \text{host extinction}}} \tag{3.18}$$

$$\overbrace{Z_{v,t+1}}^{\substack{\text{virus-killed}\\ \text{cadavers in}\\ \text{gen'n } t+1}} = \overbrace{\phi_v}^{\substack{\text{overwintering \&}\\ \text{higher susceptibility}\\ \text{in newly hatched}\\ \text{larvae}}} N_t I_{v,t} + \overbrace{\gamma_v}^{\substack{\text{long-term virus}\\ \text{survival}}} \overbrace{Z_{v,t}}^{\substack{\text{virus-killed}\\ \text{cadavers in}\\ \text{gen'n } t}} + \overbrace{g}^{\substack{\text{immigration to}\\ \text{avoid virus}\\ \text{extinction}}} \tag{3.19}$$

$$\overbrace{R_t}^{\substack{\text{fungus resting spores}\\ \text{germinating in}\\ \text{gen'n } t}} = \overbrace{(1-\gamma_f)}^{\substack{\text{resting spore}\\ \text{germination rate}}} \overbrace{Z_{f,t}}^{\substack{\text{total fungus}\\ \text{resting spores in}\\ \text{gen'n } t}} \tag{3.20}$$

$$\overbrace{Z_{f,t+1}}^{\substack{\text{total}\\ \text{resting}\\ \text{spores}\\ \text{in gen'n}\\ t+1}} = \overbrace{\frac{f_m}{1+\exp[-x_1(\log_{10}(N_t \underbrace{I_{f,R,t}}_{\substack{\text{cumulative fraction}\\ \text{infected by fungus}\\ \text{that can produce}\\ \text{resting spores}}}) - x_0)]}}^{\substack{\text{logistic function to transform}\\ \text{cadavers producing resting spores}\\ \text{into resting spore density}}} + \overbrace{\gamma_f}^{\substack{\text{long-term}\\ \text{resting}\\ \text{spore}\\ \text{survival}}} Z_{f,t} \tag{3.21}$$

In equation (3.18) and (3.19), we use $g = 10^{-6}$ to allow for immigration, thereby preventing the extinction of the host and the baculovirus. The cumulative fraction killed by the fungus $I_{f,t}$, the fraction killed by fungus that produce resting spores $I_{f,R,t}$ and the fraction killed by the virus $I_{v,t}$ can be calculated from the differential equations in the single-epizootic model equations, as follows:

$$N_t(1 - I_{f,t} - I_{v,t}) = S_{\text{last}}(1) \tag{3.22}$$

$$N_t I_{v,t} = P_{v,\text{next},\text{last}}(1) + \sum_{i=1}^{n_1} E_{vf,i,\text{last}}(1) + \sum_{j=1}^{n-n_1} E_{v,j,\text{last}}(1) \tag{3.23}$$

$$N_t I_{f,t} = P_{f,\text{last}}(1) + \sum_{i=1}^{m} E_{f,i,\text{last}}(1) \tag{3.24}$$

$$N_t I_{f,R,t} = P_{f,\text{next},\text{last}}(1) + \sum_{i=1}^{m} E_{f,i,\text{last}}(1) \tag{3.25}$$

In these equations, last(1) indicates the end of the last day of the epizootic, while $S_{\text{last}}(1)$ is the density of hosts that are uninfected at that time. Similarly, $P_{f,\text{next},\text{last}}(1)$, $P_{f,\text{last}}(1)$ and $P_{v,\text{next},\text{last}}(1)$ indicate the final densities of fungal-infected and virus-infected cadavers as calculated from equations (3.10), (3.11) and (3.12), assuming there is no cadaver

decay, to calculate the cumulative fractions infected. The final density of each exposed class is also added to the cumulative fractions infected, because extensive observations have made clear that individuals in exposed classes almost always die of their infection without pupating (G. Dwyer, unpublished). All individuals in classes exposed to the fungus at the end of the last day are therefore added to the fraction of fungus-infected individuals that produce resting spores ($I_{f,R}$). Meanwhile, because it is unlikely that fungal takeovers will be successful at the end of the epizootic, no matter whether could be coinfected by the fungus, hosts in virus exposed classes are added to the cumulative fraction infected by the virus (I_v). It is important to note, however, that number of hosts in exposed classes at the end of epizootics in the model is generally small, matching observations from the field (Dwyer et al., 2022).

In equation (3.18), host fecundity is the product of the baseline fecundity of surviving hosts λ and the stochastic term e^{ϵ}. The predation term describes the fraction surviving generalist predators, based on a Type III functional response. In equation (3.19), ϕ_v describes both the overwintering rate of virus-infected cadavers from the preceding epizootic and the increased susceptibility to the baculovirus of newly hatched larvae, while γ_v is rate at which virus-infected cadavers from earlier epizootics remain infectious over multiple years. Previous work has suggested that $\gamma_v \approx 0$ (Dwyer et al., 2022; Fuller et al., 2012), indicating that long-term baculovirus survival is very low.

Quantification of resting spore infection rates has suggested that resting spores can remain dormant for multiple years after being released from fungus-infected cadavers, while still being able to germinate and infect larvae (Weseloh and Andreadis, 1997). We therefore assume that resting spores are very stable in the environment, and that any loss of resting spores is due only to the partial germination in each year. The symbol γ_f thus represents the long-term survival rate of resting spores, and in equation (3.20) $(1 - \gamma_f)$ is the germination rate.

A key issue in constructing the long-term model has to do with how the fungus infection

rate during the epizootic affects the long-term density of resting spores. Initially we used a virus-like model for resting spore overwintering, so that resting spore density increased linearly with fungus-infected cadaver density. Because resting spores have much higher survival rates in the environment than do baculovirus occlusion bodies, however, this virus-like model produced huge fluctuations in resting spore densities, often leading to extremely high resting spore densities. Our previous work in contrast showed that resting spore densities are never very high, even during spongy moth outbreaks (Kyle et al., 2020).

To avoid unrealistically high resting spore densities, we therefore assume in equation (3.21) that resting spore densities follow a logistic function. The parameter f_m is the upper limit for this logistic function, while x_0 and x_1 control the shape of the logistic curve. By having this logistic function, we can avoid the situation where resting spore density fluctuates dramatically with fungus-infected cadaver density, which is not realistic.

3.3.5 Fitting the models to data

As we mentioned, we have estimates of all the parameters of our single-epizootic fungus-only and virus-only models (Dwyer et al., 1997, 2004; Kyle et al., 2020), and we have estimates of some long-term parameters from a model of long-term spongy moth-baculovirus dynamics (Dwyer et al., 2004). We are therefore missing estimates of parameters related to the fungus-virus interaction and to the long-term dynamics of fungus resting spores in the environment. Given that there are few long-term data sets that track the density of the spongy moth, it seemed unlikely that we would be able to estimate all of the parameters in our long-term model from existing data. We therefore estimated only the parameters that we have no information on or whose previous estimates were at best rough guesses, while fixing the remaining parameters at their point estimates from previous studies. A list of the parameter values that are fixed in the model is provided in the Appendix (Section 3.7.2).

Like the long-term dynamics for the virus (equation (3.19)), the equation for long-term

dynamics of resting spores is divided into two terms, overwintering survival and long-term survival. To simplify the resulting estimation problem, we fit the three parameters in the logistic function of resting spore overwintering to our previous estimates of resting spore density in Kyle et al. (2020); the resulting values are listed in the Appendix (Section 3.7.2). We then fit the long-term resting spore survival rate γ_f to data on spongy moth outbreaks.

The remaining parameters that we fit to the spongy moth outbreak data are the enhanced susceptibility of virus-infected hosts ζ, the initial fungus density f_{init}, the baseline fecundity λ, the standard deviation of the stochasticity (on a log-scale) in fecundity ϵ, and the degree-days above 10 $^{\circ}C$ for baculovirus infections to cause death VDD.

As we mentioned, our goal is to infer the effects of weather and the two pathogens on the dynamics of the spongy moth from data on the change in the spongy moth's dynamics since the introduction of the fungus. Quantifying spongy moth density is sufficiently logistically difficult, however, that density data are unavailable. The best available data therefore consist of measurements of defoliation rather than measurements of spongy moth density which are publicly available on the USDA Forest Service website *Lymantria dispar* Digest (U.S. Forest Service, 2022). Because our interest is in capturing the dynamics during fungus establishment and during the following period of fungus-virus competition, we use data from the era of virus-only population cycles to the present.

We focus in particular on New England, where the fungus was initially introduced and observed (Hajek et al., 1995), and which experienced its first post-fungus, region-wide outbreak in 2017. We then selected two New England states, Massachusetts and Connecticut, that show strong effects of the 2017 outbreak (see Figure 3.3 and Elkinton et al. (2019)). Since the outbreak appears to have occurred because several years of hot, dry weather temporarily suppressed the fungus, we use the New England data as an opportunity to quantify key parameters of our long-term model, and especially how some of these parameters depend on weather.

Because realistic weather data are necessary for us to fit the model to the data, for each state we chose a weather station with consistent weather data available for recent decades in the dataset Global Surface Summary of the Day from the website *https://www.ncei.noaa.gov* (National Centers for Environmental Information and National Oceanic and Atmospheric Administration, 2022). We used the weather station Chicopee Falls Westover Field to represent Massachusetts, with weather data available from 1970 to 2019, and we used the weather station Hartford Bradley International Airport to represent Connecticut, with weather data available from 1973 to 2019. We used data for daily precipitation, dew point, maximum temperature and average temperature directly from the website. We calculated daily relative humidity from dew point using a standard transformation equation (Bolton, 1980). Average values of daily maximum temperature, relative humidity and rainfall across days in each epizootic are shown in Figure 3.1.

Because the relationship between spongy moth density and defoliation is rather complicated (Liebhold et al., 1993), we used the defoliation data to provide signals of outbreaks, on the realistic assumption that peaks and outbreak lengths in the defoliation data can serve as estimates of peaks and outbreak lengths in terms of spongy moth density. Our likelihood function is then based on four separate summary statistics, as follows.

The main part of the likelihood is based on the time interval between the introduction of the fungus in 1989 (Hajek et al., 1990) and the first outbreak following the fungus introduction. For both the model output of spongy moth density and the data on defoliation, we define an outbreak as the density or defoliation peak above a threshold. In the data, we assumed that an outbreak occurred if the defoliation area in a peak was high than 20% of the maximum value of defoliation area (blue horizontal lines in Figure 3.3). As Figure 3.3 makes clear, outbreaks occur in sharp peaks, and so modest variation in this threshold is unlikely to affect our results.

Using this definition, the time between fungus introduction and the first following out-

break is $2017 - 1989 = 28$ years in both states. We then use a Poisson likelihood function to calculate the probability that we observe a 28-year interval between fungus introduction and the first outbreak afterwards given that the mean of the Poisson distribution for that interval is equal to the value found in the model output. The ways to define an outbreak in the model output (we use $10^{-0.5}$ as the threshold host density level) and calculate the interval between it and the fungus introduction, however, are more complicated. Details on how to record the outbreak and calculate the interval are listed in the Appendix (Section 3.7.3).

The second part of the likelihood function is based on the length of the first outbreak after fungus introduction. In the defoliation data (Figure 3.3), the outbreak that peaked in 2017 lasted for 5 years. To calculate the outbreak length in the model, we first recorded the peak amplitude N_p, and then we recorded the year before the peak y_{left} and the year after the peak y_{right} as the years closest to the peak for which the host density was less than another threshold value. To choose this threshold, we dynamically adjusted the threshold according to the outbreak amplitude, so that the increase during the outbreak was roughly constant over all cases. Specifically, we assumed that host density during the outbreak increases by a fold of $10^{1.5}$, on the grounds that a host density of $10^{-0.5}$ is a reasonable threshold density for an outbreak, and that a density of 10^{-2} provides a reasonable starting and ending density of an outbreak. If no years before or after the peak satisfied this criterion, we assigned y_{left} to be 10 years before the start of the weather data, and y_{right} to be 10 years after the end of weather data, giving an extremely long outbreak length. Because here we identify the best model parameters using a maximum likelihood calculation, the large value of outbreak length would likely to have little effect on our results. The equation to calculate the outbreak length in the model is thus $l = (y_{right} - 1) - (y_{left} + 1)$. We then again use a Poisson likelihood, with 5 years as our observation of outbreak length in the data, and l from model output as the theoretical mean of the Poisson distribution.

We also included a likelihood based on the density of fungal resting spore densities. In the 7 sites listed in Kyle et al. (2020), the average of $\log_{10}$(fungus density) is -3.82. As shown in Table 3.1, there is an extreme low outlier value of roughly 10^{-12}, which we exclude to avoid unrealistic outcomes. The values at the remaining 6 sites have a mean on a $\log_{10}$-scale of -2.48 and a standard deviation of 0.48. To use these summary statistics to construct a likelihood function, we used them as the theoretical mean and standard deviation of a normal distribution, and we used this normal distribution to calculate the likelihood of the average resting spore densities in the model.

Finally, because it was important to estimate the weather-dependence of the time that it takes for initial baculovirus infections to cause death, we included a likelihood value based on the pre-fungus dynamics, so that the baculovirus was the only pathogen. To avoid the cases in which the model cannot reproduce the 9-year interval between outbreaks in the pre-fungus era (Dwyer et al., 2022), we generated model simulations for the entire time period of the weather data, but without including the fungus in the model, recording the mean interval between peaks over this time period. If there were less than two peaks, we assigned a peak interval of 50 years, again on the grounds that a large value would have little effect on our results. We then again used a Poisson likelihood, with 9 years as the observation value, and the mean peak interval from model output as the theoretical mean of the Poisson distribution.

The overall likelihood function combining all parts for r realizations of the model is:

$$\bar{L} = \frac{1}{r}\sum_{i=1}^{r}[\ \overbrace{f_{Poi}(28, y_i)}^{\substack{\text{Poisson likelihood for interval}\\ \text{between fungus introduction and}\\ \text{the next outbreak}}} \times \overbrace{f_{Poi}(5, l_i)}^{\substack{\text{Poisson likelihood for length}\\ \text{of that outbreak after}\\ \text{fungus introduction}}} \times \underbrace{f_{nor}(\log_{10}\bar{(}Z_{f,i})|(-2.48), 0.48^2)}_{\substack{\text{Normal likelihood for the}\\ \text{average fungus density}\\ \text{on a } \log_{10}\text{-scale}}} \times \underbrace{f_{Poi}(9, y_{v,i})}_{\substack{\text{Poisson likelihood for cycle}\\ \text{periods when the virus}\\ \text{is the only pathogen}}} \ ] \tag{3.26}$$

Because of the stochasticity in the annual host fecundity and the daily fungus transmission rate, we averaged likelihoods across a large number of model realizations for each parameter set; in practice 200 realizations provided a consistent and accurate estimate of the overall likelihood. In each realization, initial host and virus densities were drawn randomly, so that we could average across the (unknown) initial conditions. We then used line-search to find the best parameters; in the immediate future, we will use the line-search output to construct proposal distributions using MCMC, thereby following the line-search/MCMC algorithm (Kennedy et al., 2015). Here we present only the results of the line-search algorithm, on the grounds that in general line-search typically provides a quite accurate estimate of the maximum likelihood. In line-search, each parameter to be estimated is varied in turn while the other parameters are held constant. The best value for the parameter being varied is then retained, and then the next parameter is varied until all parameters are varied a fixed number of times. We carried out 100 separate line-searches for each model, starting each line-search at a randomly selected parameter set, and we recorded the parameters that gave the maximum likelihood score across all 100 line-searches.

Although Figure 3.3 shows similar defoliation patterns in Massachusetts and Connecticut, the weather data differ between the two states; moreover, spatial variation in the data may also be operating because of differences in forest tree-species composition and data collection methods. If we assumed that spongy moth dynamics for Massachusetts and Connecticut could be described using the same parameter sets, the dynamics could be different because of differences in the weather, but it would be hard to know why the differences would occur. The conservative approach is therefore to fit the model to the data for the two states separately, so that we can find the best parameter set for each state.

To understand the extent to which generalist predators play an important role in keeping spongy moth density at a low level between outbreaks (Dwyer et al., 2004), we fit models with and without generalist predators (note that the generalist predators can be eliminated

by setting the predation rate $a = 0$). Comparing the with-predator and without-predator models also allowed us to test whether predators can help explain the long interval between the initial introduction of the fungus and the 2017 outbreak.

3.3.6 Projecting the effects of climate change

To project the effects of climate change, we inserted the best parameter set into each model together with either historical or future projected weather, and we compared summary statistics of outbreak intervals and outbreak severity between historical and future weather across different models. Weather projections were taken from a down-scaled climate change model (Wang and Kotamarthi, 2014, 2015) for a historical period from 1995 to 2004 and a future period from 2085 to 2094. Since there are only 10 years of projections in the past and future respectively, we ran the model for many additional years to produce accurate summary statistics. To do this, we randomly drew sets of weather variables from each weather data set; because each projected weather data set has 10 years, then the weather for year 11, for example, is the same as the weather in a year randomly chosen from 1 to 10. Using this random-draw approach, we expanded each data set to allow for model simulations of 200 years.

For each simulation of 200 years, we generated 500 realizations of each model, and we calculated the mean values of number of peaks, peak intervals, peak amplitudes, and the coefficient of variation of the peak intervals. We then used these summary statistics to quantify the effects of historical versus future weather on spongy moth dynamics, and thus to quantify the effects of climate change. We calculated the number of outbreaks and the intervals between outbreaks in the same way as in our likelihood function, using $10^{-0.5}$ as the threshold, and we recorded the number of ourbreaks in each realization, and then averaged over realizations. Because there may be more than one outbreak in a given realization, to calculate outbreak intervals and outbreak amplitudes we averaged all values across all

realizations, leading to a sample size that was generally larger than the 500 realizations that we generated for each model.

To generate projections, we used weather projections at a specific location in each state, with the location chosen so that it illustrated the overall trend of future weather conditions apparent in the projections in that state. The location that we used for Massachusetts was 72.05 $^{\circ}W$ 42.58 $^{\circ}N$, and the location that we used for Connecticut was 72.63 $^{\circ}W$ 41.91 $^{\circ}N$. For the location in Massachusetts, the relative differences of rainfall, relative humidity and temperature between future weather projections (2085-2094, RCP 8.5) and historical weather projections (1995-2004) are respectively -8.50%, -5.63% and 1.87%, while the absolute differences are correspondingly -2.67 cm/day, -4.20% and +0.32 $^{\circ}C$. For the location in Connecticut, the relative differences of rainfall, relative humidity and temperature between future and historical weather projections are respectively -6.96%, -3.99% and -1.73%, while the absolute differences are correspondingly -1.96 cm/day, -2.69% and -0.30 $^{\circ}C$. Across the range of the spongy moth, the mean values of relative differences of rainfall, relative humidity and temperature between future weather projections (2085-2094, RCP 8.5) and historical weather projections (1995-2004) are respectively 0.50%, -2.32% and 2.63%, while the mean values of the absolute changes in these three weather variables are -0.237 cm/day, -2.31%, and +0.46 $^{\circ}C$. Although the relative and absolute differences for the locations we used differ slightly from the mean values across the entire range of the spongy moth, Figure 2.2 makes clear that in Massachusetts conditions are projected to be hotter and drier, with decreases in both rainfall and relative humidity and increases in temperature. In Connecticut future weather is also projected to be drier, with decreased rainfall and relative humidity, but the temperature is expected to be somewhat lower. The two locations that we chose are thus representative of their respective states, while the two states are projected to show similar trends in relative humidity but different trends in temperature, and therefore provide for a useful comparison. For consistency, to make projections in each state we use

the parameter values that we estimated for that state.

3.4 Results

3.4.1 Model-fitting results

The best parameter sets for our models (Table 3.2) lead to two initial conclusions. First, most model parameters besides baseline fecundity λ vary at least modestly between Massachusetts and Connecticut. This result supports our decision to fit our models separately to the two states, and we therefore conclude that conditions were at least moderately different between the two states. Second and more importantly, models with predators have larger values of λ; for these models, explaining the data requires a larger value of λ because predator mortality reduces population rates of increase. Reassuringly, the conclusion that the values of λ for models with predators are larger is also true in previous spongy moth models that included only the baculovirus (Dwyer et al., 2000, 2004). It is also worth noting that the models with predators can explain the data for lower levels of stochasticity in fecundity.

A third conclusion from our model-fitting is that the models with predators fit the data better than the models without predators (Table 3.3); the improvement in the fit is small but detectable with respect to the Connecticut data, but it is quite large with respect to the Massachusetts data. Because our models are stochastic, it was at least possible that the differences in likelihoods between models were due only to chance variation in likelihoods between model realizations; accordingly, to ensure that the differences in likelihoods are meaningful, we used t-tests to test the null hypothesis that the difference in mean likelihoods between models are due simply to chance (Rice, 2006). In both cases, we are able to reject the null hypothesis, such that for Massachusetts $p = 0.013$ and for Connecticut $p = 0.016$.

It is important to emphasize that there is abundant evidence that generalist predators strongly affect spongy moth outbreak cycles (Elkinton et al., 1996; Jones et al., 1998), and so

demonstrating that the generalist-predator models provide a better explanation for spongy moth outbreaks is not crucial to our overall argument. Understanding why the models that include the generalist predators provide a better fit to the data is nevertheless important for understanding our later result that the importance of generalist predators exacerbates the effects of climate change. Specifically, as Figure 3.4 shows, the major advantage of the models with generalist predators is that they are better than the no-predator models at explaining the time between the introduction of the fungus and 2017 outbreak. This effect occurs because generalist predators can suppress spongy moth outbreaks, thus increasing the time interval between outbreaks. Dwyer et al. (2004) showed that this effect leads to highly variable times between outbreaks in models with only the baculovirus and generalist predators; our results here show that in models with both pathogens and generalist predators outbreak intervals are often much longer than in models with both pathogens but no generalist predators.

To emphasize the difference between the with-predator and without-predator models, Table 3.4 shows summary statistics of the model projections of the time to the first outbreak in Massachusetts and Connecticut following the introduction of the fungus. As the table shows, the mean interval is slightly longer for the with-predators model than for the no-predator model in Massachusetts and slightly shorter for the with-predator model than for the no-predator model in Connecticut. Given these small differences, Table 3.4 shows that the main reason why the with-predator models better explain the long interval between the introduction of the fungus and the 2017 outbreak is that the probability of very long intervals is much higher for the with-predator models than for the no-predator models. With respect to both Massachusetts and Connecticut, the fraction of intervals longer than 20 years is much higher for the with-predator models, as is the fraction of realizations that have no outbreaks after fungus introduction at all. In the models with predators, the predators are much more likely to maintain spongy moth densities at a low level with no outbreaks.

These effects are also apparent when we directly compare model projections to the data. As Figure 3.5 illustrates, the projections of both the with-predator and without-predator models are highly stochastic, and the fit to the data is therefore highly approximate. It is nevertheless true that in general the models with predators project later outbreaks than the models without predators, and are thus better at projecting the 2017 outbreak in both Massachusetts and Connecticut.

To quantify the dynamics of our models in the absence of the fungus, in Table 3.5 we show summary statistics for model realizations in which the fungus was never introduced. Again, the with-predator models project an average time between outbreaks that is much closer to the average outbreak interval in the pre-fungus era, therefore generating slightly higher likelihood scores with respect to the pre-fungus outbreak period. It is also worth noting that the with-predator models are more likely to project that no outbreaks will occur at all, emphasizing the importance of stochasticity in this system.

A final point is that the without-predator models do slight better at reproducing resting spore densities and the length of the 2017 outbreak (Figure 3.4, Table 3.6 and Table 3.7). As Table 3.3 makes clear, however, the overall likelihood is much more sensitive to the change in the outbreak interval, and so the with-predator models have better overall likelihoods.

3.4.2 Model phase portraits

The important role of generalist predators in spongy moth dynamics can be usefully visualized through three-dimensional phase portraits of host, virus and fungus density for each model (Figure 3.6). For models with predators, host densities spend long periods at relatively low levels, with occasional outbreaks, following a behavior similar to the analogous long-term virus-only model (Dwyer et al., 2004). This behavior thus explains the frequent occurrence of long intervals between outbreaks that gives the with-predator models better likelihood scores.

Meanwhile, in the phase portraits for the no-predator models the host density is much more variable, reflecting the high stochasticity that the no-predator models must invoke to explain the data. For the no-predator models, the model trajectories essentially fill all the space within an oval, rather than being clustered at the apparent low-density equilibrium seen in the with-predator models. The no-predator models therefore tend to produce repeated, highly stochastic cycles, so that long intervals between outbreaks typically only occur because of stochasticity rather than because the generalist predators suppress the host population.

Another important difference is that in the no-predator models host density seldom exceeds 10, whereas in the with-predator models the host density can reach values higher than 100. The with-predator models are thus better at projecting the outbreaks with high spongy moth densities that often occur in nature. As we will show, this difference in amplitudes is important because our models project that it will be strongly influenced by climate change.

3.4.3 Effects of weather

Our model fitting results show that the long interval between the introduction of the fungus and the 2017 outbreak is best explained if we include generalist predators in our models. Here we show that generalist predators will also likely play a significant role in strengthening the effect of climate change on the spongy moth.

As mentioned in the introduction of this chapter, it is at least possible that the 2017 New England outbreak was due to the suppression of the fungus due to hot, dry weather in the years before the outbreak. Indeed, as Figure 3.1 shows, maximum daily temperature rose sharply after 2010 in Massachusetts and moderately in Connecticut and relative humidity and rainfall were low around 2017 in both states, consistent with the hypothesis that the outbreak around 2017 (Figure 3.3) was partly driven by weather. To test this hypothesis more quantitatively, we replaced the weather for 2010-2019 in our models with the weather for 2000-2009, and we re-generated model summary statistics. Our goal was thus to determine

the extent to which hot, dry weather in the period 2010-2019 led to the 2017 outbreak.

As Table 3.8 shows, replacing the 2010-2019 weather data with the 2000-2009 data always leads to a larger percentage of realizations that produce no outbreaks, or outbreaks that are later than the 28 years from fungus introduction observed in the defoliation data. We therefore conclude that recent hot, dry weather helps to explain the 2017 outbreak. To the extent that this hot, dry weather is due to climate change, the 2017 spongy moth outbreak also appears to be a result of climate change.

Table 3.8 further shows that in the with-predator models the fraction of realizations in which outbreaks occur at 28 years or more after the fungus introduction is much higher than for the no-predator models. This effect occurs because the with-predator models are more likely to maintain the spongy moth near a low-density equilibrium, while models without predators are more likely to generate sustained cycles. In each state, the increase in percentages of late outbreaks when using the replacement weather data is thus larger in the model with predators than in the model without predators.

3.4.4 Projecting the effects of climate change on spongy moth outbreaks

As we mentioned, the weather projection data from our down-scaled climate-change model include only 10 years in the past and 10 years in the future, and so we generated projections by randomly drawing annual weather conditions in the years after the first 10 years. We then generated 500 realizations of each model in the representative location we chose, using random initial values of host and virus densities. For the initial fungus density, in the first year we used a value of 5.55×10^{-3}, which is the mean fungus density of estimates in Kyle et al. (2020) after excluding an outlier value (see Table 3.1). We then calculated the mean number of outbreak peaks, the mean outbreak interval and the mean outbreak amplitude across all 500 realizations, and we calculated a coefficient of variation of the outbreak interval to quantify variation in the outbreak interval.

As Table 3.9 shows, both our with-predator and no-predator models project that climate change in Massachusetts will have modest effects on the time between outbreaks. Our with-predator model, however, projects that in Massachusetts the amplitude of outbreaks will increase by a factor of more than 1.5, while the no-predator model projects that the amplitude will increase by a factor of about 1.25. Table 3.10 then shows that similar but stronger trends hold in Connecticut, where the time between peaks is projected to increase slightly in the future, and the number of peaks and the amplitude for the with-predator model are projected to increase sharply in the future, such that the amplitude will increase by a factor of 2.2. To confirm that these differences were not simply due to chance, we again used t-tests to determine if there were significant differences (Rice, 2006) between model projections that use historical weather projections (Hist) and model projections that used future weather projections (Fut, note that we have only one value for the CV of outbreak intervals, and therefore do not carry out a significance test for the CV). In all cases, $p < 10^{-5}$, confirming that the effects of climate change projected by our models are not simply due to chance.

Given that an increase in the amplitude of outbreaks can strongly increase tree mortality, our results suggest that climate change will strongly worsen the impact of the spongy moth, principally by leading to more severe outbreaks. Moreover, the high baseline for the with-predator models means that the effects of climate change are likely to be far, far worse than one would expect from the no-predator models. Allowing for both pathogens and generalist predators thus gives very different conclusions about the effects of climate change than does a model with the two pathogens but not generalist predators.

To better understand the effects of climate change, we also recorded the average fraction infected by the fungus and the baculovirus over 500 realizations. As Table 3.11 shows, in Massachusetts the average fraction infected by the fungus is projected to fall slightly in the future, while the fraction infected by the virus is projected to increase slightly. These effects

occur because in Massachusetts rainfall and relative humidity are projected to decline, while temperatures are projected to increase; because all three changes reduce fungal infection rates, the fraction infected with the fungus is projected to decline, with a consequent increase in the fraction infected by the baculovirus.

In Connecticut in contrast, the situation is reversed, in that the fraction infected by the fungus is projected to increase, while the fraction infected by the baculovirus is projected to decline. This difference likely occurs because the reductions in temperature projected for Connecticut will be beneficial for the fungus, and will apparently outweigh the negative effects of reduced rainfall and relative humidity. Meanwhile, the reductions in the fraction infected by the baculovirus are projected to be quite severe in Connecticut, and likely explains why the climate change will lead to even stronger increases in the amplitude of spongy moth outbreaks in Connecticut. These effects emphasize the complex ways in which climate change can alter pathogen competition, and illustrate the importance of this competition for long-term host-pathogen population cycles.

It is also worth noting that the coefficient of variation of the outbreak interval is always at least modestly lower in the future, suggesting that outbreaks will occur somewhat more regularly in the future. Also, the decrease in the CV of the outbreak interval tends to be larger in the with-predator models, again emphasizing that the projected effects of climate change are stronger when generalist predators are present. To see these effects more clearly, in Figures 3.7 and 3.8 we show each summary statistic with error bars (+1/-1 standard deviation) that indicate the extent of variation across realizations. As the figures show, the size of the error bars is generally smaller in Fut compared to in Hist, especially for the with-predator models, re-emphasizing that climate change has bigger effects in the with-predator models than in the no-predator models.

For models with predators, the variation in the outbreak interval comes mainly from small-scale oscillations at relatively low host densities, representing oscillations around what

appears to be a stable, low-density equilibrium. These oscillations are too small to count as outbreaks, and so the with-predator models have fewer outbreaks and longer outbreak intervals, thus increasing variation in the outbreak interval. In the no-predator models, the error bars instead result from variation due to the high levels of stochasticity that those models need to reproduce the defoliation data.

Although we have here emphasized the role of generalist predators, it is important to remember that the effects of climate change in our model are largely due to the effects of climate change on the fungus. To see this, we re-ran our models using best-fit parameter sets for both historical and future weather data, but we did not introduce the fungus. In these long-term virus-only models, weather serves to determine the speed of kill of initial virus infections and the length of epizootics; the effects of climate change are thus less profound, but as Fuller et al. (2012) showed changes in epizootic length in such models can nevertheless have strong effects on spongy moth dynamics. In our case, however, the only effect of climate change was to alter the outbreak amplitude in the with-predator models in both states very slightly (MA: historical 24.79, future 23.50, t-test $p = 0.0076$; CT: historical 17.22, future 19.19, t-test $p = 8.60 \times 10^{-5}$); all other summary statistics were the same between historical and future climates (t-test results gave $p >> 0.05$ in all cases). The effects of climate change in our models thus occur because climate change strongly affects fungus transmission and survival.

The importance of the fungus in our results suggests an explanation for why the presence of generalist predators exacerbates the effects of climate change on outbreak severity in our models. In the with-predator models, outbreaks occur when stochasticity allows the host population to increase to a level at which generalist predators are unable to control the host. At that point, mixed virus-fungus epizootics drive the host population down to low levels, so that the generalist predators can again control the host. When climate change reduces the ability of the fungus to control the host, the host is able to climb to high levels, increasing

the amplitude of outbreaks and exacerbating the effects of climate change.

In models with no predators in contrast, outbreaks are also due to stochasticity, but the model dynamics are closer to the regular cycles of classical host-pathogen population cycles. Outbreaks are therefore sufficiently regular that the model dynamics are only moderately changed by a reduction in the effectiveness of the fungus. The effect of climate change on the with-predator models is therefore to directly interfere with mechanisms that drive spongy moth dynamics, whereas the effect of climate change on no-predator models is therefore to simply alter what was already a highly stochastic system.

3.5 Discussion

By fitting our models to data on long-term defoliation caused by the spongy moth we showed that a model with predators provides a much better explanation for data from Massachusetts, and a slightly better explanation for data from Connecticut (Table 3.3). Most of the improvement in fit occurs because models with predators do better at predicting the time between the introduction of the fungal pathogen *E. maimaiga* in 1989 and the first region-wide New England outbreak in 2017. Although the no-predator models can also sometimes reproduce the long time interval between fungus introduction and the 2017 outbreak (Table 3.4), the with-predator models can generate intervals of 20 or more years much more often in Massachusetts, and slightly more often in Connecticut.

Previous work had shown that generalist predators can strongly increase variation in outbreak intervals in the spongy moth (Dwyer et al., 2004; Elkinton et al., 1996). Our fitting results are nevertheless important because they provide some of the first statistical evidence that models invoking both pathogens and predators provide a better explanation for spongy moth dynamics. Moreover, by assigning a value of more than 100 years to the interval in realizations with no outbreaks, our likelihood scores fundamentally disfavor the with-predator models, and so our approach is conservative.

The real importance of our fitting results is that they allowed us to quantify the roles of the two pathogens with and without the predators, which is essential when we try to understand the effect of climate change on spongy moth dynamics. Inserting projected weather from down-scaled climate change models into our models then yields projections that climate change will worsen spongy moth outbreaks. In both Massachusetts and Connecticut, with-predator models and no-predator models project at least mild increases in outbreak frequency in the future; more importantly, however, the with-predator models predict substantial increases in outbreak amplitudes (Table 3.9 and 3.10). This latter result is important because it makes clear that our projections of the effects of climate change strongly depend on the number of species that we include in our models.

The effect that climate change leads to more frequent and fierce *L. dispar* outbreaks in models with predators occurs because generalist predators can together help the fungal pathogen to suppress the insect host population density until a severe outbreak happens. When weather conditions become hotter and drier in the future, the fungus will be much less effective at controlling the spongy moth, but a combination of the virus and generalist predators is unlikely to be able to suppress outbreaks, as shown by previous work on long-term virus models (Dwyer et al., 2004; Fuller et al., 2012). We therefore conclude that multi-species interactions can strongly alter the projections of the ecological consequences of climate change, emphasizing the complex effects that climate change can have on natural ecosystems, and the necessity of considering multi-species interactions when studying effects of climate change on ecosystems.

Previous studies on effects of climate change on other forest insects in some cases reached different conclusions. For example, Haynes et al. (2014) showed that outbreaks of two moth species (*Panolis flammea* and *Dendrolimus pini*) were less likely at high temperatures, while outbreaks of the common pine sawfly *Diprion pini* became more likely at high temperatures. Other studies similarly showed that warm temperature can be either beneficial or deleteri-

ous to insect populations (Pureswaran et al., 2018); for example, higher temperatures almost certainly caused the recent outbreaks of some bark beetle species such as the mountain pine beetle *Dendroctonus ponderosae*. Defoliators can also respond differently to high temperature; the moth species *Thaumetopoea pityocampa* responded positively to high temperature in Europe with more outbreaks, for example, while Saturniid caterpillars appeared to have less severe outbreaks in tropical forests with high temperature.

The differences in these conclusions mainly have to do with the methods and mechanisms that were used in each study. The results in Haynes et al. (2014), for example, mostly rely on statistical regressions to connect insect population densities with weather conditions. Many other studies of the effects of climate change on different insect species attempt to understand how temperature will affect metrics of insect physiology and development, such as diapause, speed of larval growth, and waves of larval feeding (Haynes et al., 2014; Pureswaran et al., 2018), rather than how temperature will affect interactions between forest insects and their natural enemies. Other studies have focused on connecting insect density to tree or foliage growth, quantifying how high temperatures favor tree growth, generating high-quality foliage to feed more insects, or how asynchrony between insect development and tree growth could cause adverse effects on herbivorous insects (Pureswaran et al., 2018).

Studies that do allow for species interactions in contrast often face a lack of data, leading in turn to a reliance on very simple models. For example, a study on tawny owls (Millon et al., 2014) suggested that the owl population would be under the risk of extinction due to dampened prey cycles, but this conclusion was not based on mechanistic predator-prey models. The parameters related to owl physiology and demography were estimated by fitting linear models to data, and the models were used to project future dynamics for only a modest period into the future. Meanwhile, a study of the parasitoid *Trichogramma minutum* attacking spruce budworm (*Choristoneura fumiferana*) showed that the parasitoid likely benefited from higher temperature (Quayle et al., 2003), an effect that may be quite

general for parasitoids. In our case in contrast, the fungal pathogen is suppressed by increased temperature and decreased relative humidity, emphasizing the necessity of understanding the underlying biology of species interactions for projecting the ecological consequences of climate change, and the difficulties of making such projections.

Our results can provide suggestions on future spongy moth management strategies. Our projections show that climate change will likely allow spongy moth to make at least a moderately strong comeback in the 21st century, thus worsening damage to hardwood forests and oak decline (Haavik et al., 2015; Morin and Liebhold, 2016). One possible response to this change may be a broader use of the bacterial insecticide produced by *Bacillus thuringiensis* var. *kurstaki* (Btk). A shortcoming of Btk, however, is that it kills multiple species of nontarget Lepidoptera (Peacock et al., 1998), and is therefore increasingly unpopular. The species-specificity of the baculovirus spray "Gypchek" in contrast means that it has almost no non-targe effects (Wood and Granados, 1991), but baculovirus production is very expensive. Our work nevertheless suggests that finding ways to make Gypchek cheaper is an important priority for spongy moth management in the future.

3.6 Tables and figures

Table 3.1: Estimated resting spore densities at multiple sites across 3 years in the lower peninsula of Michigan from Kyle et al. (2020). The lowest value, which is around 10^{-12} at the 2011 South site, is an extreme outlier, and we therefore do not use it in our likelihood function.

Site	Median fungus density	95 % HPD
2010 South	1.83×10^{-2}	$[1.45 \times 10^{-2}, 2.23 \times 10^{-2}]$
2010 Central	5.71×10^{-3}	$[4.72 \times 10^{-3}, 6.90 \times 10^{-3}]$
2010 North	1.87×10^{-3}	$[1.48 \times 10^{-3}, 2.31 \times 10^{-3}]$
2011 South	1.08×10^{-12}	$[1.02 \times 10^{-12}, 1.15 \times 10^{-12}]$
2011 Central	2.33×10^{-3}	$[1.96 \times 10^{-3}, 2.75 \times 10^{-3}]$
2012 Central	4.39×10^{-3}	$[3.98 \times 10^{-3}, 4.86 \times 10^{-3}]$
2012 North	6.91×10^{-4}	$[4.85 \times 10^{-4}, 9.36 \times 10^{-4}]$

Table 3.2: Maximum likelihood estimates of parameters in models with and without predators in Massachusetts and Connecticut.

Parameter	Symbol	Massachusetts		Connecticut	
		With predators	No predators	With predators	No predators
DD for virus to start infection	VDD	57.36	51.40	71.31	46.28
Baseline host fecundity	λ	17.14	2.40	15.09	2.30
Enhanced susceptibility to fungus	ζ	49.05	34.37	19.98	27.62
Initial fungus density	f_{init}	2.30×10^{-5}	1.50×10^{-5}	6.40×10^{-5}	7.10×10^{-5}
Long-term fungus survival rate	γ_f	0.15	0.14	0.19	0.19
SD of stochasticity in fecundity	σ_ϵ	0.03	0.62	0.20	0.51

Table 3.3: Components of log maximum likelihood scores across models and across Massachusetts and Connecticut data.

Category	Massachusetts		Connecticut	
	With predators	No predators	With predators	No predators
Total Likelihood	-9.11	-10.38	-10.16	-10.35
Interval to 1st peak after fungus intro	-3.95	-4.78	-4.65	-4.83
Outbreak length of that 1st peak	-2.69	-2.28	-2.75	-2.23
Average fungus density	-0.47	-0.41	-0.56	-0.45
Virus-caused periods	-2.47	-2.78	-2.66	-2.83

Table 3.4: Summary statistics from fitting models to the interval between fungus introduction and the first host density peak afterwards. MA indicates Massachusetts and CT indicates Connecticut. The column "Mean interval" gives the average interval from the introduction of the fungus to the first outbreak, the column "C.V. interval" gives the coefficient of variation of the same interval, and the column "Pct. interval ≥ 20" gives the percentage of realizations for which the interval was 20 or more years. In all cases we exclude realizations with no outbreaks after the introduction of the fungus, while the last column indicates the percentage of realizations with no outbreaks after the introduction of the fungus.

Model	Mean interval	C.V. interval	Pct.interval ≥ 20	Pct.no peaks
MA with predators	13.57	0.550	24.40	16.80
MA no predators	12.72	0.469	13.40	2.60
CT with predators	12.31	0.559	18.60	17.60
CT no predators	13.55	0.435	17.20	5.40
Defo. data MA & CT	28			

Table 3.5: Summary statistics of the model projections of outbreak periods in the absence of the fungus. MA represents Massachusetts and CT represents Connecticut. The columns "Mean period" and "C.V. period" give the average periods between outbreak peaks and the corresponding coefficients of variation, excluding realizations with no outbreaks. The column "Pct. no peaks" indicates the percentage of realizations with no outbreaks.

Model	Mean period	C.V. period	Pct. no peaks
MA with predators	9.18	0.122	33.00
MA no predators	13.38	0.214	1.50
CT with predators	9.62	0.148	42.50
CT no predators	13.57	0.183	8.00
From filed observation	9		

Table 3.6: Mean values and coefficients of variation of outbreak length in the models and in the defoliation data, excluding realizations with no outbreaks or with peaks too flat to calculate outbreak lengths.

Model	Mean length	C.V. length
MA with predators	3.12	0.98
MA no predators	7.61	0.49
CT with predators	4.09	1.26
CT no predators	7.59	0.37
Defo. data MA & CT	5	

Table 3.7: Mean values, standard deviations and absolute values of coefficients of variation of $\log_{10}$ (fungus density) in our models and in the estimates from Kyle et al. (2020) given in Table 3.1. Since the mean fungus densities on a $\log_{10}$-scale are always negative, the coefficients of variation are also negative on their own, so the absolute values are shown here.

Model	Mean	Sd.	C.V.
MA with predators	-2.19	0.54	0.25
MA no predators	-2.13	0.54	0.25
CT with predators	-2.11	0.45	0.21
CT no predators	-2.10	0.40	0.19
Kyle et al. (2020) estimates	-2.48	0.48	0.194

Table 3.8: Percentages of realizations in which the interval from fungus introduction to the first outbreak is 28 years or more. "Realistic weather" refers to the model realizations generated from actual weather data while "Substitued weather" refers to model realizations in which we substitute weather data from 2000-2009 for weather data from 2010-2019.

Model	Realistic weather	Substituted weather
MA with predators	17.8	21.4
MA no predators	3.00	3.40
CT with predators	18.0	20.2
CT no predators	6.00	7.40

Table 3.9: Summary statistics for model projections with or without predators in Massachusetts. "His" refers to model realizations generated using historical weather, meaning weather from the period 1995-2004, while "Fut" refers to model realizations generated using future weather, meaning weather for the period of 2085-2094 under the RCP 8.5 climate change scenario.

Model, Weather	No. Peaks	Interval	Amplitude	CV of Interval
Predator, Hist	14.02	13.84	65.26	0.49
Predator, Fut	14.93	13.19	107.47	0.36
No Predator, Hist	13.61	13.84	1.70	0.64
No Predator, Fut	14.52	13.14	2.12	0.61

Table 3.10: Summary statistics for models with and without predators in Connecticut, with column headings as in Table 3.9. In the row "Predator, Hist", 11 realizations out of 500 generated no peaks and were therefore excluded from our calculations of summary statistics for peak interval and amplitude.

Model, Weather	No. Peaks	Interval	Amplitude	CV of Interval
Predator, Hist	7.89	20.53	32.20	1.00
Predator, Fut	11.12	17.48	71.87	0.53
No Predator, Hist	10.94	17.12	1.14	0.63
No Predator, Fut	11.95	15.77	1.31	0.60

Table 3.11: Percentage of insect hosts infected by the fungal or viral pathogen averaged over all years in 500 realizations, for models with and without predators in Massachusetts and Connecticut.

State	Model, Weather	Pct.Inf(F)	Pct.Inf(V)
MA	Predator, Hist	35.6	13.0
	Predator, Fut	34.1	14.0
	No Predator, Hist	30.6	12.3
	No Predator, Fut	29.2	11.9
CT	Predator, Hist	34.1	13.6
	Predator, Fut	35.3	10.2
	No Predator, Hist	26.7	15.4
	No Predator, Fut	28.3	13.5

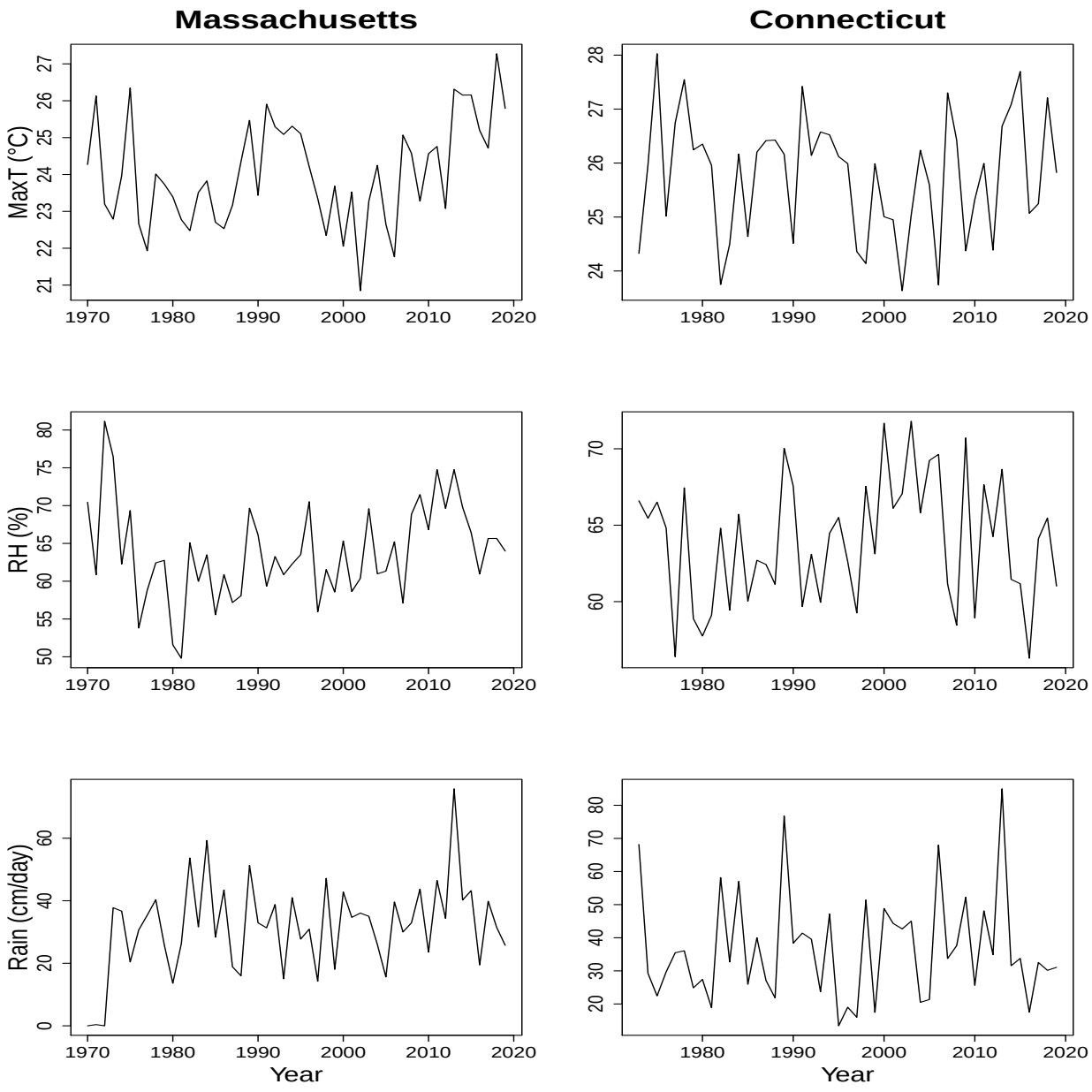

Figure 3.1: Average values of daily maximum temperature, relative humidity and rainfall in two weather stations representing Massachusetts and Connecticut respectively, calculated over the larval period of spongy moth in each year.

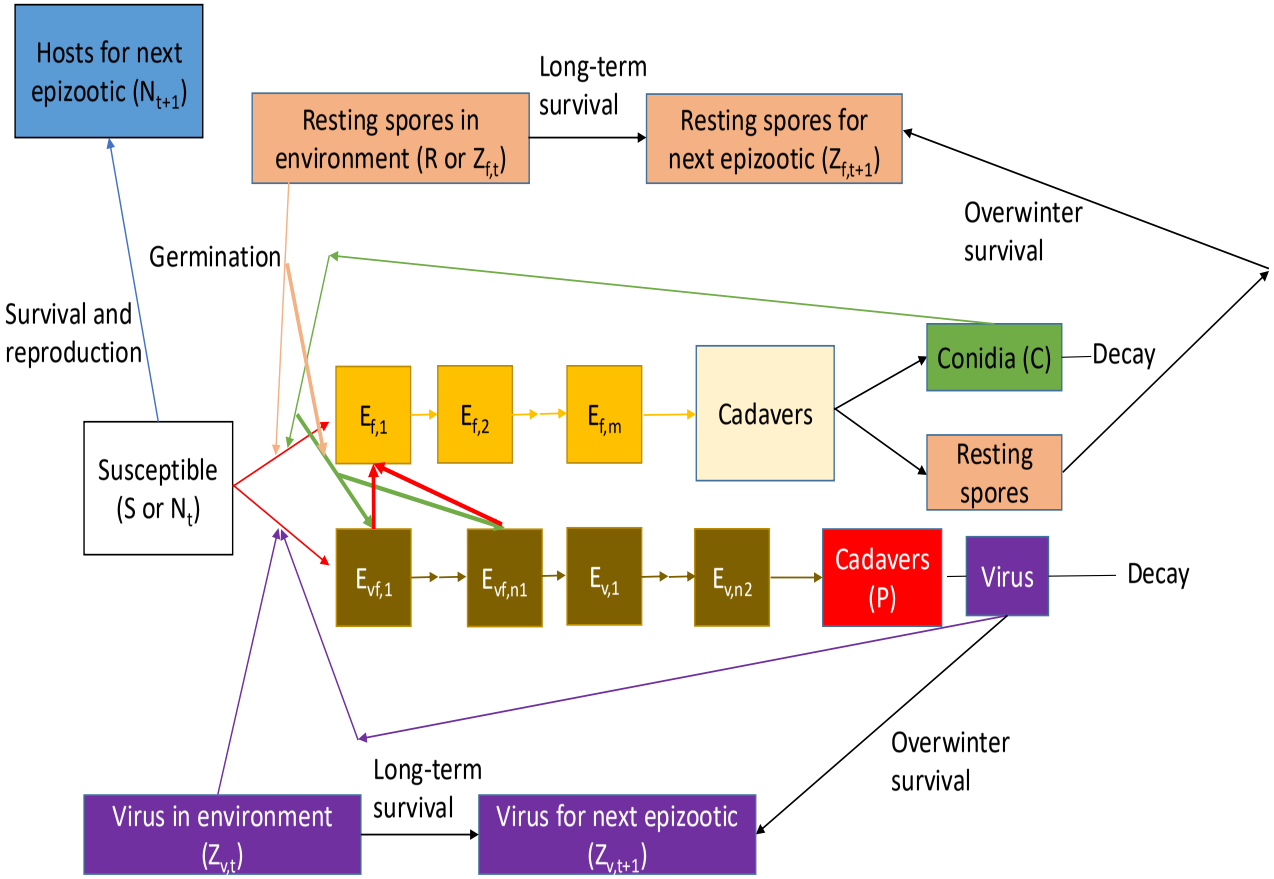

Figure 3.2: Schematic of our long-term fungus-virus model. Here susceptible hosts can be infected by either the fungus (f) or the virus (v). In the early stages after being infected by the virus, hosts in the first few virus-exposed classes, from $E_{vf,1}$ to E_{vf,n_1}, can be coinfected with the fungus, leading to fungal takeovers. This process is represented by the arrows that move into the first fungus-exposed class, $E_{f,1}$.

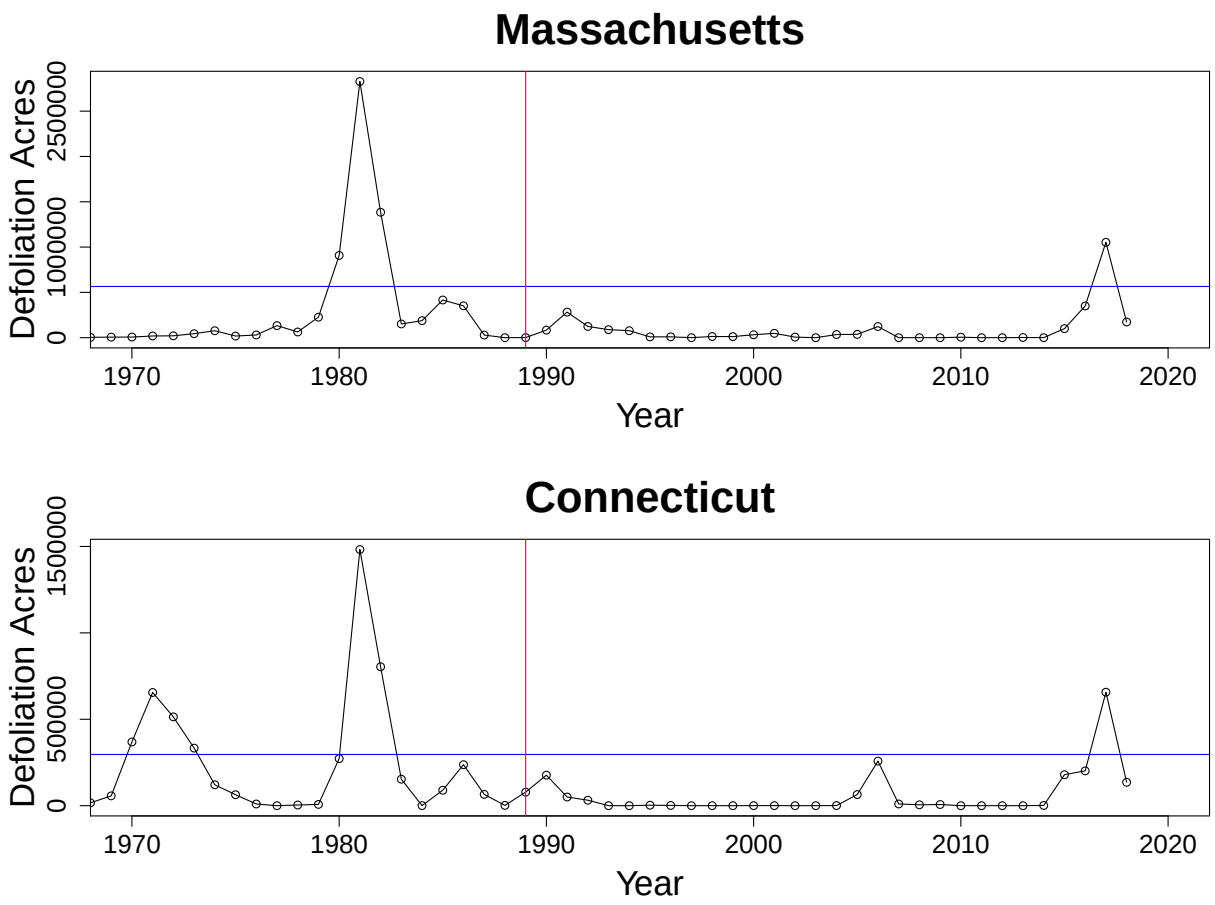

Figure 3.3: Defoliation data for the spongy moth in Massachusetts and Connecticut (U.S. Forest Service, 2022). The red vertical line indicates 1989, the year when the fungus was first introduced into North America. The blue horizontal line in each plot indicates 20% of the maximum defoliation area, which we use as a threshold to indicate when the first peak comes after the fungus introduction in 1989.

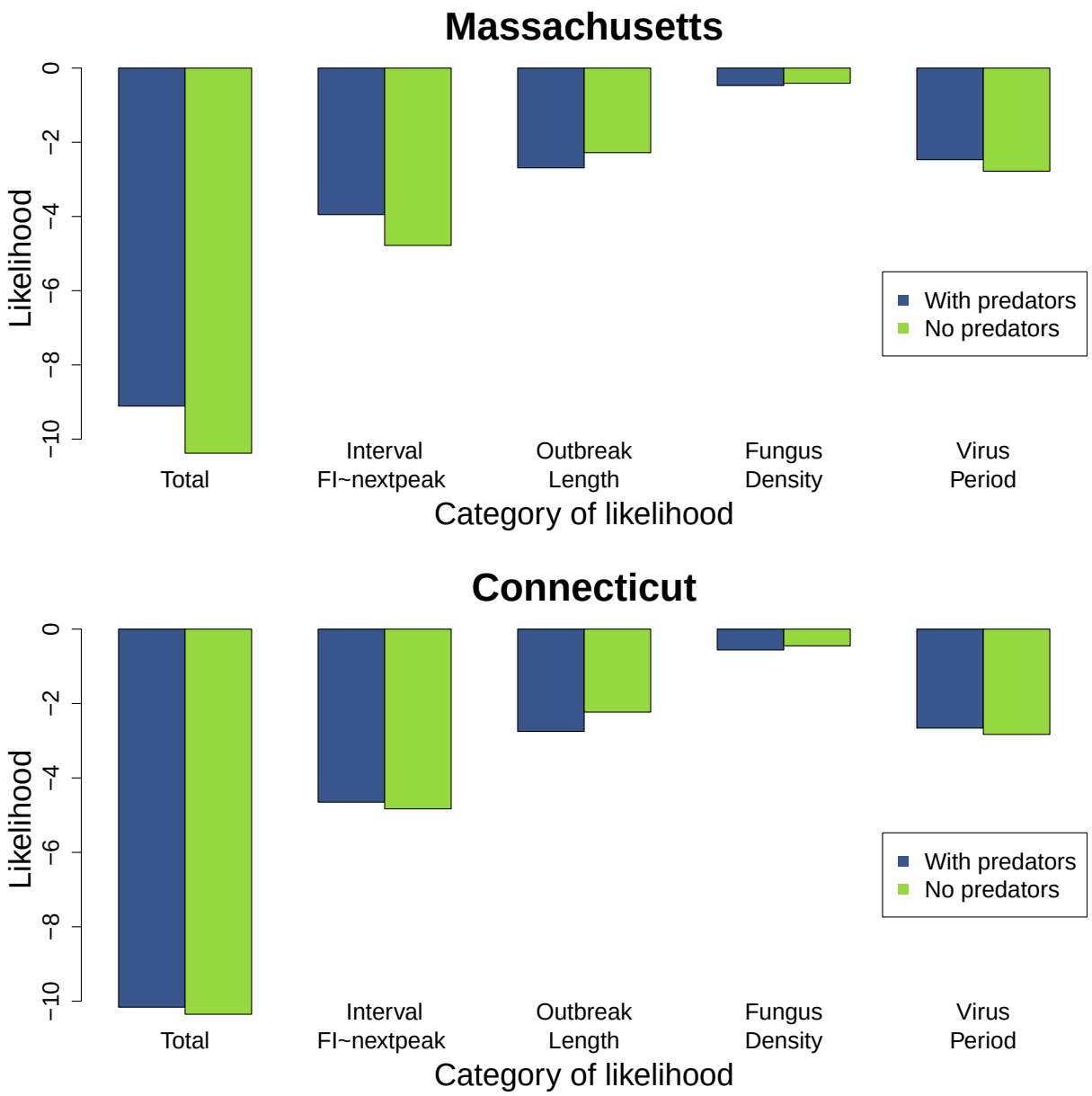

Figure 3.4: Bar plots for each component of our overall maximum likelihood on log-scales. Models with predators and without predators are indicated in different colors. In the second category, "FI∼nextpeak" means the time from the fungus introduction to the next outbreak.

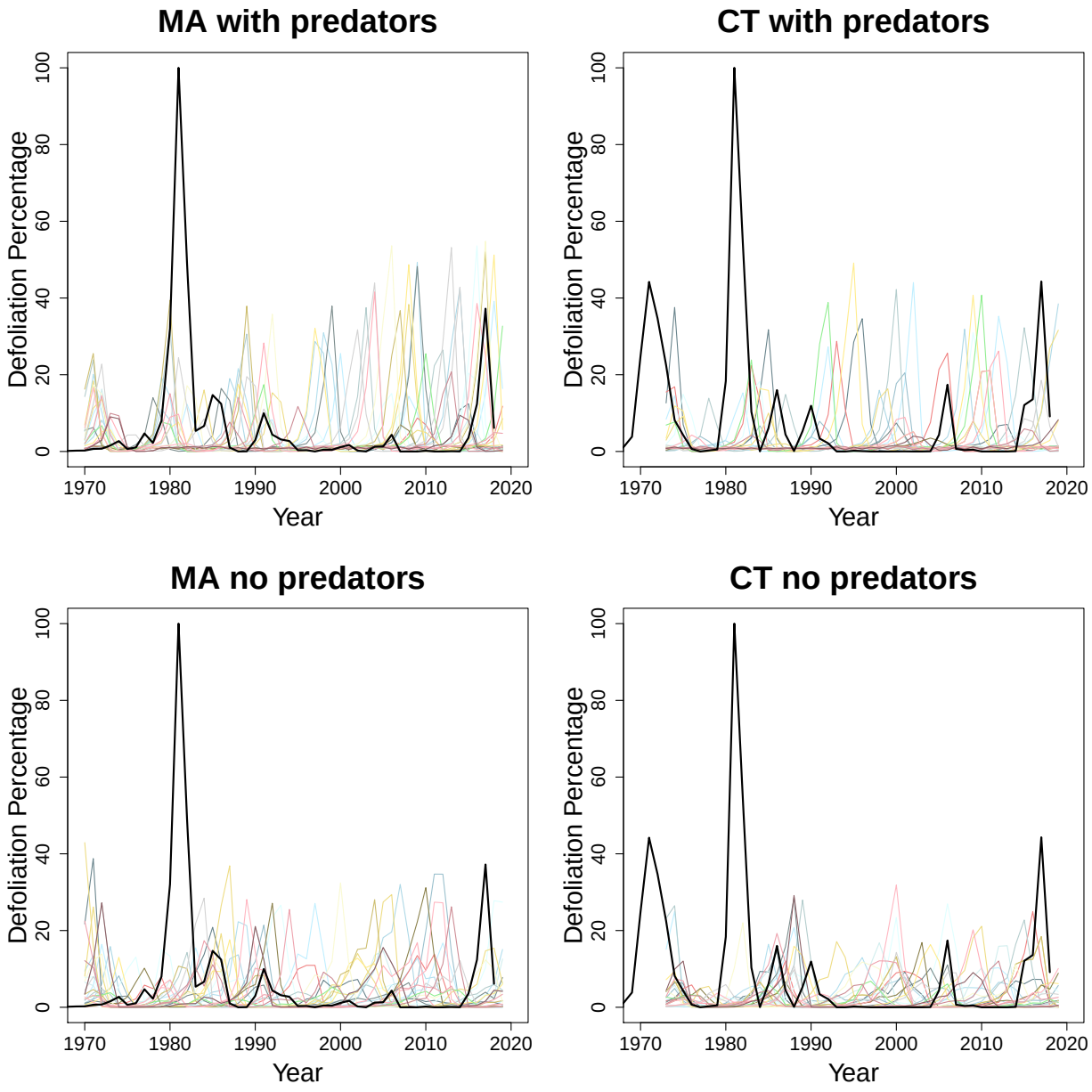

Figure 3.5: Transformed defoliation percentage from model output and from defoliation data. The black line indicates the defoliation data, while the remaining lines indicate model realizations, with each color indicating one of 25 different realizations. Methods and parameters for the transformation can be found in the Appendix (Section 3.7.2).

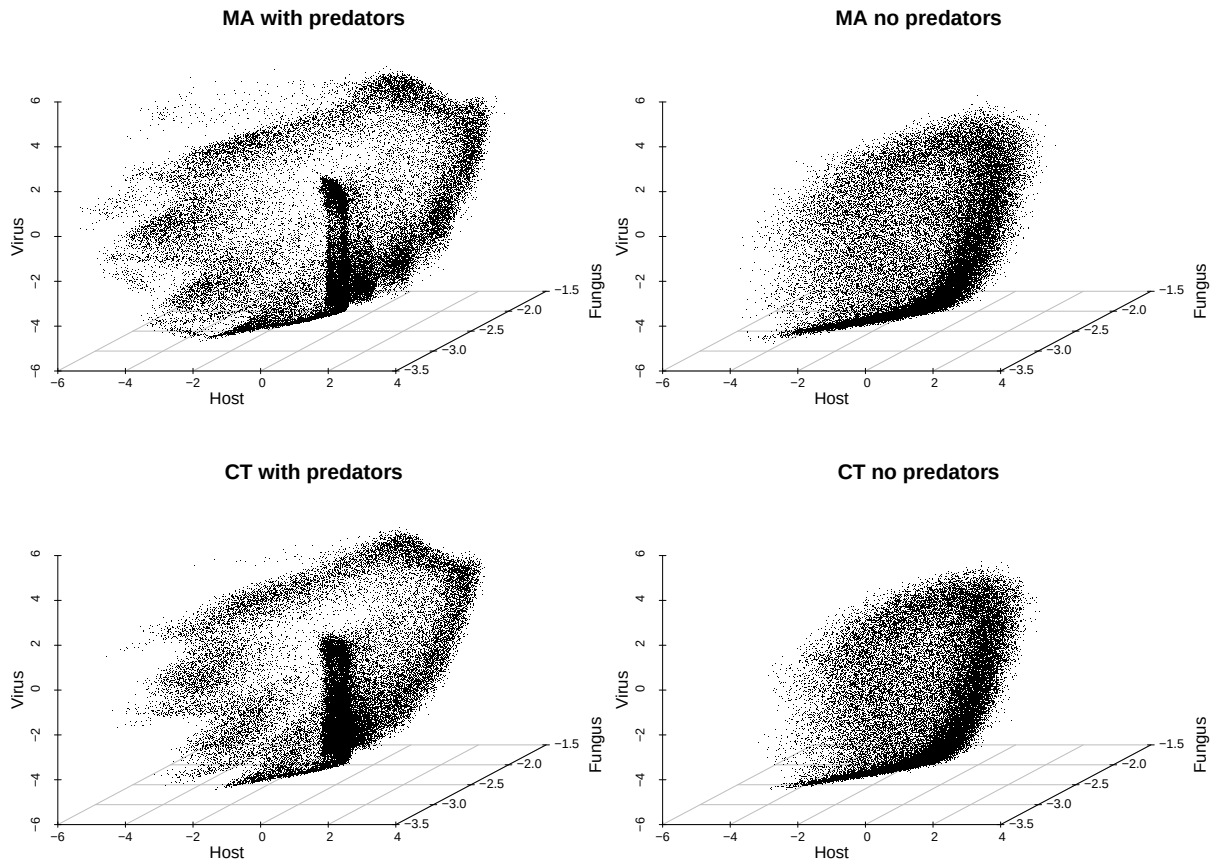

Figure 3.6: 3-dimensional phase portraits for 250 realizations of 200 years of each model under each model's best parameter set. MA represents Massachusetts and CT represents Connecticut. Host, virus and fungus densities are plotted on $\log_{10}$-scales. For years 0-49 in MA and 0-46 in CT, observed weather data are used, while for years 50-199 in MA and years 47-199 in CT, the weather conditions for each year are randomly drawn from one year in the observed weather data. The points represent model output from year 26 to year 199.

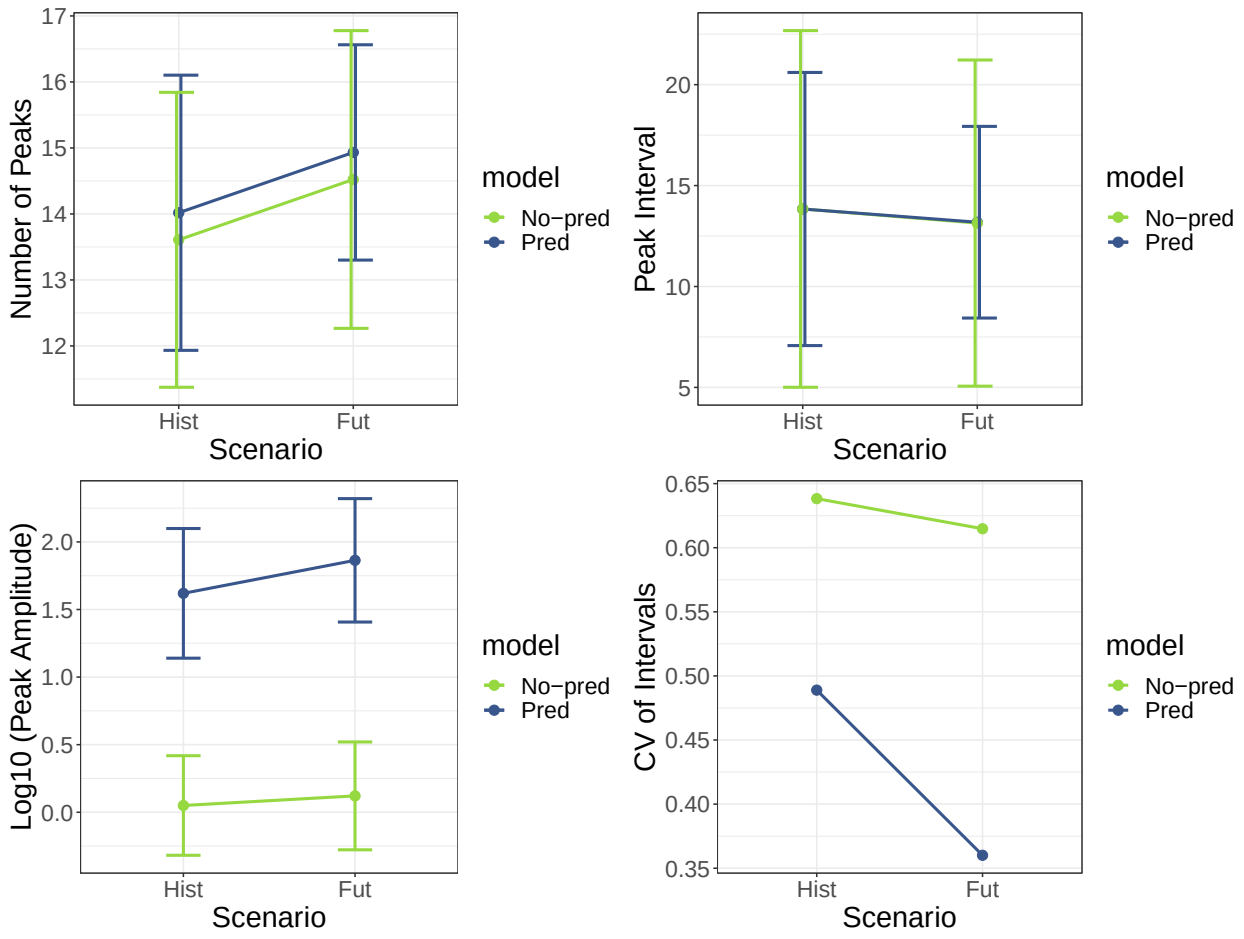

Figure 3.7: Summary statistics with error bars for the models with and without predators in Massachusetts. "Hist" indicates cases in which we used projected weather for the period 1995-2004, while "Fut" indicates cases in which we used projected weather for the period 2085-2094 under the RCP 8.5 climate change scenario. Error bars for the first three summary statistics are ± 1 standard deviation of the mean.

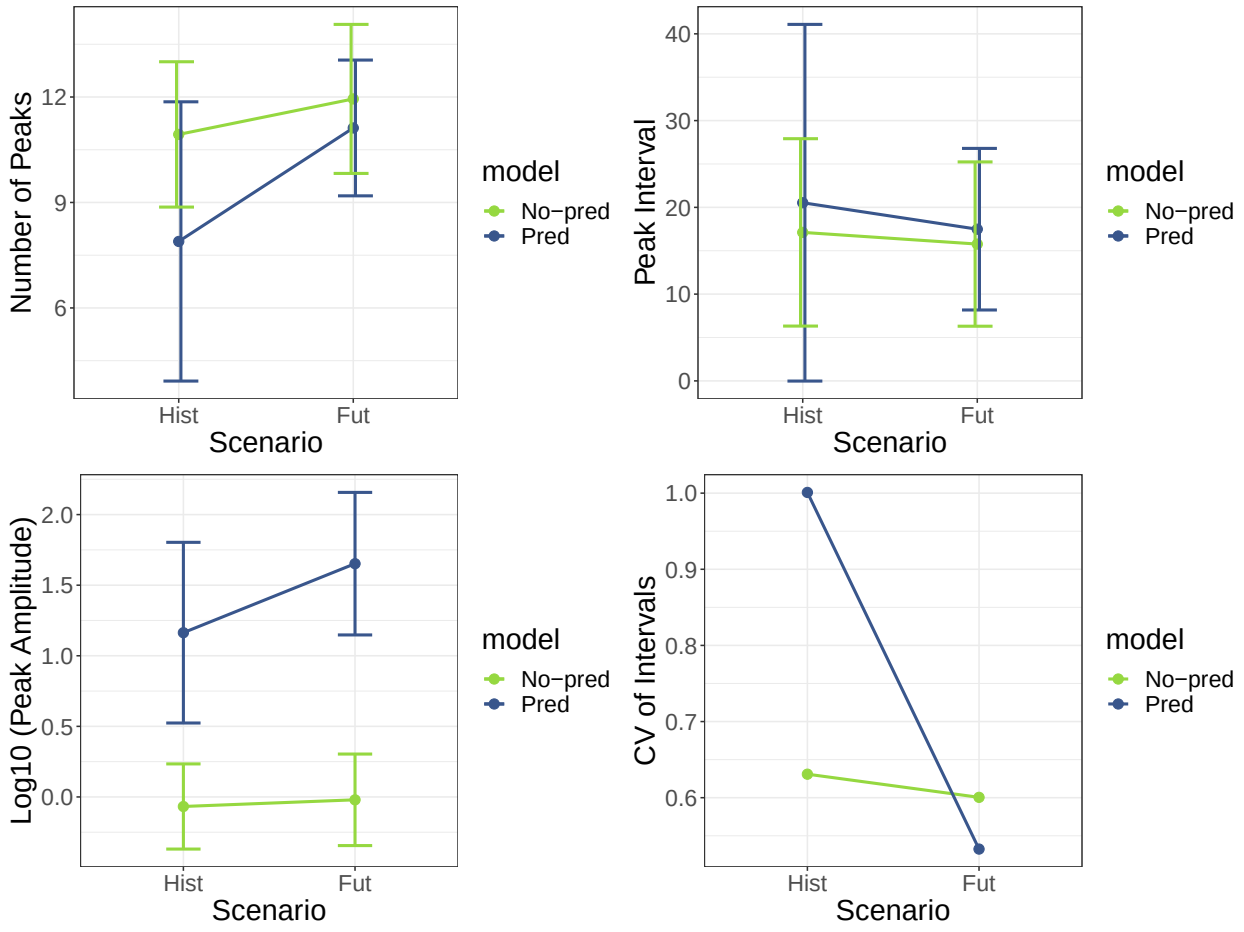

Figure 3.8: Plot of summary statistics with error bars for models with and without predators in Connecticut, as in Figure 3.7.

3.7 Appendix

3.7.1 Weather in single-epizootic models

As mentioned in Methods, we keep using the same weather dependent variables and mechanisms as those in Kyle et al. (2020), while making some extensions. In the two-pathogen single-epizootic model, degree days (DD) with different lower and/or upper thresholds are used to tell when these events should occur: larvae hatch, pupation, start of virus infection (which is equivalent to the timing of initial baculovirus deaths from larvae hatch), start and end of resting spore germination, and production of resting spores rather than conidia in late-instar larvae cadavers. Here we show the equations for calculating degree days again:

$$DD = \sum_{i=t_0}^{t_1} dd(i) \tag{3.27}$$

$$dd(i) = 0 \qquad if \quad T(i) < T_{min} \tag{3.28}$$

$$dd(i) = T(i) - T_{min} \quad if \quad T(i) \in [T_{min}, T_{max}] \tag{3.29}$$

$$dd(i) = T_{max} - T_{min} \quad if \quad T(i) > T_{max} \tag{3.30}$$

In each year, the epizootic starts when eggs hatch after 317 DD with 3 $^{\circ}C$ as the lower threshold and 40 $^{\circ}C$ as the higher threshold (Russo et al., 1993). The epizootic ends when pupation occurs 568.5 DD after hatch, with 7.65 $^{\circ}C$ as the lower threshold and 41 $^{\circ}C$ as the higher threshold (Carter et al., 1992). Resting spores start germination 100.16 DD after hatch, and end germination 267.03 DD after hatch, both with 10 $^{\circ}C$ as the lower threshold (Kyle et al., 2020). As for which type of fungus spore to be generated from fungus-infected cadavers, we use a DD roughly indicating the time when larvae reaches fourth instar. It is 291.27 DD after hatch, with 10 $^{\circ}C$ as the lower threshold (Kyle et al. unpublished work).

$X_{R,\tau} = 0$ for all the days before larvae reach fourth instar, which means they produce conidia after being infected and killed by the fungus. After larvae reach fourth instar, $X_{R,\tau} = 1$ for all days until the end of epizootic, and the fungus-infected cadavers release dormant resting spores instead of conidia into the environment. As for the time when virus starts infection, previous work has not considered the effect of DD, while just letting the virus epizootic last for a certain number of weeks (Dwyer et al., 1997; Fuller et al., 2012). However, we believe that the virus might not start infecting the larvae right after they are hatched, and there are some evidences showing the delay of virus infection from larvae hatch (Woods and Elkinton, 1987). Thus, we assume that the beginning of virus infection can also be determined by DD above 10 $^{\circ}C$ after hatch, similar to what we do to tell the resting spore germination time.

We also keep using the equations for daily transmission and decay rates from our previous single-epizootic fungus model (Kyle et al., 2020):

$$P(\tau) = \frac{\psi_1}{1 + \psi_2 \ \exp(-\psi_3 \ p(\tau))} - \frac{\psi_1}{1 + \psi_2}. \tag{3.31}$$

$$M(\tau) = \psi_4 \exp(\psi_5 \ m(\tau)), \tag{3.32}$$

$$H(\tau) = \psi_6 \exp(\psi_7 \ h(\tau)). \tag{3.33}$$

$$\nu_{R,\tau} = D(\tau) P(\tau) \exp(\epsilon_{R,\tau}), \tag{3.34}$$

$$\nu_{C,\tau} = D(\tau) M(\tau) \exp(\epsilon_{C,\tau}), \tag{3.35}$$

$$\mu_{C,\tau} = H(\tau). \tag{3.36}$$

Here $P(\tau)$ is the effect of rainfall on resting spore transmission rate on day τ, while $M(\tau)$ is the effect of relative humidity on conidia trasmission rate and $H(\tau)$ is the effect of temperature on conidia decay rate. Inside these three functions, $p(\tau)$ is the cumulative rainfall over 10 days before day τ, while $m(\tau)$ is the daily minimum relative humidity and $h(\tau)$ is the daily maximum temperature. Rainfall has a logistic effect on transmission rate of

resting spores. Relative humidity and temperature have exponential effects on transmission and decay rate of conidia. In general, cooler and wetter weather conditions are advantageous for fungal infection. In equation (3.34) and (3.35), we include a degree day function $D(\tau)$ to indicate the effect of larvae size on transmission, and we also include daily inherent environmental stochasticity since the larvae activity pattern may vary each day.

3.7.2 Fixed parameter values in models

We just estimate a few parameters by fitting the models to data. For many other parameters well-known from previous studies, we keep using the values published in literature, and here is a summary of these parameter values. We keep using the values of all parameters on fungus infection during an epizootic from Kyle et al. (2020). The mean transmission rate of virus $\bar{\nu_v} = 0.46$, decay rate of virus-infected cadavers $\mu_v = 0.41$ and number of virus-exposed classes $n = 27$ are from Dwyer et al. (2022). The mean time between baculovirus infection and virus-caused mortality $1/\delta_v = 1/16$ is from Malakar et al. (1999) and our unpublished observation data. C is greater than 1 in the latest version of virus model (Dwyer et al., 2022), but in that case the model requires very high levels of stochasticity in host reproduction, which could affect the accuracy of fitting, so we are using an old-version value $C = 0.86$ from Dwyer et al. (2000). Predation parameters $a = 0.967$ and $b = 0.083$ are from Dwyer et al. (2004). As indicated in work on long-term virus dynamics (Dwyer et al., 2004; Fuller et al., 2012), parameter for virus overwintering rate and enhanced susceptibility to virus in newly hatched larvae ϕ_v is usually in the magnitude of 10^1, and long-term virus survival rate γ_v is almost negligible. Here we use $\phi_v = 40$ and $\gamma_v = 0.001$. For the logistic function of fungus resting spore overwintering, we have $f_{max} = 0.02$, since the largest estimate of fungus resting spore density in Kyle et al. (2020) is about 0.018. We also have $x_0 = -2$ and $x_1 = 0.5$. This function is very helpful to control the fungus resting spore density within the range from 10^{-4} to 10^{-2}, which can cover the magnitudes of most estimates (excluding the

lowest outlier value in the magnitude of 10^{-12}) in Kyle et al. (2020), as Figure 3.9 shows.

To produce Figure 3.5 to see how good the models fit to defoliation data, we want to find a way to keep model output and defoliation data in the same range and unit. The easiest way is to change them into percentages. Regression models have been constructed to transform egg or egg mass density into defoliation percentage (Liebhold et al., 1993). However, we have no information about the total forest area, so we just transform defoliation area into percentages by dividing the annual defoliation area by the maximum defoliation over all years. Since the regression model in Liebhold et al. (1993) is based on different assumptions such as no pathogens, we do not choose to use it directly. Instead, we see that the relationship between host density and defoliation percentage can be roughly drawn into a logistic curve. The logistic function showing the relationship between defoliation percentage and host density N is:

$$Pct_{defo} = \frac{1}{1 + \exp(-\beta_0 - \beta_1 \log_{10}(N))} \tag{3.37}$$

We roughly fit parameters β_0 and β_1 to the defoliation percentage in data, to transform host densities from model output into defoliation percentages, making the figure look better. In Figure 3.5, parameters for models with predators are $\beta_0 = -3.02$ and $\beta_1 = 1.37$. Parameters for models with no predators are $\beta_0 = -1.96$ and $\beta_1 = 1.85$.

3.7.3 Calculating the interval between fungus introduction and the first following outbreak in the models

First, we need a threshold to define whether a host density peak in the model output is considered as an outbreak. In initial simulations of the model, we sometimes observed small sustained oscillations in host density around the magnitude of 10^{-1}; this was especially likely to occur in models with generalist predators, because generalist predators create a low-

density equilibrium (Dwyer et al., 2004). To avoid identifying such oscillations as outbreaks, we used a threshold of $10^{-0.5}$, which is modestly higher than the host densities in the oscillations. Given this definition, we estimated the time to the first outbreak after 1989 by labeling the year of the first host density peak above the threshold $10^{-0.5}$ as year p_1, the second peak as year p_2, and so on.

In rare cases there were peaks in host density almost immediately following the introduction of the fungus, when the fungus was not fully established. Because such peaks would give a false indication of the first outbreak following the introduction of the fungus, we excluded them by searching for the first clear peak in the annual cumulative fraction infected by fungus $I_{f,t}$ as calculated from equation (3.24). To do this, we identified the year of fungus establishment as the first year t in which the cumulative fraction infected by the fungus reached a local peak that was higher than 20% and that was higher than the cumulative fraction infected by virus $I_{v,t}$ (calculated from equation (3.23)). We denoted the year of fungus establishment as f_e. When f_e was very close to the year 1989, we neglected the host density peaks occurring before f_e, treating them as part of the establishment process of the fungus. However, if the establishment was slow, we could not neglect all the host density peaks before that, since they were likely to form defoliation peaks late enough after 1989, and neglecting them may result in finding a too long interval. Thus, we defined another variable t_s as the "threshold" year, and we recorded the year of the first outbreak after t_s. We then calculated the interval y between fungus introduction and the first outbreak after t_s as follows:

$$y = p - 1989 \tag{3.38}$$

$$t_s = f_e \quad if \quad f_e \leq 1992 \tag{3.39}$$

$$t_s = 1992 \quad if \quad f_e > 1992 \tag{3.40}$$

$$p = p_i \qquad if \quad p_1 \leq t_s \quad \& \quad p_i > t_s \tag{3.41}$$

$$p = p_1 \qquad if \quad t_s < p_1 \leq 2019 \tag{3.42}$$

$$p = 2100 \quad if \quad no \quad peaks \quad found \tag{3.43}$$

Here p is the year when the first outbreak occurs in the model after fungus introduction in 1989. Usually $p = p_1$, the year in which the first host density peak above the threshold after 1989; if p_1 occurs within about 3 years after fungus introduction, however, we treated it as part of the establishment process of the fungus. The threshold year t_s is then determined as the smaller of establishment year f_e and 1992. We then defined the year of the first peak above the threshold after t_s, which is p_i in equation (3.41) (typically p_2), as the year of the first outbreak. If there was no host density peak until 2019, which is the end of the weather data, we assigned a very long interval; because here we identify the best model parameters using a maximum likelihood calculation, the value of this interval is unlikely to have affected our results. We then used a Poisson likelihood function to calculate the probability that we observe a 28-year interval between fungus introduction and the first outbreak afterwards given that the mean of the Poisson distribution for that interval is equal to the value in the model.

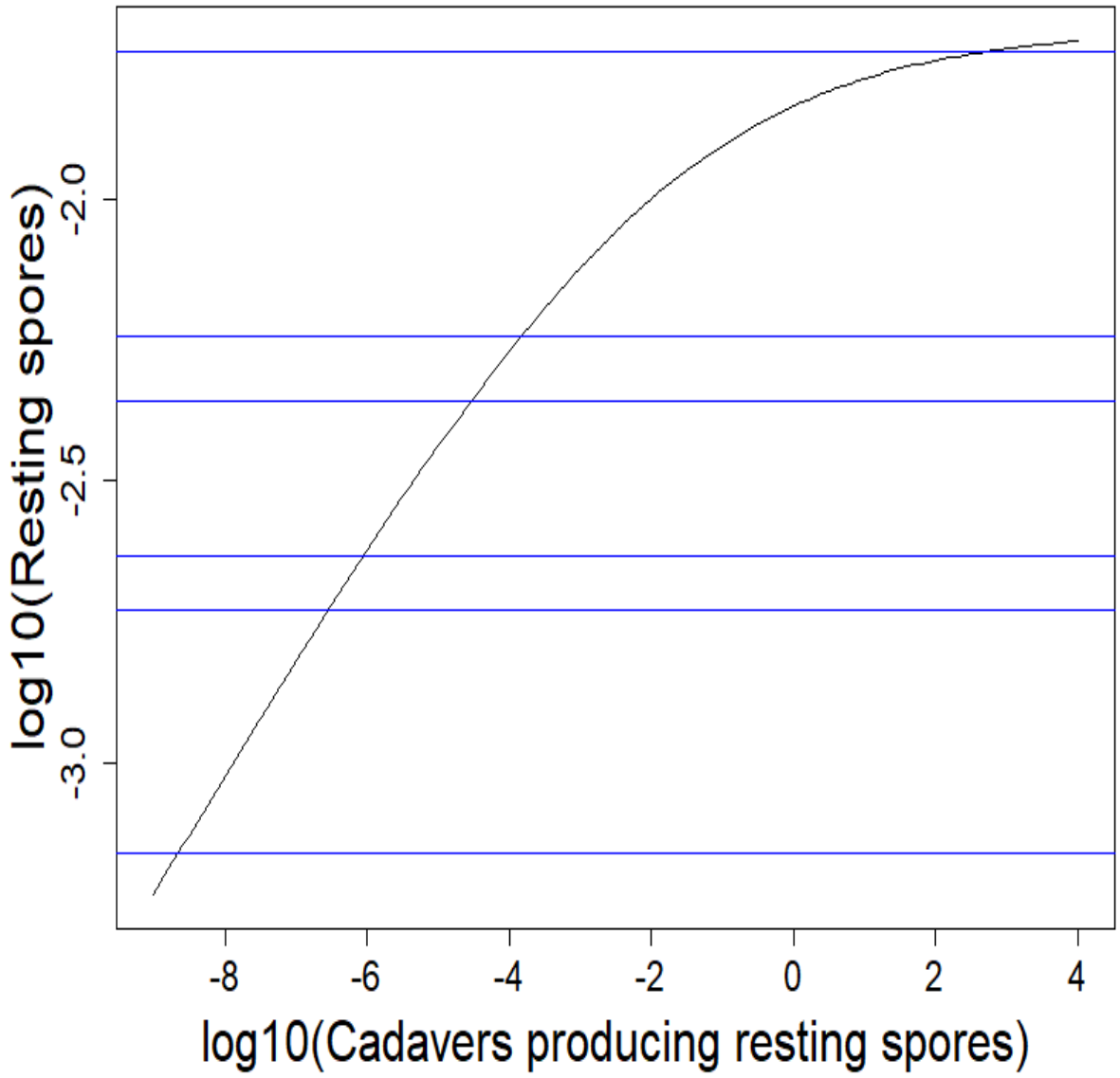

Figure 3.9: The curve for transformation between cumulative cadaver density that produces resting spores to the exact resting spore density, according to the logistic function $R_O = \frac{f_m}{1+\exp[-x_1(\log_{10}(N_t I_{f,R,t})-x_0)]}$, while $f_{max} = 0.02$, $x_0 = -2$ and $x_1 = 0.5$. R_O is the resting spore density which is generated in an epizootic and can survive overwintering, and the y axis here is $\log_{10}(R_O)$. $N_t I_{f,R,t}$ is the density of cadavers that can produce resting spores, and the x axis here is $\log_{10}(N_t I_{f,R,t})$.The blue horizontal lines are estimated resting spore densities from Kyle et al. (2020), while excluding the lowest value which is an extreme outlier.

CHAPTER 4

FUTURE STEPS

We have provided evidence that climate change will strongly affect the spongy moth. Moreover, our model projections indicate that the fungal pathogen *E. maimaiga* will likely do a worse job of controlling spongy moth population densities in the future, with the result being more frequent and more severe spongy moth outbreaks. There are nevertheless several ways in which our results could be made more general, comprehensive and persuasive. In this chapter, we list some possible future directions.

First, as we mentioned in Section 3.3.5, the best parameter sets and the likelihood scores for each model in Chapter 3 were found by line-search. Line-search can be used as the first step in a more statistically robust algorithm known as line-search Markov chain Monte Carlo, or line-search/MCMC. In line-search/MCMC, an initial line search step is used to provide a rough map of the likelihood surface, which is in turn used as input to Principle Components Analysis (PCA). The PCA output is then used to generate automated proposal distributions for MCMC (Kennedy et al., 2015). Our immediate next step will therefore be to use MCMC to generate more robust parameter estimates, as well as uncertainty estimates for the parameters. In the model fitting in Chapter 3 we were estimating the same number of parameters for every model, and so using unadjusted likelihood scores to identify the best model gives the same answer as the Akaike information criterion (AIC) (Burnham and Anderson, 2010). In the case of Connecticut, however, the difference in likelihood scores between model with predators and model without predators was not very large (Table 3.3 and Figure 3.4). Meanwhile, once we implement the MCMC step of line-search/MCMC, we will be able to use the WAIC model-selection criterion to choose between models. Unlike likelihood-based information criteria like AIC, WAIC explicitly penalizes models that produce more variable projections (Watanabe, 2013). This is important because the no-predator models can only explain the defoliation data by invoking high levels of stochasticity (Figure

3.6), and so it is likely that the no-predator models will have much worse WAIC scores than the with-predator models. Using WAIC to choose between models is therefore an important next step.

We also mentioned in Chapter 3 that we fixed the values of some parameters for now to save computing power, but our estimates of some of those parameters are highly uncertain, notably the parameters for logistic fungus overwintering and the parameters that describe predation. In our future work, we will therefore include these parameters in our fitting routines, to determine if allowing for uncertainty in these parameters changes our results. Similarly, although fitting the models to defoliation data in each state separately is in some ways a more statistically robust approach, a general model for both Massachusetts and Connecticut or even more states might be more biologically realistic. In future work we will therefore also consider models in which some parameters are assumed to be the same for different states, to determine whether models with fewer state-specific parameters provide a better fit to the data. Since it is likely that this will mean comparing models with different numbers of parameters, using WAIC to carry out model selections and identify the best model is thus an essential step.

A final next step is to include additional species interactions, and thus to make more accurate projections of the effects of climate change on the spongy moth. For example, in our with-predator models we assumed that the effect of generalist rodent predators is independent of predator densities, on the assumption that predator densities are constant. Rodents are indeed important generalist predators of the spongy moth (Elkinton et al., 1996), but some studies have shown not only that rodents have population cycles, but that climate change can collapse these population cycles (Ims et al., 2008; Kausrud et al., 2008; Korpela et al., 2013). Our assumption that the predators always have the same predation rate is therefore an over-simplification; moreover, climate change may drive changes in predator densities. A simple way to introduce effects of climate change on generalist predators into

our model is to have the predation parameter a in equation (3.18) for the host population be weather-dependent, and is therefore an important next step.

Disease-resistance evolution is another key mechanism that can alter the spongy moth's response to climate change (Urban et al., 2016). Our previous work produced a virus model that includes costly but heritable host resistance to the virus (Páez et al., 2017). Although we have little information on whether spongy moth larvae evolve resistance to the fungal pathogen, it may be possible to estimate parameters describing spongy moth fungus-resistance evolution from existing data. Constructing a model that allows the host to evolve resistance to both the fungus and the virus is therefore an additional goal.

Although our current models do not allow for variability in spongy moth host tree defenses, it is nevertheless true that such defenses can alter the feeding and development of spongy moth larvae (Barbosa and Krischik, 1987; Hemming and Lindroth, 1995; Mason et al., 2015), and the response of spongy moth larvae to the virus (Elderd et al., 2013). It may therefore be worth extending our models to allow for the effects of plant defenses on larval development and on the response of the spongy moth to the virus. Since we have shown that the number of species considered in our system can strongly alter projections of the ecological consequences of climate change, the addition of more species and interactions is an important next step in future research.

Finally, our future projections were made by using projected weather data at the end of the 21st century, but that time period is sufficiently far from now that other unpredictable changes not included in our system may also alter the ecological consequences of climate change on the spongy moth. In future research we will therefore make projections for the nearer future, such as the middle of the 21st century.

References

Andrew J Allstadt, Kyle J Haynes, Andrew M Liebhold, and Derek M Johnson. Long-term shifts in the cyclicity of outbreaks of a forest-defoliating insect. *Oecologia*, 172(1):141–151, 2013.

Roy M Anderson and Robert M May. Infectious diseases and population cycles of forest insects. *Science*, 210(4470):658–661, 1980.

Theodore G Andreadis and Ronald M Weseloh. Discovery of entomophaga maimaiga in north american gypsy moth, lymantria dispar. *Proceedings of the National Academy of Sciences*, 87(7):2461–2465, 1990.

Pedro Barbosa and Vera Aber Krischik. Influence of alkaloids on feeding preference of eastern deciduous forest trees by the gypsy moth lymantria dispar. *The American Naturalist*, 130 (1):53–69, 1987.

Alan A Berryman. What causes population cycles of forest lepidoptera? *Trends in Ecology & Evolution*, 11(1):28–32, 1996.

David Bolton. The computation of equivalent potential temperature. *Monthly weather review*, 108(7):1046–1053, 1980.

Kenneth P Burnham and David R Anderson. *Model Selection and Multimodel Inference: A Practical Information-Theoretic Approach*. Springer, 2010.

Stephen R Carpenter. Microcosm experiments have limited relevance for community and ecosystem ecology. *Ecology*, 77(3):677–680, 1996.

MR Carter, FW Ravlin, and ML McManus. Effect of defoliation on gypsy moth phenology and capture of male moths in pheromone-baited traps. *Environmental entomology*, 21(6): 1308–1318, 1992.

Intergovernmental Panel On Climate Change. Climate change 2007: the physical science basis. *Agenda*, 6(07):333, 2007.

Greg Dwyer, Joseph S Elkinton, and John P Buonaccorsi. Host heterogeneity in susceptibility and disease dynamics: tests of a mathematical model. *The American Naturalist*, 150(6): 685–707, 1997.

Greg Dwyer, Jonathan Dushoff, Joseph S Elkinton, and Simon A Levin. Pathogen-driven outbreaks in forest defoliators revisited: building models from experimental data. *The American Naturalist*, 156(2):105–120, 2000.

Greg Dwyer, Jonathan Dushoff, and Susan Harrell Yee. The combined effects of pathogens and predators on insect outbreaks. *Nature*, 430(6997):341–345, 2004.

Greg Dwyer, Joseph R Mihaljevic, and Vanja Dukic. Can eco-evo theory explain population cycles in the field? *The American Naturalist*, 199(1):108–125, 2022.

Bret D Elderd, Brian J Rehill, Kyle J Haynes, and Greg Dwyer. Induced plant defenses, host–pathogen interactions, and forest insect outbreaks. *Proceedings of the National Academy of Sciences*, 110(37):14978–14983, 2013.

Joseph S Elkinton, William M Healy, John P Buonaccorsi, George H Boettner, Anne M Hazzard, and Harvey R Smith. Interactions among gypsy moths, white-footed mice, and acorns. *Ecology*, 77(8):2332–2342, 1996.

Joseph S Elkinton, Tonya D Bittner, Valerie J Pasquarella, George H Boettner, Andrew M Liebhold, Juli R Gould, Heather Faubert, Lisa Tewksbury, Hannah J Broadley, Nathan P Havill, et al. Relating aerial deposition of entomophaga maimaiga conidia (zoopagomycota: Entomophthorales) to mortality of gypsy moth (lepidoptera: Erebidae) larvae and nearby defoliation. *Environmental entomology*, 48(5):1214–1222, 2019.

JS Elkinton and AM Liebhold. Population dynamics of gypsy moth in north america. *Annual review of entomology*, 35(1):571–596, 1990.

Songlin Fei, Randall S Morin, Christopher M Oswalt, and Andrew M Liebhold. Biomass losses resulting from insect and disease invasions in us forests. *Proceedings of the National Academy of Sciences*, 116(35):17371–17376, 2019.

Emma Fuller, Bret D Elderd, and Greg Dwyer. Pathogen persistence in the environment and insect-baculovirus interactions: disease-density thresholds, epidemic burnout, and insect outbreaks. *The American Naturalist*, 179(3):E70–E96, 2012.

Eric J Gustafson, Brian R Miranda, and Brian R Sturtevant. Can future co2 concentrations mitigate the negative effects of high temperature and longer droughts on forest growth? *Forests*, 9(11):664, 2018.

Laurel J Haavik, Sharon A Billings, James M Guldin, and Fred M Stephen. Emergent insects, pathogens and drought shape changing patterns in oak decline in north america and europe. *Forest Ecology and Management*, 354:190–205, 2015.

Ann E Hajek. Pathology and epizootiology of entomophaga maimaiga infections in forest lepidoptera. *Microbiology and molecular biology reviews*, 63(4):814–835, 1999.

Ann E Hajek, Richard A Humber, Joseph S Elkinton, Bernie May, SR Walsh, and Julie C Silver. Allozyme and restriction fragment length polymorphism analyses confirm entomophaga maimaiga responsible for 1989 epizootics in north american gypsy moth populations. *Proceedings of the National Academy of Sciences*, 87(18):6979–6982, 1990.

Ann E Hajek, Richard A Humber, and Joseph S Elkinton. Mysterious origin of entom haga malmalga in north america. *American Entomologist*, 41(1):31–43, 1995.

Ann E Hajek, Joseph S Elkinton, and Jeffrey J Witcosky. Introduction and spread of the fungal pathogen entomophaga maimaiga (zygomycetes: Entomophthorales) along the leading edge of gypsy moth (lepidoptera: Lymantriidae) spread. *Environmental Entomology*, 25 (5):1235–1247, 1996.

Ann E Hajek, Patrick C Tobin, and Kyle J Haynes. Replacement of a dominant viral pathogen by a fungal pathogen does not alter the collapse of a regional forest insect outbreak. *Oecologia*, 177(3):785–797, 2015.

Kyle J Haynes, Andrew J Allstadt, and Dietrich Klimetzek. Forest defoliator outbreaks under climate change: effects on the frequency and severity of outbreaks of five pine insect pests. *Global Change Biology*, 20(6):2004–2018, 2014.

Jocelyn DC Hemming and Richard L Lindroth. Intraspecific variation in aspen phytochemistry: effects on performance of gypsy moths and forest tent caterpillars. *Oecologia*, 103 (1):79–88, 1995.

Alison F Hunter. Ecology, life history, and phylogeny of outbreak and nonoutbreak species. *Population dynamics: new approaches and synthesis*, pages 41–64, 1995.

Rolf A Ims, John-Andre Henden, and Siw T Killengreen. Collapsing population cycles. *Trends in Ecology & Evolution*, 23(2):79–86, 2008.

Sudharsana V Iyengar, Janaki Balakrishnan, and Jürgen Kurths. Impact of climate change on larch budmoth cyclic outbreaks. *Scientific reports*, 6(1):1–8, 2016.

Derek M. Johnson, Andrew M. Liebhold, and Ottar N. Bjørnstad. Geographical variation in the periodicity of gypsy moth outbreaks. *Ecography*, 29(3):367–374, 2006.

Clive G Jones, Richard S Ostfeld, Michele P Richard, Eric M Schauber, and Jerry O Wolff. Chain reactions linking acorns to gypsy moth outbreaks and lyme disease risk. *Science*, 279(5353):1023–1026, 1998.

Naoto Kamata and Andrew Liebhold. Are population cycles and spatial synchrony a universal characteristic of forest insect populations? *Population Ecology*, 42(3), 2000.

Kyrre L Kausrud, Atle Mysterud, Harald Steen, Jon Olav Vik, Eivind Østbye, Bernard Cazelles, Erik Framstad, Anne Maria Eikeset, Ivar Mysterud, Torstein Solhøy, et al. Linking climate change to lemming cycles. *Nature*, 456(7218):93–97, 2008.

M. J. Keeling and P. Rohani. *Modeling Infectious Diseases in Humans and Animals*. Princeton University Press, 2008.

David A Kennedy, Vanja Dukic, and Greg Dwyer. Combining principal component analysis with parameter line-searches to improve the efficacy of metropolis–hastings mcmc. *Environmental and ecological statistics*, 22(2):247–274, 2015.

John B Kim, Erwan Monier, Brent Sohngen, G Stephen Pitts, Ray Drapek, James McFarland, Sara Ohrel, and Jefferson Cole. Assessing climate change impacts, benefits of mitigation, and uncertainties on major global forest regions under multiple socioeconomic and emissions scenarios. *Environmental Research Letters*, 12(4):045001, 2017.

Katri Korpela, Maria Delgado, Heikki Henttonen, Erkki Korpimäki, Esa Koskela, Otso Ovaskainen, Hannu Pietiäinen, Janne Sundell, Nigel G Yoccoz, and Otso Huitu. Nonlinear effects of climate on boreal rodent dynamics: mild winters do not negate high-amplitude cycles. *Global Change Biology*, 19(3):697–710, 2013.

Mark Kot. *Elements of Mathematical Ecology*. Cambridge University Press, 2001.

Colin H Kyle, Jiawei Liu, Molly E Gallagher, Vanja Dukic, and Greg Dwyer. Stochasticity and infectious disease dynamics: density and weather effects on a fungal insect pathogen. *The American Naturalist*, 195(3):504–523, 2020.

John H Lawton. Are there general laws in ecology? *Oikos*, 84:177–192, 1999.

Andrew Liebhold, Joseph Elkinton, David Williams, and R-M Muzika. What causes outbreaks of the gypsy moth in north america? *Population Ecology*, 42(3):257–266, 2000.

Andrew M Liebhold, Joel A Halverson, and Gregory A Elmes. Gypsy moth invasion in north america: a quantitative analysis. *Journal of Biogeography*, pages 513–520, 1992.

Andrew M Liebhold, Edward E Simons, Alan Sior, and James D Unger. Forecasting defoliation caused by the gypsy moth from field measurements. *Environmental Entomology*, 22 (1):26–32, 1993.

Andrew M Liebhold, Ann E Hajek, Jonathan A Walter, Kyle J Haynes, Joseph Elkinton, and Rose-Marie Muzika. Historical change in the outbreak dynamics of an invading forest insect. *Biological Invasions*, 24(3):879–889, 2022.

Jiawei Liu, Colin Kyle, Jiali Wang, Rao Kotamarthi, William Koval, and Greg Dwyer. Ecoclimate models project severe negative impacts of climate change on a fatal pathogen of an invasive forest pest. *PNAS*, in prep, 2022.

Raksha Malakar, Joseph S Elkinton, Ann E Hajek, and John P Burand. Within-host interactions oflymantria dispar (lepidoptera: Lymantriidae) nucleopolyhedrosis virus andentomophaga maimaiga (zygomycetes: Entomophthorales). *Journal of invertebrate pathology*, 73(1):91–100, 1999.

Charles J Mason, Kennedy F Rubert-Nason, Richard L Lindroth, and Kenneth F Raffa. Aspen defense chemicals influence midgut bacterial community composition of gypsy moth. *Journal of Chemical Ecology*, 41(1):75–84, 2015.

Hamish McCallum, Nigel Barlow, and Jim Hone. How should pathogen transmission be modelled? *Trends in Ecology & Evolution*, 16(6):295–300, 2001.

Alexandre Millon, Steve J Petty, Brian Little, Olivier Gimenez, Thomas Cornulier, and Xavier Lambin. Dampening prey cycle overrides the impact of climate change on predator population dynamics: A long-term demographic study on tawny owls. *Global change biology*, 20(6):1770–1781, 2014.

Erin A Mordecai, Jamie M Caldwell, Marissa K Grossman, Catherine A Lippi, Leah R Johnson, Marco Neira, Jason R Rohr, Sadie J Ryan, Van Savage, Marta S Shocket, et al. Thermal biology of mosquito-borne disease. *Ecology Letters*, 22(10):1690–1708, 2019.

Randall S Morin and Andrew M Liebhold. Invasive forest defoliator contributes to the impending downward trend of oak dominance in eastern north america. *Forestry*, 89(3): 284–289, 2016.

National Centers for Environmental Information and National Oceanic and Atmospheric Administration. Global surface summary of the day (online database). `https://www.ncei.noaa.gov/access/search/data-search/global-summary-of-the-day`, 2022.

David J Páez, Vanja Dukic, Jonathan Dushoff, Arietta Fleming-Davies, and Greg Dwyer. Eco-evolutionary theory and insect outbreaks. *The American Naturalist*, 189(6):616–629, 2017.

John W Peacock, Dale F Schweitzer, Jane L Carter, and Normand R Dubois. Laboratory assessment of the effects of bacillus thuringiensis on native lepidoptera. *Environmental Entomology*, 27(2):450–457, 1998.

Deepa S Pureswaran, Alain Roques, and Andrea Battisti. Forest insects and climate change. *Current Forestry Reports*, 4(2):35–50, 2018.

Debora Quayle, Jacques Régnière, Naomi Cappuccino, and Alain Dupont. Forest composition, host-population density, and parasitism of spruce budworm choristoneura fumiferana eggs by trichogramma minutum. *Entomologia Experimentalis et Applicata*, 107(3): 215–227, 2003.

Don C Radcliffe, David M Hix, and Stephen N Matthews. Predisposing factors' effects on mortality of oak (quercus) and hickory (carya) species in mature forests undergoing mesophication in appalachian ohio. *Forest Ecosystems*, 8(1):1–14, 2021.

Douglas B Rasher, Robert S Steneck, Jochen Halfar, Kristy J Kroeker, Justin B Ries, M Tim Tinker, Phoebe TW Chan, Jan Fietzke, Nicholas A Kamenos, Brenda H Konar, et al. Keystone predators govern the pathway and pace of climate impacts in a subarctic marine ecosystem. *Science*, 369(6509):1351–1354, 2020.

John A Rice. *Mathematical statistics and data analysis*. Cengage Learning, 2006.

Joseph M Russo, Andrew M Liebhold, and John GW Kelley. Mesoscale weather data as input to a gypsy moth (lepidoptera: Lymantriidae) phenology model. *Journal of Economic Entomology*, 86(3):838–844, 1993.

DR Smitley, LS Bauer, AE Hajek, FJ Sapio, and RA Humber. Introduction and establishment of entomophaga maimaiga, a fungal pathogen of gypsy moth (lepidoptera: Lymantriidae) in michigan. *Environmental Entomology*, 24(6):1685–1695, 1995.

John S Sperry, Martin D Venturas, Henry N Todd, Anna T Trugman, William RL Anderegg, Yujie Wang, and Xiaonan Tai. The impact of rising co2 and acclimation on the response of us forests to global warming. *Proceedings of the National Academy of Sciences*, 116(51): 25734–25744, 2019.

Brian R Sturtevant and Marie-Josée Fortin. Understanding and modeling forest disturbance interactions at the landscape level. *Frontiers in Ecology and Evolution*, 9(653647), 2021.

Patrick C Tobin, Barry B Bai, Donald A Eggen, and Donna S Leonard. The ecology, geopolitics, and economics of managing lymantria dispar in the united states. *International Journal of Pest Management*, 58(3):195–210, 2012.

Kévin Tougeron, Jacques Brodeur, Cécile Le Lann, and Joan van Baaren. How climate change affects the seasonal ecology of insect parasitoids. *Ecological Entomology*, 45(2): 167–181, 2020.

Mark C Urban, Greta Bocedi, Andrew P Hendry, J-B Mihoub, Guy Pe'er, Alex Singer, JR Bridle, LG Crozier, Luc De Meester, William Godsoe, et al. Improving the forecast for biodiversity under climate change. *Science*, 353(6304):aad8466, 2016.

U.S. Forest Service. Lymantria dispar digest (online database). `https://apps.fs.usda.gov/nicportal/lddigest/cfm/dsp/dsplddigesthome.cfm`, 2022.

George Copley Varley, George R Gradwell, and Michael Patrick Hassell. *Insect population ecology: an analytical approach*. Univ of California Press, 1974.

Gian-Reto Walther. Community and ecosystem responses to recent climate change. *Philosophical Transactions of the Royal Society B: Biological Sciences*, 365(1549):2019–2024, 2010.

Jiali Wang and Veerabhadra R Kotamarthi. Downscaling with a nested regional climate model in near-surface fields over the contiguous united states. *Journal of Geophysical Research: Atmospheres*, 119(14):8778–8797, 2014.

Jiali Wang and Veerabhadra R Kotamarthi. High-resolution dynamically downscaled projections of precipitation in the mid and late 21st century over north america. *Earth's Future*, 3(7):268–288, 2015.

Sumio Watanabe. A widely applicable bayesian information criterion. *Journal of Machine Learning Research*, 14(Mar):867–897, 2013.

RM Weseloh and TG Andreadis. Persistence of resting spores ofentomophaga maimaiga, a fungal pathogen of the gypsy moth, lymantria dispar. *Journal of invertebrate pathology*, 2(69):195–196, 1997.

Ronald M Weseloh and Theodore G Andreadis. Epizootiology of the fungus entomophaga maimaiga, and its impact on gypsy moth populations. *Journal of Invertebrate Pathology*, 59(2):133–141, 1992.

H Alan Wood and Robert R Granados. Genetically engineered baculoviruses as agents for pest control. *Annual review of microbiology*, 45(1):69–87, 1991.

SA Woods and JS Elkinton. Biomodal patterns of mortality from nuclear polyhedrosis virus in gypsy moth (lymantria dispar) populations. *Journal of Invertebrate Pathology*, 50(2): 151–157, 1987.

Zachary Zobel, Jiali Wang, Donald J Wuebbles, and V Rao Kotamarthi. Evaluations of high-resolution dynamically downscaled ensembles over the contiguous united states. *Climate Dynamics*, 50(3-4):863–884, 2018.